Magnetic Resonance Spectra in Polycrystalline Solids

P. C. TAYLOR,*† J. F. BAUGHER,§** and H. M. KRIZ†

U. S. Naval Research Laboratory, Washington, D. C. 20375, James Franck Institute, The University of Chicago, Chicago, Illinois 60637, and West Virginia University, Morgantown, West Virginia 26505

Contents

I. Introduction

Nuclear magnetic resonance (nmr) and electron spin resonance (esr) are invaluable tools for the chemist, physicist, or materials scientist interested in the properties of solids on an atomic scale. These techniques yield precise, detailed information about very localized magnetic and electric interactions, information which is not generally obtainable by any other means. Nmr is useful in studying static properties, such as atomic arrangements and electron charge distributions, or dynamic processes, such as diffusion and phase changes. Effects due to defects, strains, and departures from stoichiometry may also be manifested in nmr spectra. Esr is useful in studying the nature of paramagnetic impurities in a variety of materials, and in examining the nature of intrinsic and radiation-induced defects. The properties of free radicals, both induced and intrinsic, are often most easily studied by esr techniques.

Generally, the greatest amount of information concerning nuclear or paramagnetic sites in solids can be obtained from measurements in single crystals. However, there are two fundamental reasons for using powdered materials in magnetic resonance studies. ‡ First and most obvious is that some materials are available only in powdered form. Secondly, glasses and amorphous materials are inherently "powders" in the sense that they can be viewed as an ensemble of randomly oriented nuclear or paramagnetic sites. But even when powdered specimens are not dictated by the nature of the material, it may be desirable for reasons of economy or simplicity to use a polycrystalline sample. In many cases the difficulty or expense in obtaining a single crystal may not be justified by the nature of the information desired, as when the magnitude of an interaction is required but not its directional properties. Experiments on single crystals, although more precise, can be time consuming and unnecessarily tedious when compared to the speed and simplicity possible with powdered samples.

Information relating to the analysis of spectra from powdered materials is widely scattered in the literature, and important results are often contained in papers devoted to other subjects. Systematic treatments of lineshapes are not generally available, and many authors confine themselves to cursory descriptions of the very specific analysis pertinent to a particular material. Thus, the newcomer to the field is faced with the difficult problem of assimilating an extensive body of information in a piecemeal manner.

Since the first discussion of resolved dipolar interactions in powders (Pake, 1948),[1] the techniques for analyzing magnetic resonance spectra in powders have become increasingly sophisticated, and within the past few years a number of advances have been made. Of particular importance has been the realization that positions of significant features in theoretical powder patterns can be expressed analytically even in those cases where numerical methods must be resorted to in calculating the com-

‡ Throughout this review the term "magnetic resonance" will be used to mean both nuclear magnetic resonance and electron spin resonance.

plete powder pattern. In addition, high-speed computer simulation techniques have been developed which allow complete and accurate analysis of complicated spectra arising from the superposition of several distinct sites. Even the more complicated spectra resulting from the smooth distribution of Hamiltonian parameters characteristic of the random variation of local environments in glassy and amorphous materials can now be successfully analyzed.

Because details of the analytical techniques are scattered in the literature, and because many techniques for analyzing powder spectra have only recently reached full development, wide line magnetic resonance in powders has not been exploited as a routine analytical tool as has, for example, high-resolution nmr in liquids. Rather, magnetic resonance in powders remains the province of a few specialists in nmr and esr. It is hoped that this review will encourage wider use of magnetic resonance by chemists, physicists, and materials scientists interested in polycrystalline, glassy, and amorphous materials. Many of the techniques described here are also applicable to other subfields of the spectroscopy of powdered materials, namely acoustic resonance, pulsed nmr,[2] and Raman spectra of polycrystalline solids.[3]

There are two principal steps involved in the application of magnetic resonance to polycrystalline and glassy solids. First is the analysis of observed spectra in terms of phenomenological, magnetic resonance parameters. Second is the interpretation of these parameters in a physically meaningful way. In some cases the relation between the magnetic resonance parameters and chemical or physical properties may be calculated directly. At times only empirical relations are possible. In this review interpretation of the parameters is incidental to the primary purpose which is to describe the extraction of magnetic resonance parameters from experimental spectra.

No attempt has been made to review all cases of magnetic resonance studies of powdered samples, nor do the specific examples given here exhaust all applications of magnetic resonance. Rather the discussion is limited to particularly illustrative and easily understandable applications of magnetic resonance to polycrystalline and glassy inorganic solids. Excluded as examples are polymers, liquids, biological molecules, esr of rare earth ions, ferromagnetic and antiferromagnetic resonance, high-resolution and pulsed nmr, and pure nuclear quadrupole resonance (nqr). Applications of magnetic resonance to specific materials or classes of materials other than those discussed here are readily available in the literature. It is assumed that the reader is familiar with the fundamentals of magnetic resonance as presented in numerous introductory treatments.[4-23]

Section II of this review contains a general discussion of nmr and esr theory with emphasis on the formal similarities between the two magnetic resonance Hamiltonians and resulting resonance conditions. The physical origin and general properties of powder spectra are described qualitatively, and methods of computing spectra are reviewed. Sections III and IV are concerned with powder patterns encountered in nmr and esr studies, respectively. In section V the special techniques required for calculating spectra characterized by distributions of magnetic resonance parameters are described. A brief discussion of possible future developments in powder studies is presented in section VI.

List of Symbols

$\mathcal{3C}$	Magnetic resonance spin-Hamiltonian or Hamiltonian
β	Bohr magneton
$\mathbf{S}$	Electronic spin operator
$\mathbf{g}$	Electronic spin gyromagnetic tensor
g_1, g_2, g_3	Principal values of electronic g tensor
$g_{\parallel}, g_{\perp}$	Principal values of electronic g tensor in the presence of axial symmetry
$\mathbf{H}$	External applied magnetic field
$\mathbf{D}$	Fine structure interaction tensor
$\mathbf{A}$	Hyperfine interaction tensor
A_1, A_2, A_3	Principal values of hyperfine interaction tensor
$A_{\parallel}, A^*_{\perp}$	Principal values of hyperfine interaction tensor in the presence of axial symmetry
$\mathbf{I}$	Nuclear spin operator
$\mathbf{Q}$	Nuclear quadrupole moment tensor
γ	Nuclear gyromagnetic ratio
$\hbar$	Planck's constant divided by 2π
σ	Nuclear magnetic shift tensor
$\sigma_1, \sigma_2, \sigma_3$	Principal values of nuclear magnetic shift tensor
$\sigma_{\parallel}, \sigma_{\perp}$	Principal values of nuclear magnetic shift tensor in the presence of axial symmetry
$\mathbf{K}$	Knight shift tensor
ν	Frequency of applied oscillating magnetic field
θ, φ	Euler angles of external magnetic field $\mathbf{H}$ relative to principal axes of the given interaction tensor
ψ	Euler angle describing position of oscillating field $\mathbf{H}_1$
m	Nuclear magnetic quantum number
M	Electron magnetic quantum number
I	Nuclear spin
S	Electron spin
D	Axial fine structure parameter
E	Off-axial fine structure parameter
g	$g(\theta,\phi)$, effective g-factor for electron (angularly dependent)
A	$A(\theta,\phi)$, effective hyperfine coupling constant (angularly dependent)
q	zz-Component of electric field gradient tensor
Q	Nuclear quadrupole moment
η	Nuclear quadrupole interaction asymmetry parameter
$\mathbf{H}_1$	Amplitude of oscillating magnetic field
F_G	Normalized Gaussian function
σ_G	Half-width of normalized Gaussian function (half of peak-to-peak derivative width)
F_L	Normalized Lorentzian function
σ_L	Full-width at half-height of normalized Lorentzian function
$V(v)$	Voigt function
$S(H)$	Lineshape function or powder pattern
$d\Omega$	Element of solid angle
$I_m(\Omega)$	Transition probability for the mth component of the spectrum as a function of θ, φ
$P(\Omega)d\Omega$	Probability that a site is oriented in an element of solid angle $d\Omega$ at $\Omega = (\theta, \varphi)$
μ	Angular parameter, equal to $\cos \theta$
$G(a, b)$	Function used to evaluate nature of critical points in the resonance condition
$K(k)$	Complete elliptic integral of the first kind
H_1, H_2, H_3	Locations in magnetic field of ordinary singularities (shoulders and divergences) in a powder pattern
$H_{\parallel}, H_{\perp}$	Locations in magnetic field of ordinary singularities (shoulders and divergences) in an axially symmetric powder pattern

r	Internuclear separation of nuclear pair in dipolar interaction
M_2	Second moment of powder pattern
m_2	Contribution to second moment of powder spectrum due to unresolved neighboring nuclear spins
H_0	Resonance field for isotropic nuclear or electronic ($g = 2$) Zeeman interaction
ν_0	Constant applied frequency or nuclear Zeeman resonance frequency
H_d	Position in field of divergence in powder pattern
ν_d	Position in frequency of divergence in powder pattern
H_s	Position in field of shoulder in powder pattern
ν_s	Position in frequency of shoulder in powder pattern
H_{ed}	Position in field of extra divergence in powder pattern
ν_{ed}	Position in frequency of extra divergence in powder pattern
Δ_Q	Total width of powder pattern in presence of nuclear quadrupole interaction
Δ_{ss}	Distance between outermost derivative extrema in convoluted derivative spectra for the case of the nuclear quadrupole interaction
$\sigma_{iso}, \sigma_{ax},$ σ_{aniso}	Anisotropic magnetic shift parameters
Δ_M	Total width of powder pattern in presence of magnetic shift effects
ζ	Anisotropy factor for nuclear magnetic shift or electronic Zeeman powder pattern
r_{jk}	Radius vector joining nuclei j and k.
θ_{jk}	Angle between r_{jk} and the magnetic field in the spinning sample technique
ω	Angular frequency of rotation of sample
ψ_{jk}	Angle between r_{jk} and axis of rotation of spinning sample
α	Angle between the axis of rotation of the spinning sample and the magnetic field
λ_i	Direction cosines of magnetic field with respect to principal axes of magnetic shift tensor
H_{ij}	"Extra" powder pattern critical points in magnetic field
ΔH_{fs}	Total width of esr powder pattern for $S = -\frac{1}{2} \leftrightarrow +\frac{1}{2}$ transition in presence of fine structure effects
K	Resultant nuclear spin in hyperfine interactions with more than one identical nucleus
J	Strength of isotropic exchange interaction
M_3	Magnetization for ferromagnetic centers
$H_3{}^a$	Applied magnetic field for ferromagnetic center
$N_1, N_2, N_3,$ $N_i{}^e, N_2{}^e$	Demagnetizing factors for ferromagnetic center
θ', φ'	Polar and azimuthal angles, respectively
K_1/M_s	First-order anisotropy field

II. General Theory

A. Nmr and Esr Hamiltonians

For a great majority of the applications of magnetic resonance to powdered solids there is a formal identity between terms appearing in the nmr and the esr Hamiltonians. It is the purpose of this section to review briefly these two Hamiltonians with an emphasis on their formal similarity. Extensive treatments of magnetic resonance

are readily available,[4-23] and a basic theoretical understanding of nmr and esr interactions is assumed in what follows.

A reasonably general matrix representation of the esr effective spin Hamiltonian is given by[12-23]

$$\mathcal{K} = \beta \mathbf{S} \cdot \mathbf{g} \cdot \mathbf{H} + \mathbf{S} \cdot \mathbf{D} \cdot \mathbf{S} + \mathbf{S} \cdot \mathbf{A} \cdot \mathbf{I} + \mathbf{I} \cdot \mathbf{Q} \cdot \mathbf{I} - \gamma \hbar \mathbf{I} \cdot \mathbf{H} \quad (1)$$

where $\mathbf{g}$, $\mathbf{D}$, $\mathbf{A}$, and $\mathbf{Q}$ are the gyromagnetic, fine structure, hyperfine structure, and quadrupolar tensors, respectively, $\mathbf{S}$ and $\mathbf{I}$ are the electronic and nuclear spin vectors, γ is the nuclear gyromagnetic ratio, β is the Bohr magneton, and $\mathbf{H}$ is the applied magnetic field. Equation 1 does not apply in some special cases, as when there are hyperfine interactions with several nuclei, resolved superhyperfine interactions, exchange effects, or important fourth-order fine-structure terms.[10-17] Neither does it apply to the case of rare earth ions when J, and not S, is the good quantum number.

In matrix notation the nmr Hamiltonian can be represented as

$$\mathcal{K} = -\gamma \hbar \mathbf{I} \cdot \mathbf{H} + \mathbf{I} \cdot \mathbf{Q} \cdot \mathbf{I} + \gamma \hbar \mathbf{I} \cdot \sigma \cdot \mathbf{H} \quad (2)$$

where σ is a magnetic shift tensor and may represent a chemical shift in the case of diamagnetic or slightly paramagnetic substances,[4,5,7,24-26] a paramagnetic shift (or super exchange interaction) in the case of strongly paramagnetic substances,[7,27-30] or a Knight shift in the case of metallic substances.[4,5,7,9,31,32] The Knight shift tensor is usually written as K, which replaces $-\sigma$. All three magnetic shift interactions have the same functional dependence on orientation in the limit of perturbation calculations (see Appendix I), so for convenience the following discussions will be concerned primarily with the chemical shift.

A comparison of eq 1 and 2 illustrates the formal similarity of several of the nmr and esr interactions. In particular, the electronic Zeeman term ($\beta \mathbf{S} \cdot \mathbf{g} \cdot \mathbf{H}$) has the same form as the nuclear Zeeman plus magnetic shift terms ($-\gamma \hbar \mathbf{I} \cdot (\mathbf{1} - \sigma) \cdot \mathbf{H}$), and the esr fine-structure interaction ($\mathbf{S} \cdot \mathbf{D} \cdot \mathbf{S}$) is formally identical with the nmr quadrupolar interaction ($\mathbf{I} \cdot \mathbf{Q} \cdot \mathbf{I}$). However, the similarity is not complete, since there are no terms in the nmr Hamiltonian equivalent to the nuclear hyperfine and nuclear Zeeman terms in the esr Hamiltonian.

B. Powder Spectra

The energy levels of the spin system are determined by performing a diagonalization of eq 1 or 2. Once the energy levels are determined, the energy level separations that correspond to allowed transitions can be calculated. These energy level separations represent the quantum of energy (designated by $h\nu$) absorbed by the spin system. Such an expression will be referred to as a *resonance condition* and is of the form $h\nu = f(H)$. Under most experimental conditions, the frequency ν is kept constant, and the magnetic field varied, so the resonance condition is solved for H, the magnetic field at which resonance will occur.

In a single crystal, the resonance field or frequency depends on the orientation of the single crystal with respect to the applied magnetic field. The resonance condition is calculated from the energy eigenvalues obtained from eq 1 or 2. In a polycrystalline, vitreous, or amorphous sample, the nuclear or paramagnetic sites are randomly oriented with respect to the applied field. Then the magnetic resonance spectrum, referred to as a "powder pattern," is an average over the resonance conditions for all possible orientations of the nuclear or paramagnetic site.

It is an extremely lengthy process to obtain the necessary eigenvalues for all members of an ensemble of randomly oriented crystallites by exact diagonalization of the Hamiltonians as expressed in eq 1 or 2. Fortunately, in many instances the Zeeman term in the Hamiltonian predominates, and perturbation theory may be employed to derive approximate solutions. Hereafter, the discussion will deal primarily with cases where perturbation calculations are appropriate.

1. Perturbation Calculations and Resonance Conditions

Two simple resonance conditions, one pertaining to nmr and the other to esr, will be discussed here to illustrate the basic features of powder patterns most often encountered in magnetic resonance. In what follows, the orientation of the applied magnetic field with respect to the principal axes of the tensor quantities in eq 1 and 2 will be specified by the Euler angles[33] θ and φ, as shown in Figure 1. The nuclear spin quantum numbers will be denoted by I and m and the electronic spin quantum numbers S and M.

The esr resonance condition for the $M - 1 \rightarrow M$, $\Delta m = 0$ allowed transitions[34] derived from first-order perturbation theory for the hyperfine term while neglecting the fine-structure, quadrupolar, and nuclear Zeeman terms of eq 1 is

$$h\nu = g\beta H + (Am/g) \qquad (3)$$

where

$$g = [g_1{}^2 \sin^2 \theta \sin^2 \varphi + g_2{}^2 \sin^2 \theta \cos^2 \varphi + g_3{}^2 \cos^2 \theta]^{1/2}$$

$$A = [A_1{}^2 g_1{}^2 \sin^2 \theta \sin^2 \varphi + A_2{}^2 g_2{}^2 \sin^2 \theta \cos^2 \varphi + A_3{}^2 g_3{}^2 \cos^2 \theta]^{1/2}$$

If the magnetic shift term of eq 2 is neglected and the quadrupolar term is treated to second order in perturbation theory, then the following nmr resonance condition is obtained for the $m \rightarrow m - 1$ transition[35-38]

$$\nu = \gamma H/2\pi - \frac{1}{2}\left(m - \frac{1}{2}\right)\nu_Q[3\cos^2\theta - 1 - \eta\cos 2\varphi \sin^2\theta] + \frac{\nu_Q{}^2}{12(\gamma H/2\pi)}\left\{\frac{3}{2}\sin^2\theta \times\right.$$

$$[(A + B)\cos^2\theta - B] + \eta\cos 2\varphi \sin^2\theta \times$$

$$[(A + B)\cos^2\theta + B] + \frac{\eta^2}{6}[A - (A + 4B)\cos^2\theta -$$

$$\left.(A + B)\cos^2 2\varphi(\cos^2\theta - 1)^2]\right\} \qquad (4)$$

where

$$\nu_Q = \frac{3e^2qQ}{2I(2I - 1)h}$$

$$A = 24m(m - 1) - 4I(I + 1) + 9$$

$$B = \frac{1}{4}[6m(m - 1) - 2I(I + 1) + 3]$$

The three terms in eq 4 represent the Zeeman, first-order, and second-order quadrupolar perturbation terms, respectively.

As mentioned previously, several of the terms in eq 1 and 2 are formally identical so that an nmr resonance condition can be obtained from an esr resonance condition by simply making the appropriate substitutions. In particular, an nmr resonance condition containing nuclear Zeeman, nuclear quadrupolar, and magnetic shift terms may be obtained from an esr resonance condition including electronic Zeeman and fine-structure terms (provided of course that the perturbation results are valid) by making the following substitutions:[39]
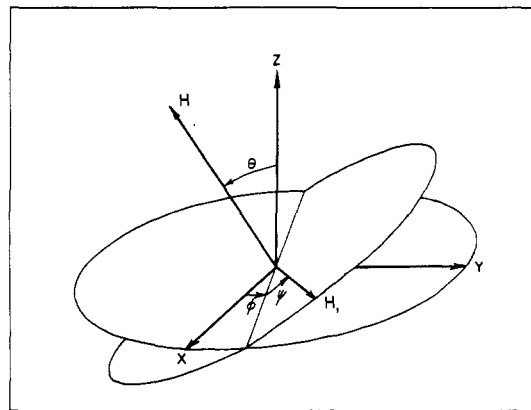

Figure 1. Definitions of the angles used in the text. The x, y, z system is the principal axis system of the interaction being considered, **H** is the static field, and H_1 is the oscillating field used to induce resonance absorption. H_1 is taken to be in a plane perpendicular to **H**. These angles are the same Euler angles as those defined by Goldstein.[33]

$$\frac{3e^2qQ}{4I(2I - 1)} \text{ for } D$$

$$[\eta/3]\frac{3e^2qQ}{4I(2I - 1)} \text{ for } E \qquad (5)$$

$$(-\hbar\gamma/\beta)(1 - \sigma_i) \text{ for } g_i \qquad i = 1, 2, 3$$

where D and E are the fine-structure parameters, e^2qQ/h is the quadrupole coupling constant in frequency units, and η is the field gradient asymmetry parameter. Also the electron-spin quantum numbers S and M must be replaced by the nuclear spin quantum numbers I and m.

The resonance conditions specified by eq 3 and 4 are the result of several simplifying assumptions. Most obvious is the assumption that the nuclear and electronic Zeeman terms predominate so that the remaining terms can be treated using perturbation theory. There are some cases in both esr and nmr where the fine structure or quadrupolar term must be taken as the dominant one, and the electronic or nuclear Zeeman term treated as a perturbation. In nmr this nuclear quadrupole resonance with Zeeman perturbation has been reviewed by Das and Hahn.[40] In intermediate cases where the Zeeman and fine structure or quadrupolar terms are of nearly equal magnitude, the entire Hamiltonian must be diagonalized exactly for each orientation of the principal axes with respect to the applied magnetic field. When there is more than one perturbation term and higher orders are calculated, the results often depend on exactly which interactions are included in the zero-order term as well as which cross terms are neglected in the perturbation expansion. These complications are discussed in Appendix I.

It is also assumed in eq 3 and 4 that all of the tensor quantities have identical principal axes. This restriction can, of course, be removed with the introduction of additional parameters specifying the relative orientations of the various tensor axes. However, in most experimental situations the powder patterns are such that a unique evaluation of these additional parameters is not possible and the assumption of coincident axes, thought not necessary, is simplest in the absence of evidence to the contrary.

Fine structure terms correct to second order in perturbation theory[41] can be added easily to eq 3 using eq 4 and the substitutions indicated in (5). Conversely, magnetic shift terms can be added to eq 4 using eq 3 and 5.[42,43] Perturbation expressions including the fine structure or quadrupolar interaction to third order[44-49] and the hyperfine interaction to third order[45,50] are quite lengthy

but have been calculated. Selected resonance conditions of this more complicated sort are discussed in Appendix I.

The ground state (or an excited state) of some molecules, usually organic radicals, can be a triplet state ($S = 1$). In this case, the dipole–dipole interaction between two electrons generates a spin-Hamiltonian term identical in form with the fine-structure term of eq 1.[51-53] The fine structure perturbation calculations listed in Appendix I can be used interchangeably to describe triplet state molecules even though the interaction results from dipole–dipole rather than crystal field effects.

A paramagnetic ion may be surrounded by ligands containing magnetic nuclei which can influence the esr spectrum *via* the super-hyperfine interaction.[54,55] The superhyperfine terms in the esr spin-Hamiltonian ($\Sigma_i \mathbf{S} \cdot \mathbf{A}^{(i)} \cdot \mathbf{I}^{(i)}$) are similar in form to the hyperfine term of eq 1 except that the electronic spin is no longer centered on the nuclear spin. The specific angular dependence of the superhyperfine terms depends on the particular geometry of the ligands that contain magnetic nuclei. Special cases are considered in section IV.

When $S > \frac{3}{2}$ the quadratic form of the fine-structure Hamiltonian ($\mathbf{S} \cdot \mathbf{D} \cdot \mathbf{S}$) in eq 1 is often not adequate, and it becomes necessary to consider fourth-order terms in the spin variables. In high-spin ferric compounds, for example, the fourth-order term can be just as important as the second.[56] Several authors[44,57-64] have performed perturbation calculations including fourth-order terms. These calculations have not been applied to powders as yet, although there is no reason why they could not be studied using computer techniques.

It is sometimes necessary to include an additional term in the nmr Hamiltonian (eq 2) to account for resolved dipole–dipole interactions. When identical nuclei occur in pairs, the interaction between the members of a pair is much stronger than the interaction between pairs. This situation, first considered by Pake,[1] is often referred to as the "Pake doublet" and occurs, for example, in the proton nmr of water molecules in many hydrated salts. The dipole–dipole interaction can usually be treated as a first-order perturbation of the nuclear Zeeman term. The resulting dipole–dipole term that must be added to the resonance condition (eq 4) has the same mathematical form as does the first-order quadrupolar term and is discussed in section III. Systems containing three identical nuclei have been studied by Andrew and Bersohn.[65] The more complicated situations including quadrupolar and resolved dipole–dipole interactions[65-68] and magnetic shift and resolved dipole–dipole effects[69,70] have also been investigated. The resonance conditions appropriate to these cases are discussed later (see section III and Appendix I).

The transition probability of an energy absorbing spin in a linearly polarized rf or microwave field, $\mathbf{H}_1$, is not always independent of the orientation of the spin with respect to the applied fields, $\mathbf{H}_0$ and $\mathbf{H}_1$. Significant angular dependence of the transition probability for the special case of an axial g tensor and no hyperfine or fine structure effects has been calculated by Bleaney.[71] To a first approximation this expression is also accurate in the presence of hyperfine effects.[72] In the case of complete g-anisotropy Isomoto, Watari, and Kotani[73] have obtained a more complicated expression. These results are discussed in Appendix I.

The problem of accounting for the effects of all of the electronic or nuclear spins in a given system is formally intractable. When the number of interacting nuclei or electronic spins becomes large, the discrete lines of the spectrum blur into a continuum, and no mathematical expression can be obtained for the lineshape in general.[74] However, it often happens that there are no spins grouped closely together (other than those specifically taken into account in the various terms of eq 1 and 2), and the orientational dependence of the dipole–dipole effects will very nearly average out. The resulting dipolar lineshape will be independent of angle, and it is usual to assume that the lineshape can be represented by a normalized Gaussian function of the form.

$$F_G(H - H') = \frac{1}{\sqrt{2\pi}\,\sigma_G} e^{-(H-H')^2/2\sigma_G^2} \qquad (6)$$

where $H'(\theta,\varphi)$ is the field at resonance as indicated by the appropriate resonance condition. The quantity σ_G is referred to as the "dipolar width" and is one-half the peak-to-peak width of the derivative of the Gaussian function. Thus when dipolar effects are taken into account, the δ-function resonance conditions indicated in eq 3 and 4 become Gaussians of half-width σ_G.

In esr an additional source of broadening may be present, in the form of the exchange interaction.[74] The exchange interaction originates from Coulomb interactions between the electrons and from the Pauli exclusion principle. The single-crystal lineshape resulting when such an interaction is present can often be approximated by a normalized Lorentzian function defined by

$$F_L(H - H') = \frac{\sigma_L}{2\pi} \frac{1}{(H - H')^2 + \frac{1}{4}\sigma_L^2} \qquad (7)$$

where $\sigma_L/\sqrt{3}$ is the peak-to-peak width of the derivative of the Lorentzian function. In dilute paramagnetic systems, with small spin–spin interactions, the lineshape is determined by spin–lattice relaxation effects which are also characterized by a Lorentzian lineshape function.[75]

In nmr, there is an analogous "exchange interaction" which can result in a Lorentzian lineshape. This is the so-called electron-coupled or indirect interaction[76] resulting from the fact that a nucleus will tend to polarize the electrons near it, which will in turn alter the polarization of other nuclei in the system. In some cases, the indirect interaction can be greater than the ordinary dipole–dipole interaction.

When two or more independent Gaussian broadening mechanisms are present, the total linewidth is given by the square root of the sum of the squares of the component linewidths as defined in eq 6. For two or more independent Lorentzian mechanisms, the total linewidth is the sum of the component linewidths as defined in eq 7. When both Gaussian and Lorentzian mechanisms are present, the total linewidth is somewhere between the square root of the sum of the squares and the sum.[77] In this case the two effects may be treated simultaneously using a convolution integral provided σ_L and σ_G are both independent of orientation. The convolution of a Gaussian with a Lorentzian function is known as a Voigt function, which has the form

$$V(v) = \int_{-\infty}^{\infty} F_L(t) F_G(v - t)\, dt \qquad (8)$$

Both approximate expressions[78] and tables[79] of this function are available.

2. Exact Diagonalization of Hamiltonians

Several authors[80-83] have considered the situation where the electronic Zeeman and fine-structure terms of eq 1 are the same order of magnitude. Bowers and Owen[18] have discussed the case of $S = \frac{3}{2}$ where the ap-

plied magnetic field H is directed along one of the principal axes of the fine-structure tensor. This discussion is useful. because these directions generally correspond to singularities (shoulders and divergences) in the powder patterns as will be discussed below. In general, progress on this problem has proven possible only by the utilization of computer techniques. Griscom and Griscom[80] have diagonalized the fine-structure Hamiltonian along its principal axes on a computer assuming an isotropic g tensor for the case of $S = \frac{5}{2}$ and $E/D = \frac{1}{3}$. Barry,[81] Dowsing and Gibson,[82] and Aäsa[83] have extended these results for general E and D, and Aäsa[83] has also considered the "extra divergences" which sometimes arise in these powder patterns for fields corresponding to orientations not along one of the three principal axes of the fine-structure tensor. The data compiled in ref 83–89 apply to both Fe^{3+} and Mn^{2+} (neglecting hyperfine terms) and are quite useful for interpreting esr spectra in powders outside of the perturbation regime.[84] Examples will be presented in section IV and in Appendix III.

3. Calculation of Powder Patterns

The general nmr or esr resonance condition, whether it is obtained from perturbation theory, as in the case of eq 3 and 4 and the more complicated expressions of Appendix I, or from numerical diagonalization of the complete Hamiltonian, can be written formally as $H_m = H_m(\mu, \varphi)$ where $\mu = \cos \theta$ and m denotes the appropriate transition (for example, the $m \rightarrow m - 1$ nmr quadrupolar transition, the $M - 1 \rightarrow M$ esr fine-structure transition or the mth hyperfine component). The powder pattern is then the ensemble average of the resonance condition over all equally probable elements of solid angle $d\Omega = d\mu d\phi$ summed over all allowed transitions. Powder patterns were first considered in detail by Pake[1] and Sands.[85] A good discussion of several uncomplicated powder patterns is contained in an article by Ibers and Swalen.[86] An extension of the basic concepts of powder patterns to the case of vitreous materials is described by Taylor and Bray.[39]

The absorption at field H in the interval dH may be written as[87]

$$S(H)\, dH = \frac{1}{4\pi} \Sigma_m \int_H^{H+dH} I_m(\Omega)\, d\Omega(H_m) \tag{9}$$

The quantity $S(H)$ is termed a *shape function* or *powder pattern* and represents the normalized amplitude of the magnetic resonance signal at field H. Equation 9 is integrated over those elements of solid angle $d\Omega(H_m)$ such that $H < H_m < H + dH$, where H_m is the appropriate resonance condition. In general, $d\Omega$ is a multivalued function of H_m, there being more than one value of μ and φ for some resonance fields H_m.

The quantity $I_m(\Omega)$ is the transition probability for the mth component of the spectrum. The nmr $(m \rightarrow m - 1)$ and esr $(M - 1 \rightarrow M)$ transitions have probabilities proportional to $I(I + 1) - m(m - 1)$ and $S(S + 1) - M(M - 1)$, respectively, which are independent of Ω except in the case of strong g anisotropy. Thus, $I_m(\Omega)$ may be taken outside the integral sign in most cases, and the powder pattern for each magnetic resonance transition need only be multiplied by one of these factors before adding all patterns together to obtain the total absorption. In some cases (i.e., low temperature) it may also be necessary to consider the relative intensity of different hyperfine transitions (for different values of m), although in most instances these intensities are essentially constant (independent of m).

There are situations where all elements of solid angle

are not equally probable, such as magnetic resonance in liquid crystals.[88] In this case an additional factor $P(\Omega)$ must be added to eq 9 where $P(\Omega)\,d\Omega$ is the probability of a site being oriented in an element of solid angle $d\Omega$ at Ω. In general, eq 9 is a double integral with an additional factor $F(H - H')$ which accounts for the Gaussian and Lorentzian broadening mechanisms mentioned in the previous section. Although there are a few instances when $F(H - H')$ is orientationally dependent,[74,89,90] in most cases the angular dependence is unimportant in the calculation of powder spectra.[7] Thus the Gaussian and Lorentzian broadening mechanisms can almost always be taken outside of the integral sign in eq 9. The lineshape corrected for Gaussian and Lorentzian broadening is thus a convolution of the ideal shape function or powder pattern with the Gaussian, Lorentzian, or Voigt functions of eq 6, 7, and 8.

There are cases where the intensity of a single-crystal resonance depends on the orientation of the oscillating field H_1 relative to the principal axis system because the transition probability depends on this angle[71,73] as described in Appendix I. This orientation is denoted by ψ in Figure 1. In this case the factor $I_m(\mu, \varphi)$ in eq 9 must be replaced by $I_m(\mu, \varphi, \psi)$ and the integral over $d\psi$ performed. The ψ integration can be performed separately since H_m does not depend on ψ, i.e.

$$I_m(\mu, \varphi) = \frac{1}{2\pi} \int_0^{2\pi} I_m(\mu, \varphi, \psi)\, d\psi$$

It should be noted that the procedures described thus far pertain to the calculation of the power absorbed by a nuclear or paramagnetic spin, but eq 9 can equally well be used in the case of magnetic resonance dispersion signals. This particular problem has not been of general interest, but analytical expressions for the nmr dispersion signal in the presence of an axially symmetric Knight shift are available.[91]

An analytical expression for the powder pattern $S(H)$ is always possible when axial symmetry is present but is usually impossible in more complicated cases. For example, if the spectrum contains only one component (no sum over m in eq 9) which results from an axially symmetric term in the Hamiltonian, then eq 9 reduces to[92]

$$S(H) = \frac{1}{2} I \left(\frac{dH}{d\mu} \right)^{-1}_{\mu = \mu(H)} \tag{10}$$

In certain cases an analytical expression can be obtained even for complete asymmetry in the spin Hamiltonian. An example is the esr resonance in the presence of a completely anisotropic g tensor to be considered in the next section. In most cases an analytical expression is not possible, and one must resort to computer-based techniques if one is to obtain the expression for the powder pattern $S(H)$.

It is not always necessary to calculate the complete powder pattern either analytically or numerically. Often it is sufficient just to determine the locations of the principal features of the powder pattern, such as shoulders and divergences. The resonance condition can be thought of as a surface in μ, φ space. The singularities of the powder pattern arise at fields corresponding to critical points[36,37,43,93,94] of the function $H = H(\mu, \varphi)$, i.e., points where

$$\left(\frac{\partial H}{\partial \mu} \right)_{a,b} = \left(\frac{\partial H}{\partial \varphi} \right)_{a,b} = 0 \tag{11}$$

Here, (a,b) are the coordinates of the critical point. A saddle point in the surface at (a,b) indicates the pres-
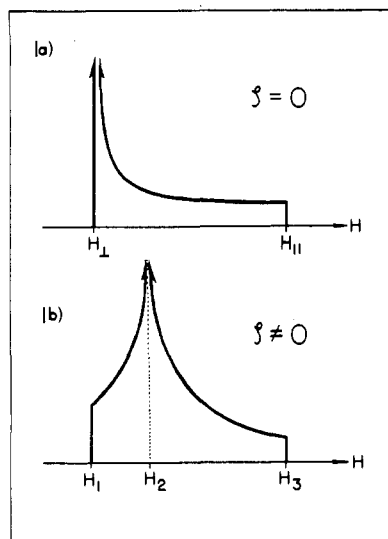
Figure 2. Powder patterns for (a) an axially symmetric g tensor and (b) a completely asymmetric g tensor. The parameter ζ is defined in section III, eq 33.

ence of a divergence in the powder pattern at the field $H = H(a,b)$, whereas a relative extremum will give rise to a shoulder or step at $H(a,b)$. The nature of the critical points can be determined by finding the sign of G, where

$$G(a,b) \equiv \left[\left(\frac{\partial^2 H}{\partial \mu \partial \varphi} \right)^2 - \left(\frac{\partial^2 H}{\partial \mu^2} \right) \left(\frac{\partial^2 H}{\partial \varphi^2} \right) \right]_{a,b} \quad (12)$$

If $G(a,b) > 0$, then (a,b) is the location of a saddle point and $H(a,b)$ corresponds to a divergence in the powder pattern. If $G(a,b) < 0$, then $H(a,b)$ is a shoulder or step in the powder pattern. In addition, the resonance field is a well-defined function only over the range $-1 \leq \mu \leq +1$. Because of this fact, there will be a shoulder in the powder pattern at $H(\pm 1, \varphi)$, even if there is no critical point corresponding to this value of μ.

In most cases, shoulders and divergences exist in the powder pattern at fields corresponding to the external field being aligned along one of the principal axes of the interaction tensor. However, at times "extra" divergences are encountered in the more complicated powder patterns, in which the corresponding field is not aligned along any principal axis. As mentioned above, Aasa[83] investigated these extra shoulders and singularities that appear in the powder pattern when he diagonalized the Zeeman plus fine structure esr Hamiltonian. The appearance of these "extra" singularities in powder patterns has been discussed by several authors.[36,37,43,95-97] Often these singularities appear when resolved hyperfine interactions with more than one nucleus are present.[96,97] Some examples will be described in section IV.

Because analytical solutions to most powder pattern problems are impossible, considerable effort[83,98-102] has been spent on numerical evaluations of eq 9, where the resonance field $H_m(\mu,\varphi)$ is obtained by exact diagonalization of the Hamiltonian. Lefebvre and Maruani[98,99] and Kopp and Mackey[100] have developed sophisticated numerical techniques. In the perturbation regime, computer methods have also proved quite effective.[39,103] In either case, the procedure consists of numerically summing the contributions to $S(H)$ over a grid in (μ,φ) space. The reader is referred to ref 39 and 98-103 for details concerning the available computer programs.

Even when closed-form expressions for $S(H)$ can be written down, they often have to be evaluated numerically.[34,72,86,104] In the two simple cases discussed in the

next section, computer techniques must be used when dipolar broadening is taken into account.[105-107] Numerical methods must also be used when the effects of statistical distributions of Hamiltonian parameters are considered in magnetic resonance experiments on glassy or amorphous materials,[39,103] or when the effects of motion alter the esr or nmr spectrum.[108]

4. An Example

An illustrative example of the calculation of powder patterns is the esr resonance condition of eq 3 including only the first term (the anisotropic g tensor). First, consider the case of axial symmetry in which $g_1 = g_2 = g_\perp$ and $g_3 = g_{\cdot\cdot}$. For constant microwave frequency ν_0, the resonance field is given by

$$H(\mu) = \frac{h\nu_0}{g\beta} = \frac{h\nu_0}{\beta} \frac{1}{\sqrt{g_\perp{}^2 - (g_\perp{}^2 - g^2)\mu^2}} \quad (13)$$

From eq 10 and 13 (assuming $g_\perp > g^{\cdot}$)

$$S(H) = \left[\frac{\beta g^3}{h\nu_0(g_\perp{}^2 - g_{\text{II}}{}^2)\mu} \right]_{\mu=\mu(H)} =$$

$$\frac{(h\nu_0)^2}{\beta^2 g_\perp \sqrt{g_\perp{}^2 - g_{\text{II}}{}^2 H^2} \sqrt{H^2 - (h\nu_0/g_\perp\beta)^2}} \quad (14)$$

for

$$\frac{h\nu_0}{g_\perp\beta} \leq H \leq \frac{h\nu_0}{g_{\text{II}}\beta}$$

$$S(H) = 0 \qquad \text{elsewhere}$$

The powder pattern described by eq 14 is shown in Figure 2a. There is a divergence at $H_\perp = h\nu_0/g_\perp\beta$ and a shoulder at $H = h\nu_0/g\beta$.

In case of complete anisotropy in the g tensor ($g_1 > g_2 > g_3$), the powder pattern can be expressed as[87]

$$S(H) = \frac{2}{\pi} \frac{H_1 H_2 H_3}{\sqrt{H^2 - H_1{}^2}\sqrt{H_3{}^2 - H_2{}^2 H^2}} K(k) \quad (H_3 \geq H \geq H_2)$$

$$S(H) = \frac{2}{\pi} \frac{H_1 H_2 H_3}{\sqrt{H_2{}^2 - H_1{}^2}\sqrt{H_3{}^2 - H^2 H^2}} K\left(\frac{1}{k}\right)$$

$$(H_2 \geq H \geq H_1) \quad (15)$$

$$S(H) = 0 \qquad \text{elsewhere}$$

where

$$k^2 \equiv \frac{(H_2{}^2 - H_1{}^2)(H_3{}^2 - H^2)}{(H^2 - H_2{}^2)(H_3{}^2 - H_1{}^2)};$$

$$H_1 \equiv \frac{h\nu_0}{g_1\beta}, \; H_2 \equiv \frac{h\nu_0}{g_2\beta}, \; H_3 \equiv \frac{h\nu_0}{g_3\beta}$$

and $K(k)$ is the complete elliptic integral of the first kind.

$$K(k) = \int_0^{\pi/2} \frac{dx}{\sqrt{1 - k^2 \sin^2 x}}$$

$$K(0) = \pi/2 \qquad K(1) = \infty$$

This powder pattern is illustrated in Figure 2b. There is a divergence at H_2 and shoulders at H_1 and H_3. The two powder patterns of Figure 2 also apply to the description of magnetic shift effects in nmr[76,109] as was pointed out earlier.

The locations of the singularities of the above powder pattern are obtained by substituting eq 15 into eq 11 to obtain two simultaneous equations for the critical points. These equations are[43]

$$-\frac{h\nu_0}{g^3\beta}(g_3{}^2 - g_1{}^2 \sin^2\varphi - g_2{}^2 \cos^2\varphi)\mu = 0$$

$$-\frac{h\nu_0}{g^3\beta}(g_1{}^2 - g_2{}^2)(1 - \mu^2)\sin\varphi \cos\varphi = 0$$

(16)

Equations 16 imply that $\mu = 0$ and either $\sin \varphi = 0$ or $\cos \varphi = 0$. Thus two singular points in the powder pattern are located at $H_1 = h\nu_0/g_1\beta$ and $H_2 = h\nu_0/g_2\beta$. Using eq 12, H_1 is found to be a shoulder and H_2 a divergence. In addition, there is a shoulder in the powder pattern at $H_3 = h\nu_0/g_3\beta$ corresponding to the $\mu = \pm 1$ "cutoff" in the resonance field.

Coope[94] has extended the above analysis of the singularities of a powder pattern characteristic of an anisotropic g tensor to derive relative peak heights of the derivative spectrum assuming a Gaussian convolution function with σ_G much smaller than the width of the powder pattern. This technique for finding the singularities of powder patterns has been applied to more complicated resonance conditions by several authors.[36,43]

C. Extracting Parameters from Powder Spectra

It is tempting to try to provide a general formula or procedure for extracting experimental parameters from powder patterns. Unfortunately, any detailed discussion would be counterproductive because of the varied nuances of powder spectra. There is no substitute for a good understanding of the specific Hamiltonian which is appropriate to the problem at hand. We therefore confine our attention in this section to a discussion of several examples which are illustrative of general problems and pitfalls often encountered in magnetic resonance spectra of powders.

Experimental magnetic resonance spectra are most often observed as derivatives of power absorption due to the method of detection used. The problem of extracting Hamiltonian parameters from the easily measurable features of derivative spectra is thus of great importance. Unfortunately, prominent features of derivative spectra (peak positions and baseline crossings) do not in general correspond to readily determined functions of the Hamiltonian parameters, unlike the situation discussed above for the singular features of powder patterns. The introduction of dipolar and relaxation broadening to the powder pattern and the effects of differentiation combine to make prominent features of the spectrum complex functions of both the Hamiltonian parameters and the Gaussian or Lorentzian broadening linewidths.

The problem is especially acute for values of the Gaussian or Lorentzian linewidth σ on the order of the spread in the powder pattern Δ $(\Delta/2\sigma \lesssim 1)$. In this case, all singularities in the powder pattern are masked and a single derivative absorption line appears.

Several authors have attacked this problem. When the Hamiltonian involves only an axial g tensor (or magnetic shift tensor, Pake doublet, quadrupole satellite transition, or fine-structure satellite transition), the interaction is dominated by the $(3 \cos^2 \theta - 1)$ term of eq 4. In this case the absorption spectrum in the presence of Lorentzian broadening can be described in closed form as an elliptic integral of the first kind.[86] Only an approximate expression can be given for the effect of Gaussian broadening on this type of axial powder pattern.[110] If the g tensor is completely anisotropic, then the powder pattern can be calculated exactly as described above, but Lorentzian broadening can be included only approximately[111] without resorting to numerical evaluation.

When the anisotropy in the powder pattern is large in comparison to the Gaussian or Lorentzian linewidth $(\Delta/2\sigma \gg 1)$, then shoulders in the powder pattern appear in the derivative spectrum as individual "absorption lines."[112] The width of these absorption lines is a measure of σ. This situation holds for any Hamiltonian for which the resulting powder pattern has a shoulder. Diver-

gences in the powder pattern do not have any simple relationship to the derivative spectra even when the Gaussian or Lorentzian broadening is small.[113,114] An empirical relation for the shift of the derivative peak relative to the position of the divergence in the powder pattern[113,114] has proved useful in some cases.

The general problem of relating peaks in derivative spectra to Hamiltonian parameters for arbitrary values of $\Delta/2\sigma$ has been investigated numerically by several authors.[115-117] The nmr powder derivative spectrum in the presence of quadrupolar effects $(m = \frac{1}{2} \leftrightarrow m = -\frac{1}{2}$ transition) and Gaussian broadening has been studied for axial symmetry[115] and for $\eta \neq 0$.[116] The derivative spectrum for an anisotropic g tensor (or magnetic shift tensor, etc.) with either Gaussian or Lorentzian broadening has also been investigated systematically.[117] Some results of these systematic studies are presented in the next section.

Several least-squares fitting procedures have been published which are applicable to simple powder pattern calculations.[86,118-120] Most of these procedures apply only to a single component powder pattern with Gaussian or Lorentzian broadening which is at least of the order of the width of the powder pattern.[119,120] Pedersen[118] has developed a least-squares procedure to analyze nmr Pake doublets in powders. Ibers and Swalen[86] have written a least-squares computer program to fit simple powder spectra for which an analytic expression (or an integral) can be obtained. As discussed above an analytic expression is most often not available, so that trial and error fitting using numerically evaluated derivative spectra remains the procedure most often employed.

Evaluation of the errors in the Hamiltonian parameters calculated for a complicated derivative spectrum is also an involved procedure. Usually no simple relationship exists which connects the degree of fit of simulated (or calculated) to experimental derivative spectra with the accuracy of the Hamiltonian parameters. "Visual" accuracy of the fit between simulated and experimental spectra often has little correlation with the accuracy to which the Hamiltonian parameters are determined.

This situation is illustrated in Figure 3 by two esr spectra each containing axially symmetric, second-order hyperfine, and electronic Zeeman interactions. Spectrum 3a is representative of an electron trapped in an oxygen vacancy surrounding what was formerly an NbO_6 octahedron in $Na_2O-Nb_2O_5-SiO_2$ glasses.[121] This spectrum consists of ten hyperfine lines since the spin of ^{93}Nb is $\frac{9}{2}$. The disagreement in the central region of the spectrum is due to other esr spectra superimposed on this broad line.[121] Error estimates were obtained[39] using trial computer simulations with slight changes in the optimum spin-Hamiltonian parameters, one at a time, while noting the effect on the simulated derivative spectrum. Error estimates are determined by the points at which there is a noticeable deterioration in the fit between the simulated and the experimental lines. The maximum error in the g values is <0.03% and in the A values is <1%.

Figure 3b displays the V_k-type centers found in alkali halide–alkali oxide–boron oxide glasses.[96] This spectrum is the sum of the hyperfine interactions due to three individual environments for the V_k-type center—a hole interacting with two ^{35}Cl nuclei, with two ^{37}Cl nuclei, and with one ^{35}Cl and one ^{37}Cl nucleus. The relative intensities due to these three environments are dictated by the relative probabilities that a hole is situated at each of the three, which is in turn controlled by the natural abundances of ^{37}Cl and ^{35}Cl. (A more complicated resonance condition than the one of eq 3 is necessary in this
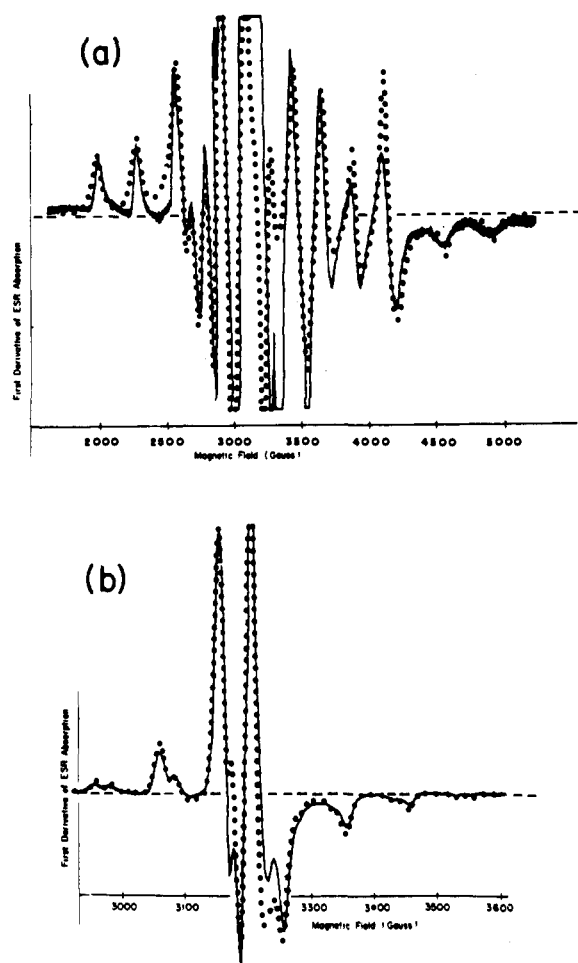
Figure 3. X-Band experimental (solid curves) and calculated (filled circles) esr spectra observed (a) in γ-irradiated Nb_2O_5-Na_2O-SiO_2 glasses at 77°K and (b) in γ-irradiated NaCl-Na_2O-B_2O_3 glasses at 300°K (after ref 39).

case.[96] Although the qualitative agreement between experimental and simulated traces for the V_k-type centers is equally as good as that obtained for the Nb-e center, the errors involved in some of the spin–Hamiltonian parameters obtained by trial simulations are much greater for the V_k-type centers. Because this spectrum is relatively insensitive to changes in parameters pertinent to the perpendicular region, errors in $g_\perp$ are 0.2% and in $A_\perp$ 30%. Thus, visual agreement between calculated and experimental spectra is not always a good estimate of the accuracy in determining the Hamiltonian parameters.

Changing several variables can often be effective in determining the Hamiltonian parameters. Perhaps the most useful variable is the radio- or microwave frequency. In addition, when the Hamiltonian contains an interaction with a nuclear spin (nmr or hyperfine interactions in esr), the nuclear isotope can sometimes be used as an additional variable.

Consider the esr spectrum observed in potassium borate ceramic $(xK_2O\cdot(1 - x)B_2O_3, 0.5 < x < 1)^{122}$ as illustrated in Figure 4. This esr response results from a paramagnetic $BO_3{}^{2-}$ radical in the material.[122] Enriching the ceramic with either ^{11}B or ^{10}B changes the esr spectrum through the hyperfine interaction of the paramagnetic center with the boron nucleus (eq 3). Boron-10 has a spin of 3 and exhibits seven hyperfine components (Figure 4b) in contrast to four for ^{11}B (Figure 4a). In fitting the esr spectra for these two cases, all of the parameters for the ^{10}B-enriched spectrum, including the convolution
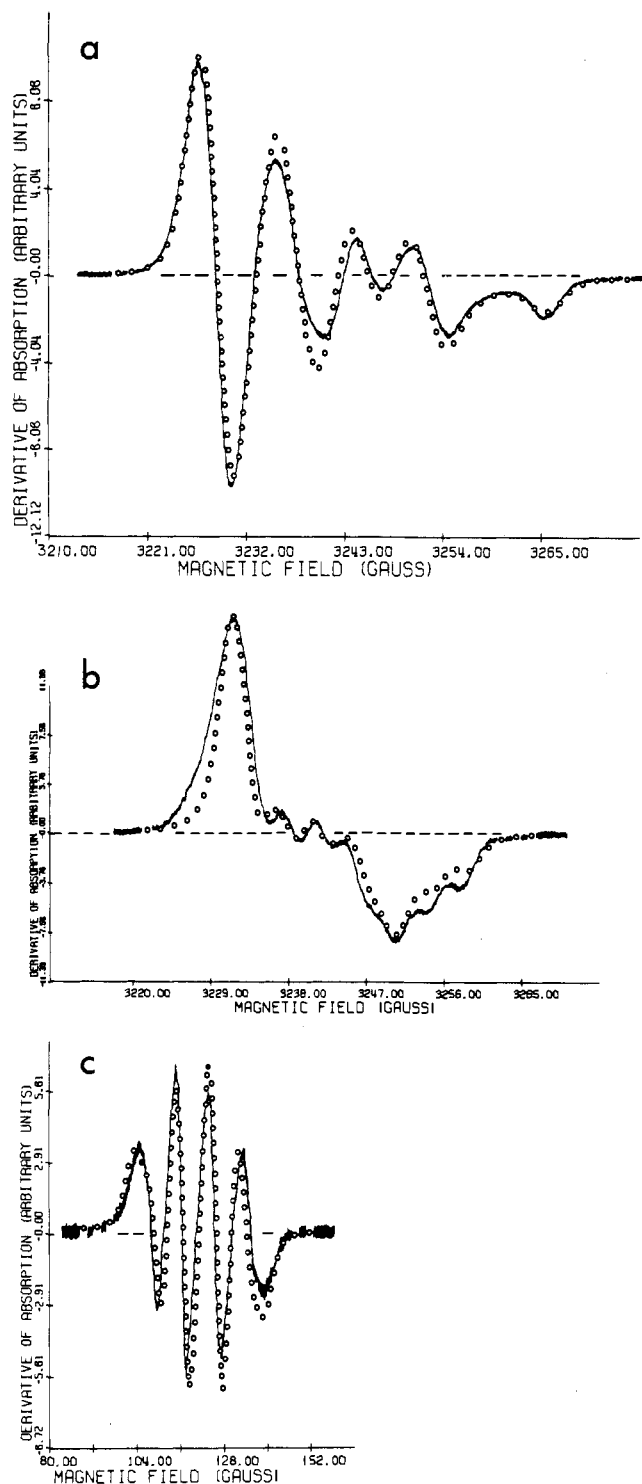

Figure 4. Esr spectra observed at 77°K in potassium borate ceramic (a) at 9 GHz, enriched in ^{11}B, (b) at 9 GHz, enriched in ^{10}B, and (c) at 0.34 GHz, enriched in ^{11}B.

linewidths, are dictated by the choice of the parameters for the ^{11}B-enriched case. The g tensor is unchanged by the substitution of ^{10}B for ^{11}B, but the hyperfine components differ by a factor of the ratio of the nuclear g factors for ^{11}B and ^{10}B.

The effect of changing the frequency is illustrated in Figure 4c. The spread in powder pattern features due to the Zeeman interaction decreases linearly with frequency (eq 3) while the hyperfine splitting remains constant. At 0.34 GHz (Figure 4c) the spectrum is dominated by the hyperfine terms, but at 9.1 GHz the effects due to the anisotropic g tensors are evident (Figure 4a). Consistent
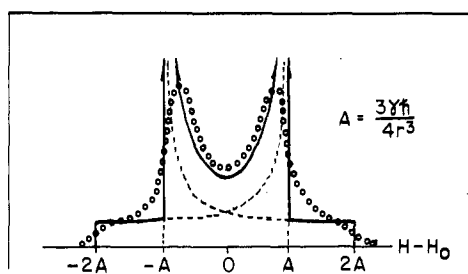
Figure 5. Pake doublet powder pattern for a pair of identical nuclei. The dashed lines show the individual components while solid lines indicate the sum of the two components. The powder pattern corrected for unresolved dipolar effects is shown by the open circles.

spin-Hamiltonian parameters are, of course, used in fitting all three spectra of Figure 4.

Sometimes it is advantageous to correct for instrumental effects (other than differentiation). Corrections for the effects on powdered lineshapes of magnetic field modulation are discussed in Appendix II. Also considered in this Appendix are derivatives of dispersion signals at high power which can under appropriate conditions yield lineshapes similar to absorption spectra.

III. Nuclear Magnetic Resonance

A. Introduction

In this section, the powder spectra of particular interest in nmr are considered. No attempt has been made to review all applications of nmr in powders. Rather the various types of spectra arising from particular interactions of a nucleus with its magnetic and electric environment are discussed, and representative examples are given. The Pake doublet problem was one of the first applications of powder patterns to nmr, and this is discussed in some detail in section B. The nuclear quadrupole interaction is perhaps the most studied effect in nmr in powders, and powder patterns in the presence of this effect are discussed in section C. In certain special cases, both nuclear dipole and nuclear quadrupole effects are important, and these are discussed in section D. The effects of magnetic shifts on powder spectra are discussed in section E. There are certain situations in which magnetic shift and nuclear quadrupolar effects are both important, and these are considered in section F. Section G describes some miscellaneous effects such as diffusion and molecular rotation. Finally, section H is devoted to a discussion of the spinning sample technique.

B. Dipole–Dipole Interactions between Pairs of Nuclei—The "Pake Doublet"

The Pake doublet[1,5,7,9] is the nmr spectrum that arises from the dipole–dipole interactions between the members of a pair of identical nuclei, each with $I = \frac{1}{2}$. If the dipole–dipole interaction is treated as a first-order perturbation of the nuclear Zeeman energy, then the resonance condition is

$$h\nu = \gamma \hbar H \pm \frac{3}{4} \frac{\gamma^2 \hbar^2}{r^3} (1 - 3\mu^2) \qquad (17)$$

where r is the distance between nuclei, θ is the angle between the line joining the two nuclei and the external field, and $\mu = \cos \theta$. There are two resonance lines, at the field locations

$$H = H_0 \pm \frac{3}{4} \frac{\gamma \hbar}{r^3} (1 - 3\mu^2) \qquad (18)$$

where $H_0 = 2\pi\nu_0/\gamma$ and ν_0 is the fixed radiofrequency.

Since the resonance field has axial symmetry (depends only on θ), the powder pattern for each component can be calculated by using eq 10. The powder patterns for the components with the positive and negative signs in eq 18 are given, respectively, by[7]

$$S_+ (H) = \frac{1}{6}(\gamma\hbar/r^3)^{-1/2}\left(H_0 - H + \frac{3}{4}\frac{\gamma\hbar}{r^3}\right)^{-1/2} \qquad (19a)$$

for

$$H_0 - \frac{3}{2}\frac{\gamma\hbar}{r^3} \le H \le H_0 + \frac{3}{4}\frac{\gamma\hbar}{r^3}$$

$$S_- (H) = \frac{1}{6}(\gamma\hbar/r^3)^{-1/2}\left(H - H_0 + \frac{3}{4}\frac{\gamma\hbar}{r^3}\right)^{-1/2} \qquad (19b)$$

for

$$H_0 - \frac{3}{4}\frac{\gamma\hbar}{r^3} \le H \le H_0 + \frac{3}{2}\frac{\gamma\hbar}{r^3}$$

where $S_+ (H)$ and $S_- (H)$ vanish outside the defined ranges. The normalization of each powder pattern has been chosen so that the total area under both powder patterns is unity. The composite powder pattern is shown in Figure 5. The dotted lines indicate the individual components, and the solid line indicates the sum of the two components. The individual components are mirror images of each other, about the field H_0. There are divergences at the fields $H_0 \pm (3/4)(\gamma\hbar/r^3)$, and shoulders at the locations $H_0 \pm (3/2)(\gamma\hbar/r^3)$.

The utility of this interaction for studying solids lies in the dependence of the width of the powder pattern on the distance r between the two nuclei in the pair. In addition, the shape and width of the powder pattern are independent of the applied frequency ν_0, and help to identify dipole–dipole effects in a magnetic resonance spectrum.

Interactions between neighboring pairs of spins will broaden the theoretical powder pattern, so that the true absorption spectrum will not be as sharp. This broadening is accounted for by convoluting the theoretical powder pattern $S_+ (H) + S_- (H)$ with a broadening function as described in section II. The true absorption spectrum is indicated by the open circles in Figure 5.

A technique that has often been used to evaluate the Pake doublet powder pattern is that of the second moment, defined by[7]

$$M_2 = \int_{-\infty}^{\infty} (H - H_0)^2 (S_+ (H) + S_- (H)) \, dH =$$

$$\frac{3}{5} \frac{\gamma^4 \hbar^2 I(I + 1)}{r^6} \qquad (20)$$

A measurement of the second moment of the resonance lineshape will give a measure of r, the separation of the two nuclei in the pair. One difficulty with this technique is that errors are introduced by the presence of interactions between neighboring pairs. These interpair interactions tend to increase the second moment, so that the second moment of the lineshape is in reality a more complicated expression containing M_2 and m_2, where m_2 is the contribution to the second moment from interactions between pairs.[76] Since both of these second moments M_2 and m_2 are frequency independent, complicated procedures such as isotopic replacement must be used to determine separately M_2 and m_2.[76]

Another commonly used technique is to compare the locations of easily measured features in the experimental spectrum to the theoretical powder pattern. This technique, however, can result in systematic errors, since there is no study available which relates powder pattern features to features of the broadened lineshape. An earlier review[123] lists studies of the Pake doublet (in both
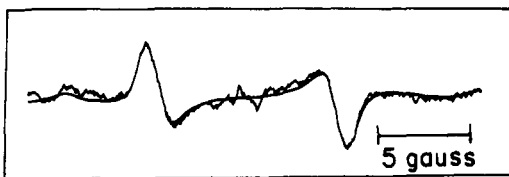
Figure 6. Computer-simulated Pake-doublet spectrum (smooth curve) superimposed on an experimental proton spectrum of potassium oxalate monohydrate (after ref 118).

single crystal and powdered materials) up to the year 1961.

Recently, computer simulation techniques have been used to study the Pake doublet lineshape.[118,124,125] An example is shown in Figure 6, which shows a lineshape computed for appropriate parameters superimposed on an experimental proton spectrum for potassium oxalate monohydrate. In both cases, the derivative of the absorption spectrum is shown. The two strong lines are a result of the divergences in the powder pattern, whereas the two "bumps" in the wings of the spectrum are due to the shoulders in the powder pattern.

When a nuclear pair consists of two nonidentical nuclei, with $I_1 = I_2 = \frac{1}{2}$ slightly different results are obtained. The powder pattern has exactly the same shape as that for the case of two identical nuclei, but divergences occur at the fields $H_0 \pm \gamma_2 \hbar / 2r^3$ and shoulders at the fields $H_0 \mp \gamma_2 \hbar / r^3$, where $H_0 = 2\pi\nu_0 / \gamma_1$, and it is assumed that the nmr spectrum of nucleus 1 is being observed.

Systems in which both direct and indirect dipole–dipole interactions are present have been studied.[69,70] Also, systems with three identical nuclei have been discussed.[65] In the latter case, the transition probability depends on θ, which must be taken into account when the powder pattern is computed. An exact analytical solution can be obtained for these cases,[65] but the systems are specialized and not of general applicability.

C. Nuclear Quadrupole Interaction

For a variety of reasons, the nmr powder spectra for the nuclear quadrupole interaction have been studied more extensively than those for any other nmr interaction. The magnitude of the quadrupole interaction parameters for many different nuclei in diverse materials are such that well-resolved powder lineshapes can often be obtained. In addition, the interaction is sometimes frequency dependent, a fact which facilitates the separation of quadrupolar effects from those of other interactions. Quite often the quadrupolar parameters can be simply related to structural features of the solid being studied.

Quadrupolar effects through second order in perturbation theory have been considered by a number of reviews.[5,7,9,35] The resonance condition for the $m \leftrightarrow m - 1$ transition correct to second order in the nuclear quadrupolar interaction is given by eq 4. When the nuclear spin I is half-integral, there is a central ($m = \frac{1}{2} \leftrightarrow m = -\frac{1}{2}$) transition that is affected only by second-order quadrupolar terms, flanked by "satellites" that are affected by both first- and second-order terms.

1. Central Transition ($m = \frac{1}{2} \leftrightarrow m = -\frac{1}{2}$)

The resonance frequency for the second-order quadrupolar interaction for the central ($m = \frac{1}{2} \leftrightarrow m = -\frac{1}{2}$) transition is given by eq 4 with $m = \frac{1}{2}$.[36,37] The resonance frequency to terms in third order in the quadrupolar interaction has been calculated.[48] Note that terms of first order in ν_Q do not appear for the central transition.
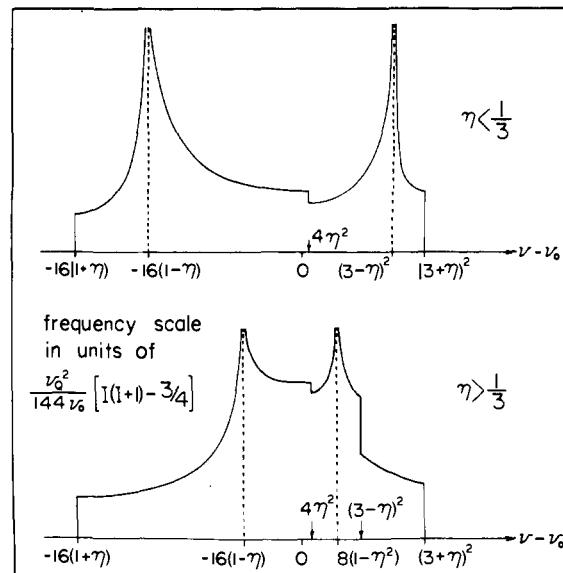

Figure 7. Powder pattern for the $m = \frac{1}{2} \leftrightarrow m = -\frac{1}{2}$ transition broadened by second-order quadrupole effects. The locations of the divergences and shoulders are indicated. There are two distinct cases, $\eta < \frac{1}{3}$ and $\eta > \frac{1}{3}$ (after ref 116).

An exact analytical expression for the powder pattern in this case has not been given, but the locations of the shoulders and divergences have been determined by use of the technique outlined in section II.[36,37] These locations are shown in Figure 7. This figure is drawn assuming constant magnetic field H_0 with frequency being swept. The results for fixed frequency (sweeping H) are identical to first order as discussed in section E below. Numerical methods have been used to study the lineshape in detail.[115,116]

The expressions for the locations of the divergences and the step on the high-frequency side of the powder pattern depend on whether the electric field gradient asymmetry parameter is less than or greater than $\frac{1}{3}$. For all values of η, the total width of the powder pattern is given by

$$\Delta_Q = \frac{\nu_Q^2 [I(I+1) - \frac{3}{4}]}{144\nu_0}(\eta^2 + 22\eta + 25) \qquad (21)$$

The relative positions of the spectral features are determined by η, whereas the coupling constant, which is proportional to ν_Q, determines the magnitude of the splitting between features. When $\eta = 0$, that is, when the electric field gradient at the nuclear site has axial symmetry, the high- and low-frequency shoulders merge with the divergences, and the powder pattern can be calculated exactly.[35] As η increases two shoulders move outward while the two divergences move toward one another and merge, when $\eta = 1$, at the position corresponding to the Larmor frequency.

Systematic studies of the dipolar-broadened derivative spectrum arising from the second-order quadrupolar powder pattern have been published.[115,116] Figure 8 shows representative computer-evaluated derivative spectra for various values of η and the dimensionless parameter $\Delta_Q / 2\sigma_G$, where $2\sigma_G$ is the width between derivative extrema of the Gaussian function (eq 6) used to simulate the effects of dipolar broadening. This ratio provides a convenient measure of the relative strengths of the dipolar and quadrupolar interactions, and it is inversely proportional to ν_0.

Generally, as $\Delta_Q / 2\sigma_G$ increases, more structure appears in the derivative spectrum. For large values of $\Delta_Q / 2\sigma_G$, one can determine the quadrupolar parameters
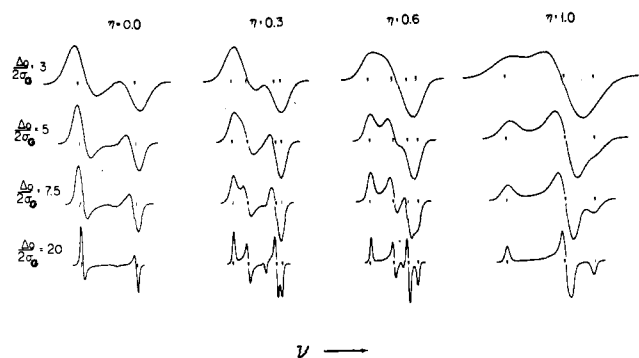
Figure 8. Computer-evaluated derivative spectra for the $m = \frac{1}{2}$ $\leftrightarrow m = -\frac{1}{2}$ transition broadened by second-order quadrupolar effects for various values of $\Delta_Q/2\sigma_G$ and η where these parameters are defined in the text (after ref 116).
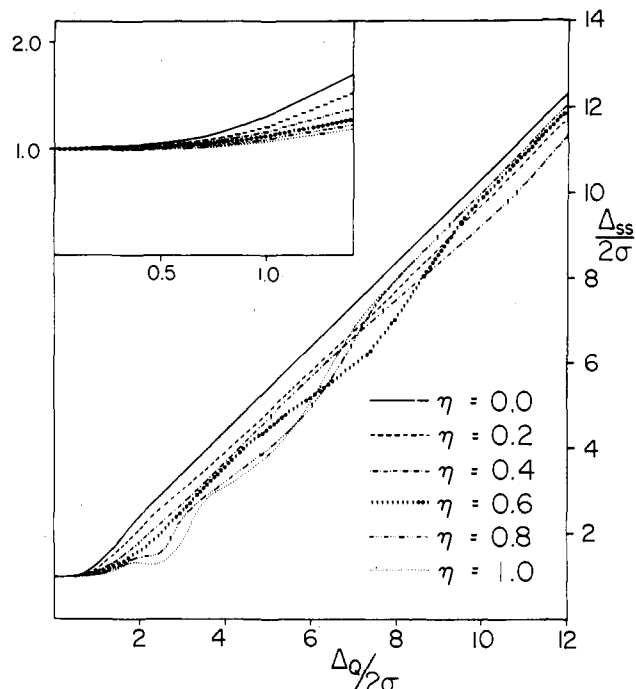

Figure 9. Computer-evaluated peak-to-peak normalized line width $\Delta_{ss}/2\sigma_G$ plotted as a function of $\Delta_Q/2\sigma_G$ (after ref 116).

Figure 10. Computer-evaluated derivative spectra for three combinations of e^2qQ/h and η superimposed on several ^{11}B nmr spectra obtained from polycrystalline $Li_2O \cdot 2B_2O_3$ at $\nu_0 = 16.000$ MHz. In all cases $\sigma_G = 2.4$ kHz. The strong central resonance is from a second ^{11}B site which does not experience a second-order quadrupole interaction and has been driven off scale (after ref 116).

with precision by comparing the experimental spectrum to computer-simulated lineshapes (ref 37, 39, 43, 46, 115, 116, 126–133). The reader is referred to a number of more recent studies which illustrate the application of nmr measurements of the second-order quadrupolar interaction to polycrystalline and glassy materials (ref 37, 39, 43, 46, 67, 115, 116, 126–145).

It is useful to consider the dependence on $\Delta_Q/2\sigma_G$ of the dimensionless ratio $\Delta_{ss}/2\sigma_G$, where Δ_{ss} is the distance between the outermost derivative extrema of the spectrum.[115,116] This dependence is illustrated in Figure 9 for various values of η. In principle, e^2qQ/h, η, and σ_G can be obtained from measurements of the frequency dependence of the linewidths of spectra using Figure 9. However, the method is a very insensitive measure of η, and only a rough estimate of the parameters can be obtained by this means unless there is some additional evidence for the precise value of the asymmetry parameter.

Examples of computer-based measurement techniques are shown in Figures 10 and 11. Figure 10 shows examples of computed derivative spectra superimposed on experimental B^{11} spectra from lithium diborate. The strong resonance driven off the recorder scale is due to B^{11} at a site in the crystal which does not experience a strong quadrupole interaction. The remaining lineshape is a sec-
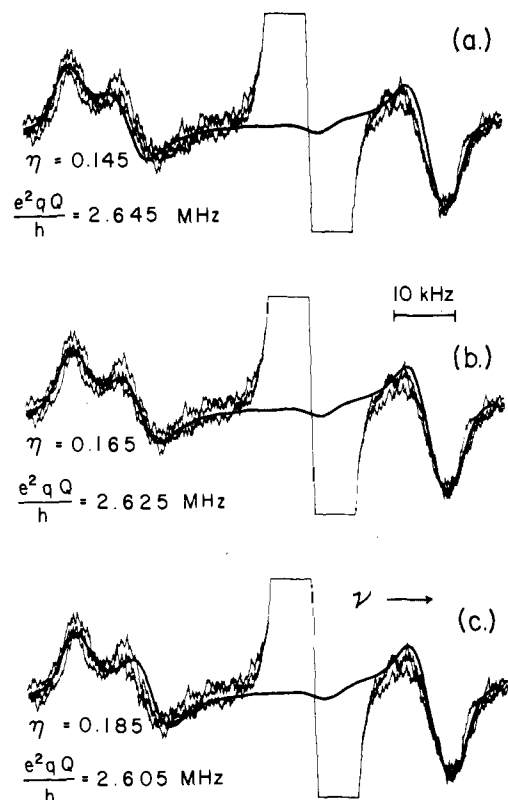
ond-order broadened central transition with small asymmetry parameter. The spectrum is highly sensitive to small changes in the quadrupole parameters and illustrates the high precision sometimes possible with powdered samples. Figure 11 shows the well-resolved spectrum observed in sodium niobate where η is large.[46]

Considerable care must be taken in using the values of the quadrupole coupling constant published before the advent of computer simulation. Prior to the mid-1960's, most authors assumed that the asymmetry parameter η was equal to zero and then measured either the width of the derivative lineshape or the frequency dependence of this linewidth. The systematic errors that can be introduced by unjustified assumptions of zero asymmetry parameter have been discussed by Kriz and Bray.[126]

2. "Satellite" Transitions ($m \neq \frac{1}{2}$)

For the nmr "satellite" transitions of a nucleus with a half-integral spin, the resonance condition is given by eq 4. In this case, terms in ν_Q to both first and second order appear. However, in most cases only terms to first order in ν_Q (second term in eq 4) are required for the discussion of satellite transitions.

In first order, the powder patterns for the satellite transitions can be calculated exactly, both for zero and non-zero asymmetry parameter η. The reader is referred to the review by Cohen and Reif[35] for the details of the calculation, which are quite similar to those outlined in section II. As in most powder pattern analyses, it is important to determine the location of the principal features of the powder pattern. There is a divergence at the frequency

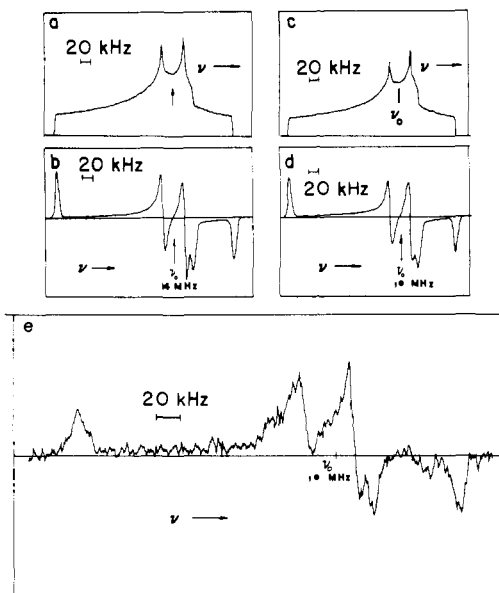$$\nu_d = \nu_0 + \frac{1}{4}\nu_Q(2m - 1)(1 - \eta) \qquad (22)$$

Figure 11. Computer-evaluated powder pattern (a) and derivative spectrum (b) of $m = \frac{1}{2} \leftrightarrow m = -\frac{1}{2}$ transition for ^{93}Nb ($I = \frac{9}{2}$, $e^2qQ/h = 19.7$ MHz, $\eta = 0.82$, $\sigma_G = 3.7$ kHz) in polycrystalline NaNbO$_3$ at 300°K. Central portion of computer-evaluated powder pattern (c) and derivative spectrum (d) of $m = \frac{1}{2} \leftrightarrow m = -\frac{1}{2}$ and $m = \pm\frac{3}{2} \leftrightarrow m = \pm\frac{1}{2}$ transitions in NaNbO$_3$ powder. (e) Experimental derivative spectrum in NaNbO$_3$ powder (after ref 46).

and two shoulders at the locations

$$\nu_s = \nu_0 + \frac{1}{4}\nu_Q(2m - 1)(1 + \eta) \qquad (23)$$

$$\nu_s = \nu_0 - \frac{1}{2}\nu_Q(2m - 1) \qquad (24)$$

It is apparent from these equations that the central transition ($m = \frac{1}{2} \leftrightarrow -\frac{1}{2}$) is unaffected in first order by the nuclear quadrupole interaction.

Figure 12 shows the first-order powder patterns for the $m = \frac{3}{2} \leftrightarrow \frac{1}{2}$ and $m = -\frac{1}{2} \leftrightarrow -\frac{3}{2}$ transitions. The magnitude of the nuclear spin I is included in the quantity ν_Q, which acts as a scale factor. The first-order powder patterns for the $m \leftrightarrow m - 1$ and $-(m - 1) \leftrightarrow -m$ transitions are mirror images of each other, about $\nu = \nu_0$. For nuclei of integral spin I, there are $2I$ such powder patterns. For half-integral spin, there are $2I - 1$ satellites flanking a single central ($m = \frac{1}{2} \leftrightarrow -\frac{1}{2}$) line which is unshifted in first order.

No systematic study of dipolar broadening comparable to that for the second-order quadrupolar-broadened central transition has been carried out for the $m \neq \frac{1}{2}$ powder pattern. A recent study by Creel and Barnes[146] discusses a computer evaluation of $\eta \neq 0$ first-order satellites for different values of dipolar broadening. The effects of dipolar broadening can be discussed in terms of the anisotropic magnetic shift interaction, and the results can be carried over to the present situation by a simple change in the scale factor determining the width of the powder pattern. The width of the first-order quadrupolar powder pattern is independent of ν_0 while the magnetic shift linewidth is proportional to ν_0. The reader is referred to section E of this review which deals with the anisotropic magnetic shift.

Second-order effects also influence the transitions for $m \neq \frac{1}{2}$, but only the case of $\eta = 0$ has been considered in detail. The discussion is confined to that case. The resonance condition is obtained from eq 4 with $\eta = 0$. Again, it is most useful to discuss the powder pattern in terms of the locations of the shoulders and singularities.
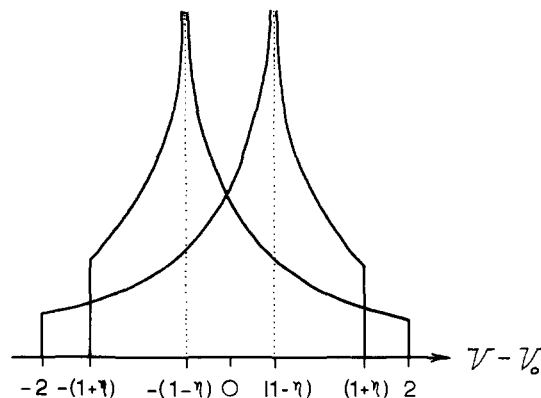

Figure 12. Powder patterns for the $m = \frac{3}{2} \leftrightarrow m = \frac{1}{2}$ and $m = -\frac{1}{2} \leftrightarrow m = -\frac{3}{2}$ transitions broadened in first order by the quadrupolar interaction. The frequency is expressed in units of $\nu_Q/2$.

The divergence found in the first-order calculation (eq 22 with $\eta = 0$) is shifted slightly to

$$\nu_d = \nu_0 + \frac{\nu_Q}{4}(2m - 1) - \frac{\nu_Q^2}{16\nu_0}\{[I(I + 1) - \frac{3}{4}] - 3(m - \frac{1}{2})^2\} \qquad (25)$$

while the location of the shoulder is unaffected and lies at

$$\nu_s = \nu_0 - \frac{\nu_Q}{2}(2m - 1) \qquad (26)$$

Note that the separation of the divergences at ν_d for the mirror image powder patterns for the $m \leftrightarrow m - 1$ and $-(m - 1) \leftrightarrow -m$ transitions is independent of second-order effects and provides a convenient measure of the coupling constant.

An additional complication arises from the presence of an "extra" divergence, the term "extra" indicating a feature in the powder pattern that is present only for special values of the experimental parameters (see section II). This extra divergence appears at the frequency

$$\nu_{ed} = \nu_0 + [\nu_09b^2 - 3\nu_Qb(a - 5b^2) + \nu_Q^2(a - 6b^2)/\nu_0](9a - 15b^2) \qquad (27)$$

where

$$a = I(I + 1) - \frac{3}{4} \qquad b = (m - \frac{1}{2})$$

This divergence appears only when the quantity $2\nu_0/\nu_Q$ lies between A_1 and A_2 where

$$A_1 \equiv (-27b^2 + 5a)/6b$$

$$A_2 \equiv (24b^2 - 4a)/6b$$

The signs of A_1 and A_2 are opposite for all values of I and m, and the detailed behavior of the extra divergence will depend on which of the two quantities is positive. When A_1 is positive, the extra divergence will split from the divergence at ν_d and move toward ν_s as ν_0 is lowered. When A_2 is positive, the extra divergence first appears at ν_s and moves toward ν_d as ν_0 is lowered. In an intermediate frequency range the shoulder at ν_s will change smoothly from a finite step to an infinite singularity as ν_0 is decreased. The reader is referred to the paper by Barnes, et al., for the details.[147] Numerous additional papers contain discussions of first-order quadrupolar powder patterns (ref 134, 135, 143–145, 148–157).

As with the second-order lineshape for the central transition, considerable caution must be exercised in

TABLE I. ^{11}B Nmr Frequencies and Relative Intensities of $m = \frac{1}{2} \leftrightarrow m = -\frac{1}{2}$ Transitions in BF_3 Molecule

| | | Magnetic quantum numbers of fluorine nuclei | | | Rel |
Frequency		m_1	m_2	m_3	intensity
$\Delta\nu_1 = A(1 - 9\mu^2)(1 - \mu^2) - (3C/4)(1 - 3\mu^2)$		$-\frac{1}{2}$	$-\frac{1}{2}$	$-\frac{1}{2}$	1
$\Delta\nu_2 = A(1 - 9\mu^2)(1 - \mu^2) - (C/4)(1 - 3\mu^2) + (3C/2)(1 - \mu^2) \cos 2\alpha$		$\frac{1}{2}$	$-\frac{1}{2}$	$-\frac{1}{2}$	3
$\Delta\nu_3 = A(1 - 9\mu^2)(1 - \mu^2) + (C/4)(1 - 3\mu^2) - (3C/2)(1 - \mu^2) \cos 2\alpha$		$-\frac{1}{2}$	$\frac{1}{2}$	$\frac{1}{2}$	3
$\Delta\nu_4 = A(1 - 9\mu^2)(1 - \mu^2) + (3C/4)(1 - 3\mu^2)$		$\frac{1}{2}$	$\frac{1}{2}$	$\frac{1}{2}$	1

TABLE II. Locations of Shoulders and Divergences In Powder Patterns Arising from Frequency Functions Given in Table I

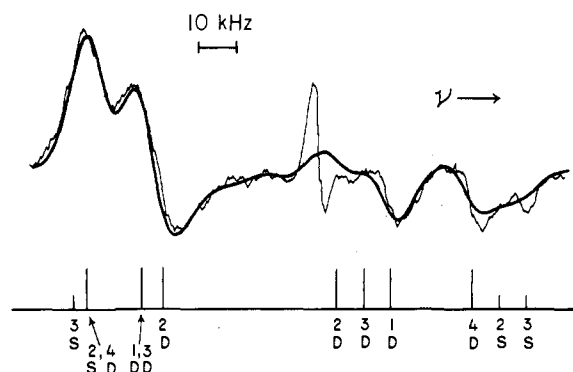|	Low-frequency shoulder	Low-frequency divergence	High-frequency divergence	High-frequency shoulder
$\Delta\nu_1$		$-(16/9)A + C/2 - (9/64)(C^2/A)$	$A - 3C/4$	
$\Delta\nu_2$	$-(16/9)A - C/2 - (9/64)(C^2/A)$	$-(16/9)A + (5/6)C - C^2/64A$	$A - 7C/4$	$A + 5C/4$
$\Delta\nu_3$	$-(16/9)A - (5/6)C - C^2/64A$	$-(16/9)A + C/2 - (9/64)(C^2/A)$	$A - 5C/4$	$A + 7C/4$
$\Delta\nu_4$		$-(16/9)A - C/2 - (9/64)(C^2/A)$	$A + 3C/4$	

Figure 13. Experimental spectrum of BF_3 at $\nu_0 = 11.13$ MHz (light line) superimposed on a computer-simulated spectrum (heavy line) calculated for $A = 30.6$ kHz, $C = 14.7$ kHz, and $\sigma = 4.0$ kHz. Long vertical lines below the spectrum indicate the positions of divergences (D) and short lines indicate shoulders (S) in the four underlying powder patterns. The numbers indicate the frequency function from which each feature arises. The narrow resonance near the center of the spectrum is due to four-coordinated boron in the glass sample holder and is not a part of the spectrum of BF_3 (after ref 68).

using values of the quadrupole coupling parameters obtained in early studies of the satellite ($m \neq \frac{1}{2}$) transitions. Often the shoulders of the powder patterns are broadened beyond visibility, and yet it has often been arbitrarily assumed that the asymmetry parameter η was equal to zero. No systematic review of this early work has ascertained the extent of these errors.

D. Combined Nuclear Quadrupole and Dipole–Dipole Interactions

An unusual nmr spectrum occurs in polycrystalline boron trifluoride. The ^{11}B nmr spectrum is accounted for by the combined effects of the central transition of an axially symmetric, second-order nuclear quadrupole interaction and the dipole–dipole interaction between the boron nucleus and its three nearest neighbor fluorine nuclei in the planar BF_3 triangle.[67] This situation is rather special, but it illustrates a number of points.

The nmr resonance condition for the $m = \frac{1}{2} \leftrightarrow -\frac{1}{2}$ transition of ^{11}B in BF_3 can be calculated by the use of perturbation theory. The shift of the nmr resonance frequency away from the unperturbed value is the sum of the first-order dipolar shift due to the fluorine–boron interaction plus the second-order quadrupolar shift.[67] There are four lines, whose resonance frequencies relative to ν_0 and relative intensities are given in Table I. The quantities A and C in Table I are given by

$$A = 3(e^2qQ/h)^2/64\nu_0$$

$$C = g_F g_B \mu_0^2/hr^3$$

where g_F and g_B are the nuclear g factors for fluorine and boron, r is the distance between boron and the nearest neighbor fluorine, and μ_0 is the nuclear magneton. In Table I, the quantity $\mu = \cos\theta$, where θ is the angle between the normal to the BF_3 triangle and the magnetic field. The quantity α in Table I is the angle between the projection of the magnetic field on the BF_3 plane and the line between the boron and one of the fluorine atoms. Note that lines 1 and 4 have axial symmetry, while lines 2 and 3 do not (Table I). The details of this calculation are given elsewhere.[66,67]

The locations of the shoulders and singularities are determined by using the procedure outlined in section II. They are listed in Table II. A complete analysis of a spectrum of this complexity is difficult without a numerical calculation, though a value of the quadrupole coupling constant can be obtained from the frequency dependence of the linewidth.[67] Figure 13 shows the results of a computer simulation of the spectrum.[68] The narrow resonance in the center of the trace results from boron in the glass sample holder. It must be remembered that this analysis depends on the assumption, perhaps unjustified, that the asymmetry parameter is equal to zero.

The ^{19}F nmr spectrum has also been studied in BF_3. The influence of the nuclear quadrupole interaction on the B–F dipolar interaction has been evaluated, and the powder pattern for the F^{19} nmr has been discussed.[66]

E. Magnetic Shift Interactions

Because of the simplicity of the equations for the axially symmetric chemical shift, it will be useful here to discuss a point, usually neglected, which can be confusing even to experienced workers in magnetic resonance. Confusion can arise between sweeping the magnetic field and sweeping the frequency, for the two ways of performing magnetic resonance experiments are not equivalent and could in principle yield different results whenever the interaction of interest is a function of the applied field. Although in practice the difference between sweeping field and frequency is negligible, the point is worth examining since it is usual to sweep magnetic field while using expressions for the linewidth in frequency units, as in the case of the second-order quadrupole interaction. It will be seen that to first order the expressions for linewidths are identical whether frequency or field is swept so that as a practical matter the problem may be ignored

(although this is not always the case in electron spin resonance as will be discussed in section IV). Frequency formulas are usually applied because they are simpler in form and evolve naturally from the perturbation theory.

The resonance condition for the magnetic shift is given by the first term of eq 3 with the substitutions indicated in (5). The coordinate system of Figure 1 can be chosen so that $\sigma_3 > \sigma_2 > \sigma_1$. If the field is kept fixed at H_0 while the frequency is varied, then the resonance appears at the frequency

$$\nu = \frac{\gamma H_0}{2\pi}[(1 - \sigma_1)^2 \sin^2 \theta \sin^2 \varphi + (1 - \sigma_2)^2 \sin^2 \theta \cos^2 \varphi + (1 - \sigma_3)^2 \cos^2 \theta]^{1/2} \quad (28)$$

However, if the frequency is kept fixed at ν_0 while the field is varied, then the resonance appears at the field

$$H = \frac{2\pi\nu_0}{\gamma}[(1 - \sigma_1)^2 \sin^2 \theta \sin^2 \varphi + (1 - \sigma_2)^2 \sin^2 \theta \cos^2 \varphi + (1 - \sigma_3)^2 \cos^2 \theta]^{-1/2} \quad (29)$$

The equations are different, since the square root appears in the denominator in eq 29 and in the numerator of eq 28. In the case of fixed field, variable frequency, the locations of the shoulders and divergences are found by using the procedure outlined in section II. The powder pattern has a divergence at the frequency

$$\nu_2 = (\gamma H_0/2\pi)(1 - \sigma_2) \quad (30)$$

and shoulders at the frequencies

$$\nu_3 = \frac{\gamma H_0}{2\pi}(1 - \sigma_3), \quad \nu_1 = \frac{\gamma H_0}{2\pi}(1 - \sigma_1) \quad (31)$$

The powder pattern is shown in Figure 14b. In the case of axial symmetry, $\sigma_1 = \sigma_2$, and the right-hand shoulder merges with the divergence, as indicated in Figure 14a.

The total shoulder-to-shoulder width of the powder pattern is

$$\Delta\nu = \nu_1 - \nu_3 = (\gamma H_0/2\pi)(\sigma_3 - \sigma_1) \quad (32)$$

The width of the powder pattern is proportional to H_0, a fact which helps to identify and measure magnetic shift effects. We define an empirical parameter ζ which is useful in characterizing the asymmetry of a magnetic shift powder pattern. This parameter has no theoretical significance and should not be confused with the asymmetry parameter η which is related to the asymmetry of the electric field gradient tensor. The "anisotropy factor" ζ is defined as the ratio of the width (in frequency units) between the high-field shoulder and the divergence and the total width (eq 32).

$$\zeta = \frac{\nu_1 - \nu_2}{\nu_1 - \nu_3} = \frac{\sigma_2 - \sigma_1}{\sigma_3 - \sigma_1} \quad (33)$$

When $\zeta = 0.5$ the power pattern is symmetric about the divergence, and the limiting cases of $\zeta = 0$ and $\zeta = 1$ correspond to axial symmetry.

When the frequency is fixed, and the field is varied, the results are different. The shape of the powder pattern is the same but the divergence lies at the field

$$H_2 = \frac{2\pi\nu_0}{\gamma} \frac{1}{1 - \sigma_2} \quad (34)$$

and shoulders at the fields

$$H_3 = \frac{2\pi\nu_0}{\gamma} \frac{1}{1 - \sigma_3}; \quad H_1 = \frac{2\pi\nu_0}{\gamma} \frac{1}{1 - \sigma_1} \quad (35)$$

This situation is shown in Figure 2 where H_1, H_2, H_3 now refer to $H(\sigma_1)$, $H(\sigma_2)$, $H(\sigma_3)$, respectively. Note that the left-right asymmetry of the powder pattern for constant frequency is reversed from that for constant field. The total shoulder-to-shoulder width of the powder pattern is

$$\Delta H = H_3 - H_1 = \frac{2\pi\nu_0}{\gamma}\left[\frac{1}{1 - \sigma_1} - \frac{1}{1 - \sigma_3}\right]$$

$$\approx \frac{2\pi\nu_0}{\gamma}[\sigma_3 - \sigma_1] \quad (36)$$

only for σ_1, σ_2, $\sigma_3 \ll 1$

The anisotropy factor ζ is equal to

$$\zeta = \frac{\dfrac{1}{1 - \sigma_2} - \dfrac{1}{1 - \sigma_1}}{\dfrac{1}{1 - \sigma_1} - \dfrac{1}{1 - \sigma_3}} \quad (37)$$

$$\approx \left(\frac{\sigma_2 - \sigma_1}{\sigma_3 - \sigma_1}\right) \quad \text{only for } \sigma_1, \sigma_2, \sigma_3 \ll 1$$

The exact mathematical form for the powder pattern is given in section II in terms of esr notation (eq 15).

The difference in the expressions for the two types of magnetic resonance experiments should not be surprising, since the two experiments are not equivalent. However, the magnetic shift parameters are usually less than about 10^{-3}, and the two linewidth expressions (eq 32 and 36) are identical in first order and can be used interchangeably. Similar results can be demonstrated for the second-order quadrupole interaction, which also depends on the applied magnetic field. It is always possible, as long as perturbation theory is applicable, to use the constant field equations or constant frequency equations interchangeably.

The powder pattern for the magnetic shift interaction is quite similar in form to that for the "satellite" transitions in the presence of the first-order nuclear quadrupole interaction (section C above). In fact, it can be shown that if eq 28 is expanded in powers of σ_1, σ_2, σ_3 and only first-order terms are kept, one obtains

$$\nu = \frac{\gamma H_0}{2\pi}[1 - \sigma_{\text{iso}} - \sigma_{\text{ax}}(3 \cos^2 \theta - 1) - \sigma_{\text{aniso}} \sin^2 \theta \cos 2\varphi] \quad (38)$$

where

$$\sigma_{\text{iso}} = \tfrac{1}{3}(\sigma_1 + \sigma_2 + \sigma_3)$$

$$\sigma_{\text{ax}} = \tfrac{1}{6}(2\sigma_3 - \sigma_1 - \sigma_2)$$

$$\sigma_{\text{aniso}} = \tfrac{1}{2}(\sigma_2 - \sigma_1)$$

which is formally identical to the resonance frequency in the presence of the first-order nuclear quadrupole interaction (second term in eq 4).

Note that only the differences between the magnetic shift parameters can be obtained from linewidth measurements. Complete evaluation of the parameters requires that an accurate field and frequency determination be made at some point on the spectrum.

The subject of the dipolar broadening of the magnetic shift powder pattern has been discussed in section II. Ibers and Swalen[86] and Searl, Smith, and Wyard[106] have obtained closed expressions for the absorption pattern when the axially symmetric powder pattern is broadened by a Lorentzian function. These authors considered the additional complication of an angular-dependent transition probability, which can be ignored in most nmr applications. The resulting expression is complicated and it is necessary to use a computer to evaluate it. In the case
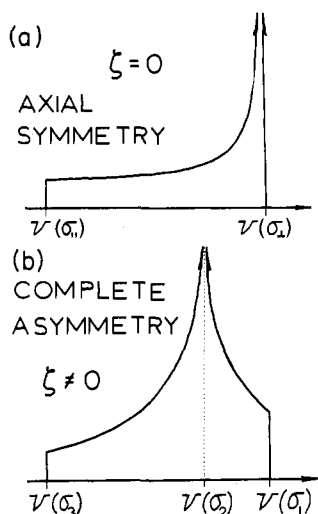
Figure 14. Powder patterns for the magnetic shift interaction for the cases of (a) axial symmetry and (b) complete asymmetry where the anisotropy factor ζ is defined in the text.

Figure 15. Computer-evaluated derivative spectra for the magnetic shift powder pattern in the presence of a Gaussian broadening function. Relevant parameters are defined in the text.

Figure 16. Computer-evaluated derivative spectra for the magnetic shift powder pattern in the presence of a Lorentzian broadening function. Relevant parameters are defined in the text.

of complete anisotropy, it is necessary to use computer-based techniques to obtain the convoluted lineshape.

Searl, Smith, and Wyard[106] and Hughes and Rowland[107] have used computer-based techniques to study the convolution of the theoretical powder pattern with both Gaussian and Lorentzian functions. Systematic studies of the magnetic shift powder pattern using computer evaluated derivative spectra are shown in Figure 15 for the case of a Gaussian convolution function and in Figure 16 for a Lorentzian convolution function.[117] The quantity σ_G in Figure 15 is defined in eq 6 and represents the peak-to-peak derivative width of the Gaussian convolution function. The quantity σ_L' in Figure 16 is the peak-to-peak derivative width of the Lorentzian convolution function and is equal to $\sigma_L/\sqrt{3}$ where σ_L is defined in eq 7. The ratio $\Delta_M/2\sigma$ gives a measure of the relative strengths of the dipolar and anisotropic magnetic shift interactions. Δ_M stands for the total width of the powder pattern, in either field or frequency units. For small values of $\Delta_M/2\sigma$, a single structureless asymmetric spectrum is observed. As the ratio $\Delta_M/2\sigma$ is increased, more and more structure appears, and the shoulders become resolved, the amount of resolution increasing with $\Delta_M/2\sigma$. The lines for the Gaussian and Lorentzian functions are quite similar, but the Lorentzian has a longer "tail" than does the Gaussian. As a result, the structure is somewhat less pronounced in the Lorentzian case.

There are three methods that are most often used in determining the magnetic shift parameters σ_1, σ_2, σ_3 from experimental spectra. The most commonly used technique is to measure the linewidth of the spectrum as a function of applied frequency.[91] This can often lead to errors, since there is no direct relationship between Δ_M and the linewidth of the experimental trace. Furthermore, axial symmetry is often assumed in measurements of this sort, sometimes with no obvious justification. The usual precautions must be observed in accepting published values of magnetic shift parameters, especially in earlier papers.

A second technique that is often used is to measure the second moment of the experimental lineshape as a function of applied frequency.[158-160] The second moment of the experimental line when magnetic shift and dipolar broadening effects are present can be shown to be[76]

$$M_2 = \left\{ \frac{16\pi^2}{45\gamma^2}[(\sigma_3 - \sigma_1)^2 + (\sigma_2 - \sigma_1)(\sigma_2 - \sigma_3)] \right\}^2 \nu_0^2 + m_2 \quad (39)$$
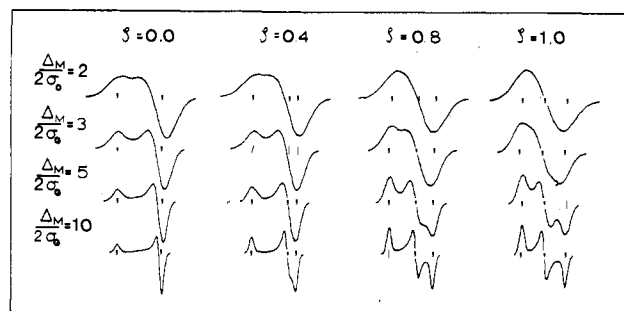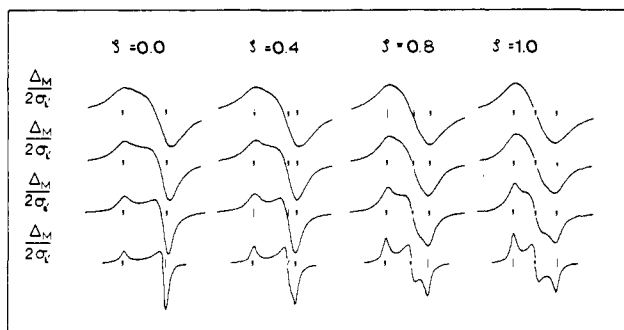
where M_2 is the second moment of the experimental trace and m_2 is the contribution due to dipolar broadening effects. The second moment thus depends on the square of the applied frequency ν_0, and the quantity in the brackets can be measured by taking the slope of a M_2 vs. ν_0^2 plot. However, since the bracket in eq 39 depends on the three parameters σ_1, σ_2, σ_3, some independent information is needed to determine σ_1, σ_2, σ_3 separately. This procedure will not work for a Lorentzian convolution function, as m_2 is infinite for that case. The method of moments usually requires an experimental trace with a fairly high signal-to-noise ratio, as the measurement of the second moment is subject to large errors. Finally, axial symmetry is often assumed without any a priori justification.

A third technique that has recently become important is that of computer simulation. Several workers[161-163] have compiled libraries of computer-evaluated derivative spectra in the presence of anisotropic magnetic shifts, and have determined magnetic shift parameters by comparing these computer evaluated traces with experimental spectra.

F. Combined Magnetic Shift and Nuclear Quadrupole Interactions

When both magnetic shift and nuclear quadrupole effects are present, the resonance condition is given by the sum of eq 4 and 28, where nuclear quadrupole effects are considered to second order in perturbation theory. This problem has been extensively considered by Jones, Graham, and Barnes[42] for the case of axial symmetry and by Baugher, Taylor, Oja, and Bray[43] for complete anisotropy in the magnetic shift and electric field gradient tensors. All of these authors assume that the anisotropic shift effects are small enough so that the magnetic shift term can be replaced by its approximate form (eq 38).

In the case of axial symmetry where quadrupolar terms are only considered to first order, the resonance frequen-

cy for the case of constant magnetic field (see section E) is given by

$$\nu = \nu_0(1 - \sigma_{iso} - \sigma_{ax}(3\mu^2 - 1)) - \nu_Q(m - \tfrac{1}{2})(3\mu^2 - 1) \quad (40)$$

where $\mu^2 = \cos^2\theta$ and σ_{iso}, σ_{ax} are defined in the previous section (eq 38). The magnetic shift and nuclear quadrupolar terms both have the same angular dependence. The divergence for each component will appear at the frequency

$$\nu_d = \nu_0(1 - \sigma_\perp) + \nu_Q(m - \tfrac{1}{2}) \quad (41)$$

and the shoulder is at the frequency

$$\nu_s = \nu_0(1 - \sigma_{||}) - \nu_Q(2m - 1) \quad (42)$$

where $\sigma_{||} = \sigma_3$, $\sigma_\perp = \sigma_1 = \sigma_2$. The effect of the magnetic shift on the first-order nuclear quadrupole powder pattern is simply to displace all the divergences by an amount $\nu_0(1 - \sigma_\perp)$ and all the shoulders by the amount $\nu_0(1 - \sigma_{||})$. The separation between the divergences and the m and $-(m - 1)$ components is, however, independent of the magnetic shift (and independent of magnetic field). This discussion is valid for both integral and half-integral spins, provided the value $m = \tfrac{1}{2}$ is excluded. For the central transition ($m = \tfrac{1}{2}$), only magnetic shift effects are observed in this approximation.

When second-order nuclear quadrupole terms are included, the resonance frequency for the central transition becomes

$$\nu = \nu_0(1 - \sigma_{iso} - \sigma_{ax}(3\mu^2 - 1)) - (\nu_Q^2/16\nu_0)[I(I + 1) - \tfrac{3}{4}](1 - \mu^2)(1 - 9\mu^2) \quad (43)$$

Now the magnetic shift and nuclear quadrupole terms have different angular dependencies. A divergence appears at the frequency

$$\nu_d = \nu_0(1 - \sigma_\perp) - (\nu_Q^2/16\nu_0)[I(I + 1) - \tfrac{3}{4}] \quad (44)$$

for all values of the quadrupolar and magnetic shift parameters. There is a shoulder at the frequency

$$\nu_s = \nu_0(1 - \sigma_{||}) \quad (45)$$

which is independent of quadrupolar effects. In addition, there is an extra divergence located at the frequency

$$\nu_{ed} = \nu_0\left(1 - \sigma_{iso} - \frac{2}{3}\sigma_{ax}\right) + \frac{4\sigma_{ax}^2\nu_0^3}{\nu_Q^2[I(I + 1) - (3/4)]} + \frac{\nu_Q^2}{9\nu_0}\left[I(I + 1) - \frac{3}{4}\right] \quad (46)$$

which only exists when

$$0 \le \frac{5}{9} + \frac{1}{6}r \le 1 \quad (47)$$

where

$$r = \frac{16\sigma_{ax}\nu_0^2}{\nu_Q^2[I(I + 1) - (3/4)]}$$

The parameter r provides a convenient measure of the relative strengths of the nuclear quadrupole and magnetic shift interactions.

The behavior of the "extra" divergence depends on the sign of σ_{ax}. When $\sigma_{ax} < 0$, r is a negative number, and the inequality in eq 47 reduces to

Figure 17. Powder patterns for the $m = \tfrac{1}{2} \leftrightarrow m = -\tfrac{1}{2}$ nmr transition broadened by axially symmetric, second-order quadrupolar and magnetic shift effects for various values of the parameter r (eq 47) for $\sigma_{ax} < 0$. The horizontal axis is $\nu - \nu_0$ in units of $\nu_Q^2[I(I + 1) - \tfrac{3}{2}]/16\nu_0$ (after ref 42).
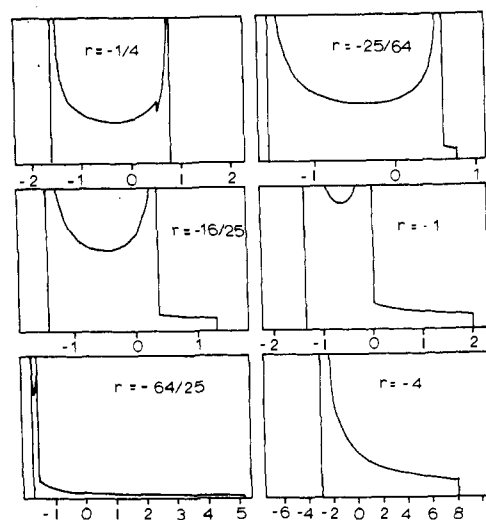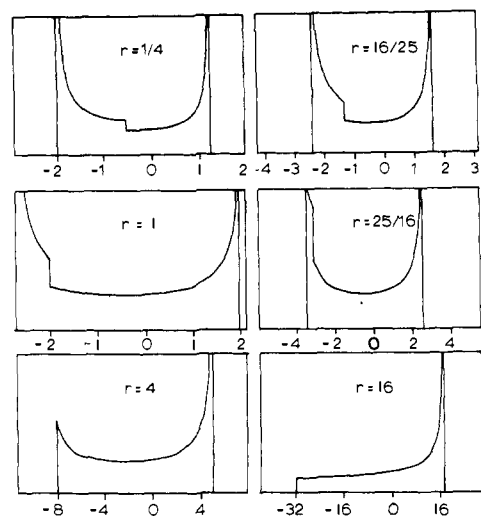

Figure 18. Powder patterns for the $m = \tfrac{1}{2} \leftrightarrow m = -\tfrac{1}{2}$ nmr transition broadened by axially symmetric, second-order quadrupolar and magnetic shift effects for various values of the parameter r (eq 47) for $\sigma_{ax} > 0$. The horizontal axis is $\nu - \nu_0$ in units of $\nu_Q^2[I(I + 1) - \tfrac{3}{2}]/16\nu_0$ (after ref 42).

$$\nu_0^2 \le \frac{5\nu_Q^2[I(I + 1) - (3/4)]}{24|\sigma_{ax}|}$$

The behavior of the powder pattern is shown in Figure 17. When r has a large (negative) value, the powder pattern is essentially that due to magnetic shift effects alone. When ν_0^2 decreases below the limit $5\nu_Q^2[I(I + 1) - \tfrac{3}{4}]/24|\sigma_{ax}|$, an additional divergence will split off from the original divergence at ν_d and will move across the powder pattern toward the shoulder as r is increased. Eventually, the extra divergence and the shoulder will cross, and the powder pattern becomes similar to that for the pure quadrupolar case for small values of ν_0.

When $\sigma_{ax} > 0$, r is a positive number, and the inequality in eq 47 reduces to

$$\nu_0^2 \le \frac{\nu_Q^2[I(I + 1) - (3/4)]}{6\sigma_{ax}}$$

The behavior of the powder pattern when $\sigma_{ax} > 0$ is shown in Figure 18. When r is large, the powder pattern is essentially that due to the magnetic shift interaction.

P. C. Taylor, J. F. Baugher, and H. M. Kriz

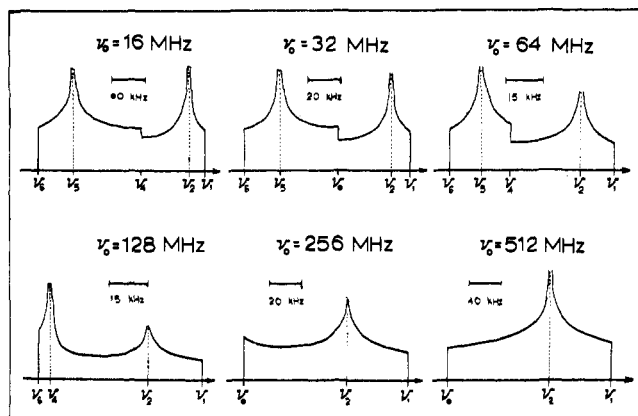**Figure 19.** Examples of powder patterns for the $m = \frac{1}{2} \leftrightarrow m = -\frac{1}{2}$ transition in the presence of quadrupolar and magnetic shift effects. The following parameters have been used: $\nu_Q = 1.0$ MHz, $\eta = 0.2$, $\sigma_1 = -2.0 \times 10^{-4}$, $\sigma_2 = -0.5 \times 10^{-4}$, $\sigma_3 = 2.0 \times 10^{-4}$. The powder patterns were calculated for the six indicated values of the applied frequency ν_0. The locations of the shoulders and singularities are indicated using the nomenclature of ref 43. The evolution of the powder pattern from purely quadrupolar to purely chemical shift as the frequency ν_0 is raised is apparent.

As r decreases, the shoulder begins to become sharper. When ν_0^2 decreases so that the above inequality is satisfied, a divergence splits away from the shoulder. The powder pattern becomes similar to that due to quadrupole effects only as r is lowered further. This behavior is expected, of course, since the magnetic shift linewidth varies linearly with frequency while the quadrupolar linewidth varies as $1/\nu_0$.

The case of complete asymmetry of the combined magnetic shift and quadrupolar interactions is more complex, even under the simplifying assumption that the principal axis systems of both interaction tensors are coincident. When only first-order quadrupolar terms contribute, the resonance condition is[43]

$$\nu = \nu_0[1 - \sigma_{iso} - \sigma_{ax}(3\mu^2 - 1) - \sigma_{aniso}(1 - \mu^2)\cos 2\varphi] - \frac{\nu_Q}{4}(2m - 1)[(3\mu^2 - 1) - \eta(1 - \mu^2)\cos 2\varphi] \quad (48)$$

As before, the $m = \frac{1}{2}$ transition will exhibit only magnetic shift effects, but all other transitions for both integral and half-integral spins will exhibit a combination of effects. Since both terms have the same angular dependence as the first-order quadrupole interaction, the powder pattern will be identical in form to that discussed in section C. It can be shown that a divergence will appear at

$$\nu_d = \nu_0(1 - \sigma_3) + \nu_Q(m - \frac{1}{2}) \quad (49)$$

provided that

$$-1 \leq \frac{-6\nu_0\sigma_{ax} + 3\nu_Q(m - \frac{1}{2})}{(\sigma_1 - \sigma_2)\nu_0 - \nu_Q(m - \frac{1}{2})} \leq +1 \quad (50)$$

This can be shown to be equivalent to the condition that ν_3 lies between the frequencies

$$\nu_1 = \nu_0(1 - \sigma_1) - (\nu_Q/2)(1 - \eta)(m - \frac{1}{2}) \quad (51)$$

and

$$\nu_2 = \nu_0(1 - \sigma_2) - (\nu_Q/2)(1 + \eta)(m - \frac{1}{2}) \quad (52)$$

which will be the positions of shoulders in the powder pattern. When eq 50 is not satisfied, ν_3 will be the location of a shoulder, the intermediate value frequency will be a divergence, and the remaining frequency will corre-
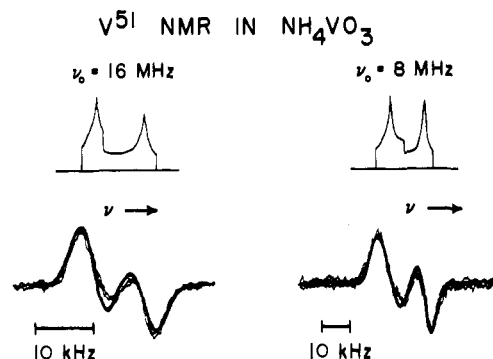
V^{51} NMR IN NH$_4$VO$_3$

Figure 20. ^{51}V nmr in NH$_4$VO$_3$, at both 16 and 8 MHz. Located above each experimental trace is the corresponding powder pattern. Superimposed on each experimental trace is the corresponding convoluted derivative spectrum (after ref 43).

spond to a shoulder at the opposite end of the powder pattern from ν_3. Details are available in ref 43.

Combined effects for the central $(m = \frac{1}{2} \leftrightarrow m = -\frac{1}{2})$ transition may also be considered by summing the magnetic shift term in eq 48 and the expression for the second-order quadrupole interaction given in eq 4. The locations of features in the powder pattern and whether the locations correspond to shoulders or divergences depend on the relative values of the various interaction parameters. Note that the powder pattern reflects primarily magnetic shift effects at higher frequencies and quadrupolar effects at lower frequencies just as in the axial case. A complete discussion is available elsewhere.[43,158] Figure 19 illustrates the transition of the powder pattern from the shape characteristic of a pure second-order quadrupole interaction to that for a pure magnetic shift.

The complexity of this powder pattern and the large number of parameters involved necessitates the use of exact computer simulation of the experimental derivative lineshape at a number of frequencies for precise determination of the magnitudes of the Hamiltonian parameters. An example of such a computer fit is shown in Figure 20. A detailed discussion of the successive approximations necessary in computer fitting in the case of complete anisotropy is presented elsewhere.[164]

The reader is referred to a number of nmr studies in which the combined effects of quadrupolar and magnetic shift interactions have been encountered in polycrystalline or glassy solids (ref 42, 43, 48, 114, 147, 155, 162, 165–174).

G. Miscellaneous Effects

Several additional effects, although not of general importance, are sometimes encountered in magnetic resonance spectra of powders. In this section we describe briefly effects due to the indirect interaction,[76,175,176] to diffusion, and to molecular rotation. The indirect interaction is a second-order dipolar effect which involves a coupling between two nuclear spins via the orbital electrons as an intermediary. The strength of this interaction depends on the amount of electron orbital overlap between atoms, but otherwise its mathematical form is identical with the dipole–dipole interaction. The indirect interaction is handled mathematically in exactly the same way as the ordinary dipolar interaction as far as the broadening of magnetic resonance powder patterns is concerned (eq 6). In powders containing thallium this effect is large and has been studied in some detail.[177]

Often when materials are heated, the nmr linewidth of a given nucleus in the material is observed to narrow as the various broadening mechanisms are averaged out owing to nuclear diffusion or molecular rotation.[7,178] De-

tails of the narrowing of nmr (or esr) spectra in powders are beyond the scope of the present article. Numerous examples from both nmr and esr are available in the literature, including the effects of molecular rotation on proton nmr in organic powders[179,180] and on esr in liquids,[87] and Monte Carlo computer simulations of the effects of motion on esr of free radicals.[108]

H. Spinning Sample Technique

The large nuclear dipole–dipole coupling characteristic of solids is the principal cause of difficulty in the analysis of the nmr spectra of polycrystalline and glassy materials. In some cases the dipolar broadening completely dominates the spectrum so that no fine structure can be observed in the spectrum. Even when the anisotropic interactions are large enough to produce observable fine structure in the derivative spectrum, easily measured features such as derivative extrema and baseline crossings are often displaced from the corresponding features of the theoretical powder pattern by the dipolar broadening.

The situation in solids contrasts sharply with that in mobile fluids, where the rapid molecular motion effectively averages the dipolar broadening to zero and causes the anisotropic interactions to be replaced by their isotropic means.[181] As a result, mobile fluids exhibit highly resolved, sharp-line spectra which are determined primarily by the scalar chemical shift and electron-coupled nuclear spin–spin interactions. Similar spectra can be obtained in a solid by elimination of dipole broadening through rapid, macroscopic rotation of the solid sample about an axis inclined at an angle $\alpha = \cos^{-1} 1/\sqrt{3}$ to the magnetic field. The resulting nmr spectrum of the solid can then be studied in a manner analogous to that in fluids. Though the spectrum is not a powder pattern in the sense used so far, the technique is worth describing briefly here. The spinning sample technique has been used very successfully by Andrew and coworkers, and more detailed accounts of the theory and applications of this technique are available elsewhere.[182-188]

To see how sample rotation results in narrowing of the spectrum, consider the usual truncated form of the Hamiltonian for dipole–dipole coupling

$$\mathcal{K}_d = \frac{\hbar^2}{4} \sum_{j,k} \gamma_j \gamma_k \frac{(3 \cos^2 \theta_{jk} - 1)}{r_{jk}^3} (I_j \cdot I_k - 3I_{jr}I_{kr}) \quad (53)$$

where γ_j is the gyromagnetic ratio of nucleus j, I_j is the nuclear spin of nucleus l, r_{jk} is the radius vector joining nuclei j and k, and θ_{jk} is the angle between r_{jk} and the applied field H_0. If the system of nuclear spins is rotated at an angular velocity ω about an axis inclined at an angle α to the applied field, then θ_{jk} will be explicitly time dependent so that

$$\cos \theta_{jk} = \cos \alpha \cos \psi_{jk} + \sin \alpha \sin \psi_{jk} \cos \omega t \quad (54)$$

where ψ_{jk} is the angle between r_{jk} and the axis of rotation. Substituting eq 54 into eq 53 results in a time-dependent dipolar Hamiltonian which can be written

$$\mathcal{K}_d = \overline{\mathcal{K}}_d + \mathcal{K}_d(t) \quad (55)$$

where the time-independent part is given by

$$\overline{\mathcal{K}}_d = \frac{\hbar^2}{8} (3 \cos^2 \alpha - 1) \sum_{jk} \gamma_j \gamma_k \frac{(3 \cos^2 \psi_{jk} - 1)}{r_{jk}^3} \times$$
$$(I_j \cdot I_k - 3I_{jr}I_{kr}) \quad (56)$$

The time-dependent part of the Hamiltonian will generate satellite spectra spaced at integral multiples of ω on either side of the central spectrum. Provided the rotation
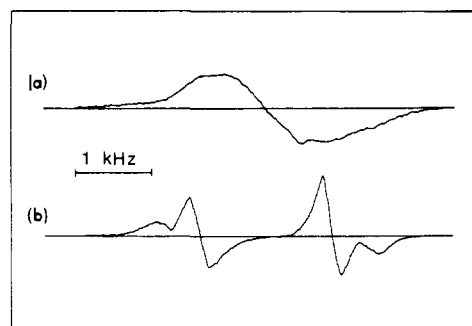

Figure 21. ^{31}P nmr spectrum of polycrystalline phosphorus sesquisulfide (P_4S_3) at $\nu_0 = 8.2$ MHz: (a) the broad, structureless line observed in the static specimen; (b) the chemical shift fine structure resolved by rotation of the sample at 2.5 kHz about the magic axis. First satellites of each line occur outside the other line (after ref 183).

rate is greater than the static dipolar width, the satellite lines will not interfere with the central spectrum, and for sufficiently high rotation rates the satellites will become unobservably weak. The width of the central portion of the spectrum is then determined solely by $\overline{\mathcal{K}}_d$. From eq 56 it is seen that $\overline{\mathcal{K}}_d = 0$ when $\cos^2 \alpha = \frac{1}{3}$ ($\alpha = 54°$ 44'). This axis is referred to as the "magic axis," and $\alpha = 54° 44'$ is called the "magic angle." It should be noted that elimination of dipolar broadening by spinning the sample will occur in both single-crystal and powder samples because the factor $(3 \cos^2 \alpha - 1)$ appears in the dipolar interaction between every pair of nuclei.

The Hamiltonian for the chemical shift is given by the last term in eq 2. Chemical shifts are small relative to the Zeeman interaction, and to first-order in perturbation theory

$$\mathcal{K}_c = \gamma \hbar H_0 I_z \sum_{i=1}^{j} \lambda_i^2 \sigma_i \quad (57)$$

where the σ_i are the principal values of the chemical shift tensor and the λ_i are direction cosines of H_0 with respect to the principal axes of σ. When the nuclear system is rotated, the λ_i become explicitly time dependent, and, as in the case of the dipolar interaction, the chemical shift Hamiltonian can be written

$$\mathcal{K}_c = \overline{\mathcal{K}}_c + \mathcal{K}_c(t) \quad (58)$$

Again in analogy to the dipolar interaction, $\mathcal{K}_c(t)$ contributes to the satellite spectra and can be ignored for large ω. The time-independent part of the chemical shift involves only the trace of σ and can be written

$$\overline{\mathcal{K}}_c = \gamma \hbar H_0 I_z \left[\frac{1}{2} \sin^2 \alpha \ \mathrm{Tr} \ \sigma + \right.$$
$$\left. \frac{1}{2} (3 \cos^2 \alpha - 1) \sum_i \sigma_i \cos^2 \beta_i \right]$$

where β_i is the angle between the axis of rotation and the ith principal axis of the shift tensor. When $\cos^2 \alpha = \frac{1}{3}$ the interaction reduces to

$$\overline{\mathcal{K}}_c = \gamma \hbar H_0 I_z \left(\frac{1}{3} \mathrm{Tr} \ \sigma \right) = \gamma \hbar H_0 I_z \bar{\sigma}$$

which is identical with the expression for a liquid.

As an example of the application of the spinning sample technique, consider the ^{31}P nmr spectrum of polycrystalline phosphorus sesquisulfide,[182,183] shown in Figure 21. The upper spectrum is from the static specimen, while the lower portion of the figure shows the spectrum from the sample when it is rotating at 2.5 kHz about the
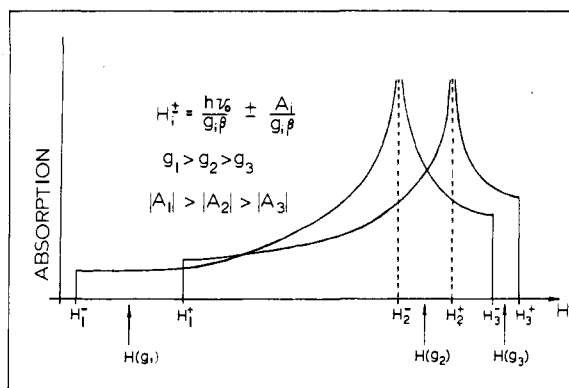
Figure 22. Powder patterns in the presence of electronic Zeeman and first-order hyperfine interactions where the nuclear spin I is $\frac{1}{2}$. This figure is drawn for the case where the anisotropy in the Zeeman term is larger than the splitting introduced by the hyperfine term. $H(g_i) = h\nu_0/g_i\beta$.

magic axis. It is seen that spinning the sample reveals the chemical shift fine structure which is obscured in the static sample by dipolar broadening and perhaps by broadening due to anisotropy of the chemical shift.

Nmr studies in spinning samples can be desirable for a number of reasons, despite the loss of information regarding the anisotropic nature of the nuclear interactions. Most important, of course, is the resolution of fine structure normally obscured by large dipolar broadening, particularly when measurements in the liquid state are not feasible. For example, melting of a solid may cause decomposition or a material may be insufficiently soluble in a liquid. In addition, studies of materials having a molecular form in the solid state which is different from that in solution, or investigations of differences in the liquid and solid environment for compounds whose molecular form in solution is similar to that in the solid, are possible. Spin–spin multiplets have rarely been resolved in solid samples, but they can easily be studied using spinning samples.[182,184,185] Little has been done with nuclei possessing quadrupole moments. Because the quadrupole interaction tensor is traceless, spinning the sample will eliminate first-order quadrupole effects. Second-order effects will remain in a modified form, however, and these could be studied in the absence of dipolar broadening.[186,187] Finally, additional structure can be revealed by the spinning sample technique even when there is partial narrowing due to molecular reorientation or diffusion.[189]

In order to achieve significant narrowing of a spectrum, it is necessary to spin the sample at a rate greater than the static linewidth of the nmr signal. Thus, the rotation rate must be at least of the order of several kilohertz. An account[188] of the development of high-speed, gas-driven rotors indicates that rotation rates are limited by the velocity of sound in the propelling gas, and ultimately by the strength of the rotor materials. Reliable operation at rotation rates of 8 kHz has been achieved using helium-driven gas turbines, and experimental turbines have been operated at 12.5 kHz. Routine analysis at such high rotation rates may be precluded by the difficulties of rotor construction (since the rotor is constructed around the sample), but spectra whose static width is only 1 or 2 kHz can be studied without undue difficulty.

IV. Electron Spin Resonance

A. Introduction

The powder spectra most often encountered in esr are discussed in this section. As in the previous section on

nmr, no attempt will be made to review all applications of esr to powdered or glassy materials. Instead, the various interactions of the paramagnetic spin with its environment are discussed and selected examples are presented.

The most simple esr powder spectrum results when only the electronic Zeeman term is present. The powder pattern (which in its most general form consists of two shoulders spanning a divergence) can be calculated exactly[85,87] and was described in detail in the example presented in section II (see Figures 2 and 14 and eq 15). This powder pattern is identical in form with several others encountered in nmr (magnetic shift, Pake doublet, quadrupole satellite transition), and the reader is referred to the appropriate paragraphs in section III for details. In particular, the effects of Gaussian and Lorentzian broadening on this powder pattern are shown in Figures 15 and 16.

In many cases, the electronic Zeeman term dominates the esr Hamiltonian so that the remaining interactions may be treated using perturbation combinations of the hyperfine, fine-structure, and quadrupolar interactions. When the electronic Zeeman term is of the same order as other terms in the spin-Hamiltonian, one must resort to exact diagonalization of the entire spin-Hamiltonian. This technique is described in section C. Finally, section D is devoted to special experimental techniques which are sometimes useful for powdered samples.

B. Perturbation Approach

Perturbation techniques are most often employed in evaluating the esr spectra of powders, and several reviews of the resonance conditions appropriate to a variety of situations most often encountered in esr have been published.[17-23] In the discussion which follows, the esr spin-Hamiltonian (eq 1) is solved exactly for the electronic Zeeman term, and the remaining terms are treated to an appropriate order in perturbation theory.

1. Zeeman and Hyperfine Interactions

The resonance condition for the combined effects of the Zeeman and hyperfine interactions is given in eq 3 where the hyperfine term is treated to first order and all tensors have the same principal axes. The resonance condition including second-order hyperfine terms is discussed by Low[17] and de Wijn and van Balderen[45] for the case of axial symmetry and by Baugher[50] for the case of complete asymmetry (see Appendix I, eq A-12).

The critical points of the powder pattern arising from the resonance condition of eq 3 (first-order hyperfine effects) have been calculated for the case of axial symmetry[85,190] and for complete asymmetry in both tensors.[191] When the magnetic field is swept and the frequency held constant, eq 3 becomes

$$H = (h\nu_0/g\beta) - (Am/g\beta) \tag{59}$$

where A and g are as defined in eq 3. Critical points occur at the fields

$$H_i = (h\nu_0/g_i\beta) - (A_im/g_i\beta) \tag{60}$$

where the nature of the critical points (shoulder or divergence) depends on the somewhat complicated conditions listed in Table III.

Often the anisotropy in the Zeeman term of eq 59 is considerably greater than the splitting introduced by the hyperfine terms. In this case, the powder patterns take on the general form described in Figure 22 which is drawn for the case of $I = \frac{1}{2}$. The splitting $H_i^+ - H_i^-$ is

Table III. Occurrence of Ordinary Divergences and Shoulders in Powder Patterns Arising from the Resonance Condition of Eq 59 at Fields Indicated by Eq 60

Field	Condition for occurrence of divergence	Condition for occurrence of shoulder
H_1	$J_1, L_1 > 0$ or $J_1, L_1 < 0$	$J_1 < 0, L_1 > 0$ or $J_1 > 0, L_1 < 0$
H_2	$J_2, L_2 > 0$ or $J_2, L_2 < 0$	$J_2 < 0, L_2 > 0$ or $J_2 > 0, L_2 < 0$
H_3	$I_1, I_2 > 0$ or $I_1, I_2 < 0$	$I_1 < 0, I_2 > 0$ or $I_1 > 0, I_2 < 0$

$$I_i = (-1)^{i+1}\left[h\nu_0(g_i^2 - g_3^2) + \frac{m}{A_3}(g_i^2 A_i^2 - g_3^2 A_3^2) - 2A_3 m(g_i^2 - g_3^2) \right]$$

$$J_i = h\nu_0(g_3^2 - g_i^2) + \frac{m}{A_i}(g_3^2 A_3^2 - g_i^2 A_i^2) - 2A_i m(g_3^2 - g_i^2)$$

$$L_i = (-1)^{i+1}\left[h\nu_0(g_1^2 - g_2^2) + \frac{m}{A_i}(g_1^2 A_1^2 - g_2^2 A_2^2) - 2A_i m(g_1^2 - g_2^2) \right]$$

TABLE IV. Occurrence of Extra Divergences and Shoulders in Powder Patterns Arising from the Resonance Condition of Eq 59 at Fields Indicated by Eq 61

Field	Condition for occurrence of extra singularity	Condition for occurrence of divergence	Condition for occurrence of shoulder
H_{12}	$A_1 < A_{12} < A_2$ or $A_2 < A_{12} < A_1$	$J_{12} > 0$	$J_{12} < 0$
H_{13}	$A_1 < A_{13} < A_3$ or $A_3 < A_{13} < A_1$	$L_{13} > 0$	$L_{13} < 0$
H_{23}	$A_2 < A_{23} < A_3$ or $A_3 < A_{23} < A_2$	$L_{23} < 0$	$L_{23} > 0$

$$J_{12} = \frac{1}{m}\left[h\nu_0(g_3^2 - g_{12}^2) + \frac{m}{A_{12}}(g_3^2 A_3^2 - g_{12}^2 A_{12}^2) - 2A_{12} m(g_3^2 - g_{12}^2) \right]$$

$$L_{13} = \frac{1}{m}\left[h\nu_0(g_1^2 - g_2^2) + \frac{m}{A_{i3}}(g_1^2 A_1^2 - g_2^2 A_2^2) - 2A_{i3} m(g_1^2 - g_2^2) \right]$$

equal to $A_i/g_i\beta$ which is the ith hyperfine coupling constant in magnetic field units. Each hyperfine multiplet ($2I + 1$ components) is centered about the Zeeman field in the absence of hyperfine effects. That is, for $I = \frac{1}{2}$ (Figure 22), $H(g_i) = (h\nu_0/g_i\beta) = (H_i^+ + H_i^-)/2$, where $H_i^\pm$ is defined in Figure 22.

The splittings of the resonance fields for the Zeeman term alone, $H(g_i)$, are proportional to frequency, while the hyperfine splittings are independent of frequency (eq 59). Thus one may separate the effects of these two terms by examining the resonance at different frequencies. The reader is referred to the example cited in section II and depicted in Figure 4.

In addition to the singular points described by eq 60, extra singularities as discussed in section II (and encountered in section III) can sometimes occur. In the case of complete asymmetry, extra singularities occur at the fields

$$H_{ij} = \frac{h\nu_0}{g_{ij}\beta} - \frac{A_{ij}m}{g_{ij}\beta} \qquad i = 1, 2; j = 2, 3 \qquad (61)$$

where

$$A_{ij} = \frac{h\nu_0}{4m} \pm \sqrt{\left(\frac{h\nu_0}{4m}\right)^2 + \frac{1}{2}\frac{g_i^2 A_i^2 - g_j^2 A_j^2}{g_i^2 - g_j^2}}$$

$$g_{ij} = \sqrt{g_i^2 + (g_j^2 - g_i^2)\cos^2\varphi} \qquad (62)$$

$$\cos^2\varphi = 1 \Big/ \left(1 + \frac{g_j^2 A_j^2 - A_{ij}^2}{g_i^2(A_{ij}^2 - A_i^2)}\right)$$

provided that the conditions listed in Table IV are met.

The esr spectrum of BO_3^{2-} in potassium borate ceramics[122] provides a good example of the ordinary and extra singularities encountered in powder patterns resulting from electronic Zeeman and first-order hyperfine terms. The hyperfine interaction is with the ^{11}B nucleus of spin $I = \frac{3}{2}$.

At 300 K, the powder patterns appear as in Figure 23a. The ordinary singularities H_1, H_2, H_3 of eq 60 and

Table III are determined to be low-field shoulders, divergences, and high-field shoulders, respectively, using the spin-Hamiltonian parameters listed in the figure caption. In addition, an extra shoulder corresponding to H_{13} of eq 61 and Table IV occurs overlapping H_2 in the $I = \frac{3}{2}$ powder pattern. This shoulder adds to the strength of the derivative in the region of the ordinary divergence but is otherwise unnoticeable. The derivative spectrum at 300 K is shown in Figure 4a.

At 77 K, the ordinary singularities H_1, H_2, H_3 are again, respectively, low-field shoulders, divergences, and high field shoulders for the $M = -\frac{3}{2}$, $-\frac{1}{2}$, $\frac{1}{2}$ components as shown in Figure 23b. For the $M = \frac{3}{2}$ component H_1 is a low-field divergence while H_2 and H_3 are shoulders. H_3 is just on the edge of becoming a divergence ($I_1, I_2 \sim 0$ in Table III). In addition, an extra divergence H_{23} occurs in the $M = \frac{3}{2}$ component overlapping H_3 as indicated in Figure 23b.

The situation in the special case of axial symmetry has been discussed by Neiman and Kivelson[190] and Gersmann and Swalen[92] who have observed extra divergences in the hyperfine spectra of a number of copper and vanadyl complexes. Lee and Bray[192,193] have also described the axial case for hyperfine interactions with boron nuclei. An analytical expression for the powder pattern cannot be calculated even in the case of axial symmetry. When one solves for $S(H)$ using eq 10 and 3, the angular variable θ cannot be explicitly eliminated.[190] However, if the g tensor is isotropic, then an exact expression for the powder pattern can be calculated which is identical with that presented in section II for the anisotropic g tensor[87] (or magnetic shift in nmr[35,76,109]). When the effects of the nuclear Zeeman term are included,[194,195] the powder pattern can be expressed analytically if the g tensor is isotropic. The nuclear Zeeman term (final term of eq 1) introduces an additional doublet in the energy levels which in turn can produce additional features in the powder spectra.[195] The reader is referred to the literature for details (ref 35, 109, 187, 194–197).

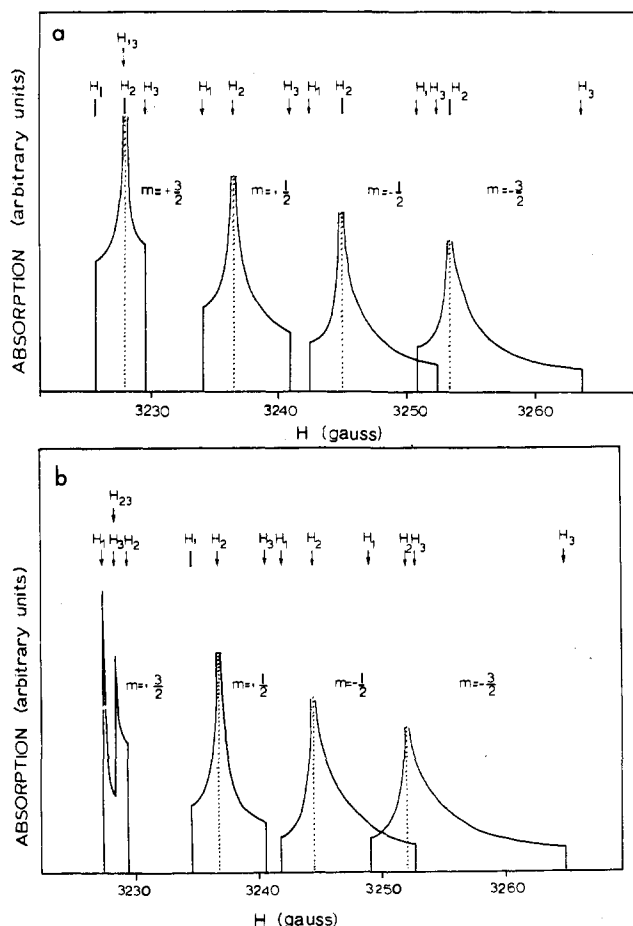There are two very special cases where the general

Figure 23. Powder patterns observed in ^{11}B-enriched potassium borate ceramic (a) at 300°K and (b) at 77°K. The fields H_1, H_2, H_3, H_{13}, H_{23} are defined in eq 60 and 61. Conditions for ordinary singularities (H_i) are defined in Table III and those for extra singularities (H_{ij}) in Table IV.

conditions expressed in Table III are indeterminate. When the g tensor is isotropic, the hyperfine tensor has axial symmetry, and either $A_{\parallel}$ or $A_{\perp}$ is zero, then some of the quantities I_i, J_i, L_i of Table III are undefined. These two special cases have been treated by Blinder[194] who finds that when $A_{\perp} = 0$ the powder patterns are rectangular step functions containing two shoulders and no divergences, and extending from $H(g_0)$ to $H(g_0, A$ When $A_{\parallel} = 0$, then the powder patterns contain a divergence at $H(g_0, A_{\perp}, m)$ and go to zero without a finite step at $H(g_0)$.[194]

Sometimes there are resolved hyperfine effects with nearest-neighbor nuclei other than the nucleus with which the paramagnetic spin is primarily associated. These so-called superhyperfine (shf) effects depend on the exact position of the surrounding nuclei, and no general calculation of powder spectra in the presence of shf effects is possible. An example of superhyperfine effects in the special case of Cu^{2+} in powdered phthalocyanine has been discussed by Chen, Abkowitz, and Sharp.[95,198,199] Extra divergences also play an important role when superhyperfine effects are present, although calculations are difficult and again depend on the exact symmetry of the surrounding nuclei.

Hyperfine effects can often be large enough so that second-order perturbation terms become important. Calculations of the positions of the singularities similar to those expressed in eq 60 and 61 and in Tables III and IV are not available. The resonance condition including electronic Zeeman, hyperfine, quadrupolar, and nuclear Zeeman terms correct to second order in perturbation

theory is listed in Appendix I (eq A-13). Since the ordinary divergences and shoulders occur at fields H_i corresponding to evaluation of the resonance condition along the three principal axes, we list these fields for reference ($M - 1 \leftrightarrow M$, $\Delta m = 0$ transition).

$$H_1 = \frac{h\nu_0}{g_1\beta} - \frac{A_1 m}{g_1\beta} - \frac{I(I+1) - m^2}{4h\nu_0 g_1\beta}(A_2{}^2 + A_3{}^2) - \frac{m(2M-1)A_2 A_3}{2h\nu_0 g_1\beta} - \frac{m[2m^2 + 1 - 2I(I+1)](h\nu_Q)^2(\eta+3)^2}{288M(M-1)g_1\beta A_1} \quad (63a)$$

$$H_2 = \frac{h\nu_0}{g_2\beta} - \frac{A_2 m}{g_2\beta} - \frac{I(I+1) - m^2}{4h\nu_0 g_2\beta}(A_1{}^2 + A_3{}^2) - \frac{m(2M-1)A_1 A_3}{2h\nu_0 g_2\beta} - \frac{m[2m^2 + 1 - 2I(I+1)](h\nu_Q)^2(\eta-3)^2}{288M(M-1)g_2\beta A_2} \quad (63b)$$

$$H_3 = \frac{h\nu_0}{g_3\beta} - \frac{A_3 m}{g_3\beta} - \frac{I(I+1) - m^2}{4h\nu_0 g_3\beta}(A_1{}^2 + A_2{}^2) - \frac{m(2M-1)A_1 A_2}{2h\nu_0 g_3\beta} - \frac{m[2m^2 - 1 - 2I(I+1)](h\nu_Q)^2\eta^2}{72M(M-1)g_3\beta A_3} \quad (63c)$$

where ν_Q and η are as defined in eq 4 and where H_i has been set equal to $h\nu_0/g_i\beta$ in the second-order hfs terms (see Appendix I).

Note that there is no contribution in eq 63 from the nuclear Zeeman term along the three principal axes. An important exception to the predictions of eq 63 concerns hyperfine interactions with protons. In this case, the nuclear Zeeman terms cannot always be taken as a perturbation. A good discussion of the effect of a strong nuclear Zeeman interaction on powder patterns is available in the article of Lefebvre and Maruani.[98]

One can see from the third terms in eq 63a-c that the primary effect of the second-order hyperfine terms is to increase the separation of hyperfine components with increasing magnetic field (decreasing m values) and to displace the center of gravity of each hyperfine multiplet away from the resonance field in the absence of hyperfine effects [$H(g_i)$].

Second-order hyperfine effects have been studied most often in powders containing transition metal ions such as Cu^{2+}, V^{4+} and VO^{2+}. The reader is referred to several illustrative references (72, 101, 108, 200–208).

Sometimes the electronic spin is not centered on a single nucleus but is delocalized, more or less uniformly, on two or more nuclei. If the nuclei are identical, then one may approximate the interactions with all of the nuclei of spin I by introducing a resultant spin $\mathbf{K} = \Sigma_i I_i$.[97,209-211] Maruani has studied the delocalized esr spectra of the trifluoromethyl radical in a polycrystalline matrix including the effects of extra singularities.[97,211] Owens and Vincow have investigated the naphthalene radical where the unpaired spin is extensively delocalized,[212] and Taylor, Griscom, and Bray have studied the hole centers trapped on two equivalent boron nuclei in γ-irradiated alkali diborate crystals.[213,214]

A simple example of hyperfine interactions in the presence of delocalized spins is the esr spectrum of V_K centers in alkali halide–alkali oxide glasses.[96] A V_K center is a hole trapped on an $X_2{}^-$ radical where X is a halogen atom. Thus for V_K centers, the spin is delocalized on only two atoms. The appropriate resonance condition includes nuclear Zeeman and second-order hyperfine terms (Ap-

pendix I). The esr spectrum for the case of Cl_2^- is shown in Figure 3b. The spin of ^{35}Cl is $\frac{3}{2}$ so the appropriate resultant spin to use in the resonance condition is $K = 3$. Shoulders from five of the seven ($2K + 1 = 7$) hyperfine powder patterns are visible on the high-field side of the spectrum of Figure 3b. The ordinary singularities of these powder patterns can be obtained using eq 63 with $K = I = 7$.

There is an additional complication in the Cl_2^- spectrum resulting from the fact that there are two abundant isotopes of chlorine (^{35}Cl and ^{37}Cl) with differing hyperfine effects. The spectra due to $^{35}Cl-^{37}Cl$ pairs are more difficult to evaluate because a resultant spin K as defined above cannot be introduced. Details are available elsewhere.[96,215-217]

In addition to the allowed transitions ($M - 1 \leftrightarrow M$, $\Delta m = 0$), there are weak transitions which are forbidden to first order ($M - 1 \leftrightarrow M$, $\Delta m = \pm 1$) (ref 20, 45, 52, 218-224). The intensity of these transitions is of the order of $[h\nu_Q/(A/g)]$ compared to the allowed transitions where ν_Q, A, g are defined in eq 3 and 4. The resonance condition for these transitions has been calculated by Bleaney[20] assuming second-order hyperfine effects and axial symmetry. For a hyperfine interaction of ~100 G and a quadrupole coupling constant of ~10 MHz, the forbidden transitions are ~10^{-2} of the allowed transitions. Although a number of studies have reported the occurrence of weak forbidden hyperfine transitions in powders (ref 39, 45, 52, 80, 84, 225), these transitions usually do not account for any strong features in the powder patterns. An example is presented in the next section.

The preceding discussion on hyperfine effects has assumed that all of the tensor quantities have identical principal axes. The powder patterns are, of course, altered when these tensors have different principal axes. A discussion of the effects on powder spectra when the hyperfine and g tensors have noncoincident axes is available in ref 98.

2. Zeeman and Fine Structure Interactions

When the crystal field effects are weak enough, or the operating frequency is great enough, then the fine structure interaction (second term in eq 1) can be treated as a perturbation. If the g tensor is isotropic, the resonance condition is given by eq 4 with the substitutions listed in eq 5. As first pointed out by Burns,[47] the powder patterns are identical with those considered in section III for the nuclear quadruple interaction.[5,7,9,35] In esr notation, the resonance condition for axial symmetry is given by Bleaney,[20] where the fine structure is considered to second order in perturbation theory. Third-order axial fine structure terms have also been calculated.[45,47] Appendix I lists the resonance condition for complete asymmetry for terms up to second order. Third-order calculations are also available.[44-49]

When the electronic spin S is half integral, there is a central ($M = -\frac{1}{2} \leftrightarrow M = \frac{1}{2}$) transition that is affected only by second-order fine-structure terms, flanked by satellite lines which are affected by both first- and second-order terms. When the electronic spin is integral, there is no central transition.

Shoulders and divergences for the second-order central transition have been calculated (assuming an isotropic g tensor) using the technique outlined in section II.[36,37] Figure 7 of section III indicates the positions of the singularities in nmr notation for which one must make the substitutions D for $h\nu_Q/2$, E for $\eta(h\nu_Q)/6$, and E/D for $\eta/3$. Figure 24 represents the situation in esr notation
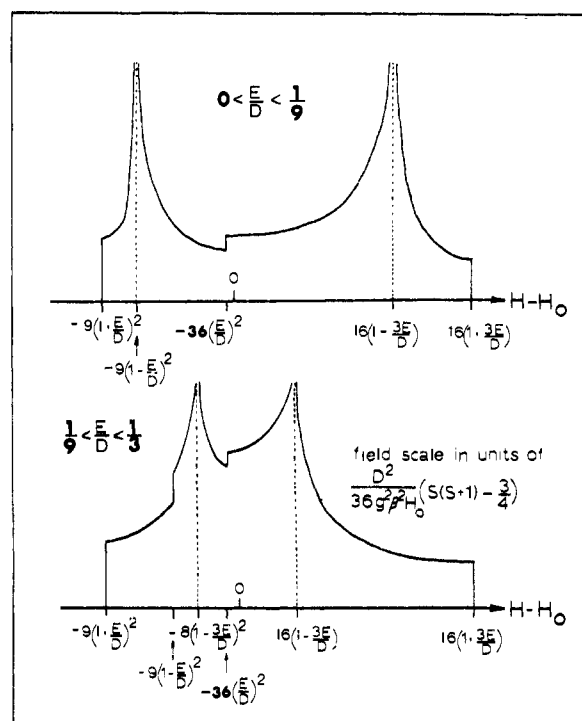

Figure 24. Powder patterns for the $M = -\frac{1}{2} \leftrightarrow M = \frac{1}{2}$ fine-structure transition broadened to second order. Locations of the divergences and shoulders are indicated. There are two distinct cases, $E/D < 1/9$ and $E/D > 1/9$.

assuming that the frequency is constant and the magnetic field is being swept.

Note that expressions for the locations of some of the low-field singularities depend on whether E/D is less than or greater than $\frac{1}{9}$. For all values of E/D ($0 \leq E/D \leq \frac{1}{3}$) the total width of the powder pattern is given by

$$\Delta H_{FS} = \frac{D^2}{36g_0^2\beta^2H_0}[S(S + 1) - \frac{3}{4}] \times$$
$$[9(E/D)^2 + 66(E/D) + 25] \quad (64)$$

The relative positions of shoulders and divergences are determined by E/D while D determines the magnitude of the splitting between features (Figure 24). For axial symmetry ($E/D = 0$), the low- and high-field shoulders merge with the divergence, and the powder pattern can be calculated exactly.[35] As E/D increases, two shoulders move outward while the two divergences move toward one another and merge when $E/D = \frac{1}{3}$ at the Zeeman field H_0.

Systematic studies of the dipolar broadened derivative spectrum in the presence of second-order fine structure effects (central transition)[115,116] were discussed in section III. In particular, Figure 8 shows representative derivative spectra for various values of $\eta = 3E/D$ and the dimensionless parameter $\Delta H_{FS}/2\sigma_G$ where σ_G is defined in eq 6. This ratio, which measures the relative strengths of the fine structure and dipolar interactions, is inversely proportional to the operating frequency ν_0. The reader is referred to section III for details and, in particular, to Figures 8 and 9.

For the satellite transitions both first- and second-order perturbation terms contribute, but in many cases first-order terms provide a sufficiently good approximation. In first order, the powder patterns can be calculated exactly for all values of E/D. Details are available in ref 35 which uses nmr notation. For reference, we list the field positions of the one divergence and two shoulders.

$$H_d = H_0 - \frac{D}{2g_0\beta}(2M - 1)(1 - 3E/D) \quad (65)$$

$$H_s = H_0 - \frac{D}{2g_0\beta}(2M - 1)(1 + 3E/D) \quad (66)$$

$$H_s = H_0 + \frac{D}{g_0\beta}(2M - 1) \quad (67)$$

where $H_0 = h\nu_0/g_0\beta$.

First-order powder patterns for the case of $S = \frac{3}{2}$ are shown in Figure 12 (section III) in nmr notation with frequency being swept. Note from eq 65, 66, and 67 that the electronic spin and the fine-structure constant D act as a scale factor through the product $(2M - 1)D$. The ratio E/D determines the relative positions of the shoulders and the divergence. Powder patterns for the $M - 1 \leftrightarrow M$ and the $-M \leftrightarrow -(M - 1)$ transitions are mirror images of one another about $H = H_0$.

For systematic studies of the effects of dipolar or relaxation (Lorentzian) broadening on first-order satellite transitions, the reader is referred to ref 106, 107, and 146 and to the discussion in section III. In particular, Figures 15 and 16 show a systematic parameterization of derivative spectra in the presence of Gaussian and Lorentzian broadening, respectively. These figures were drawn for the magnetic shift interaction which has the same functional form as the first-order fine-structure satellite transitions.

Second-order effects on the fine structure satellite powder patterns have been considered in detail only for axial symmetry $(E/D = 0)$. The divergence of eq 65 is shifted by second-order effects to

$$H_d = H_0 - \frac{D}{2g_0\beta}(2M - 1) + \frac{D^2}{4g_0{}^2\beta^2 H_0}\{[S(S + 1) - \frac{3}{4}] - 3(M - \frac{1}{2})^2\} \quad (68)$$

while the shoulder remains as given by eq 67. The separation of the divergences (H_d of eq 68) for the mirror image axial powder patterns of the $M - 1 \leftrightarrow M$ and $-M \leftrightarrow -(M - 1)$ transitions is independent of second-order effects and provides an accurate measure of D.

There is sometimes an extra divergence in the second-order satellite powder pattern which occurs at

$$H_{ed} = H_0 - \left[H_0 9b^2 - \frac{6Db(a - 5b^2)}{g_0\beta} - \frac{4D^2(a - 6b^2)}{g_0{}^2\beta^2 H_0}\right](9a - 15b^2) \quad (69)$$

where $a = S(S + 1) - \frac{3}{4}$ and $b = (M - \frac{1}{2})$. This divergence only exists when $A_1 < g_0\beta H_0/D < A_2$ or $A_2 < g_0\beta H_0/D < A_1$ where

$$A_1 = (5a - 27b^2)/6b$$

$$A_2 = (24b^2 - 4a)/6b$$

Further details are available in section III above and in ref 147.

An illustrative example of the application of perturbation techniques to the study of fine-structure effects in powders is presented in Figure 25. This figure shows the axially symmetric esr spectrum of Cr^{3+} $(S = \frac{3}{2})$ in powdered $NH_4(0.01Cr + 0.99Al)SO_4 \cdot 12H_2O$ after Burns.[47] Additional examples are available in the literature (ref 39, 52, 80, 84, 226–229).

When the fine structure terms are large in comparison with the electronic Zeeman term, the Zeeman term can be treated as the perturbation. This procedure was first adopted by Castner, Newell, Holton, and Slichter[41] to explain the Fe^{3+} resonance occurring at an effective g value of 4.3 in various oxide glasses. This situation repre-
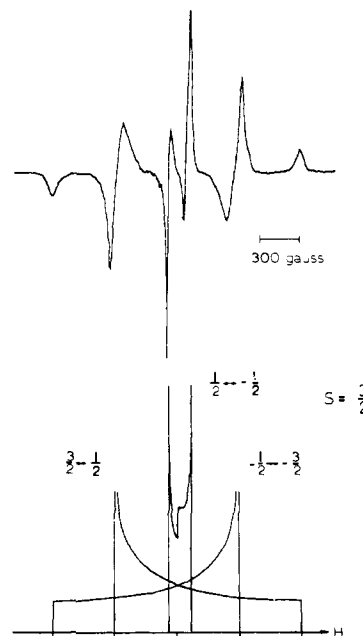

Figure 25. Derivative spectrum and powder pattern for Cr^{3+} $(S = \frac{3}{2})$ in powdered $NH_4(0.01 Cr + 0.99 Al) SO_4 \cdot 12H_2O$ at $297°K$ (after ref 47).

sents a limiting case of the matrix diagonalization procedures to be discussed in section C below, and we defer further comments until that section.

Except for the resonance condition referred to in Appendix I, the preceding discussion has assumed that the electronic Zeeman term is isotropic. In practice, the anisotropy in the Zeeman term is usually small in comparison to the fine-structure effects and can be neglected to a first approximation. Anisotropies in the g tensor are reflected in a transition probability which varies with orientation (see Appendix I) and in the occurrence of extra divergences in the powder spectra.[230]

Forbidden transitions of the form $M - 2 \leftrightarrow M$ can contribute to the powder spectra.[20] When both hyperfine and fine-structure interactions are present, forbidden transitions of the form mentioned in the preceding section $(\Delta m = \pm 1)$ can also contribute (ref 20, 45, 52, 218–224). An illustrative example is presented in Figure 26 (after de Wijn and van Balderen[45]) which shows the central fine-structure transition split into six allowed hyperfine transitions and ten forbidden $(\Delta m = \pm 1)$ hyperfine transitions for various values of A and D. The hyperfine coupling constant is assumed to be isotropic and the fine-structure tensor to be axial in this example. The spectrum of Figure 26 applies specifically to Mn^{2+} where $S = \frac{5}{2}$ and $I = \frac{5}{2}$.

The powder spectra when the electronic Zeeman and fine-structure terms are coupled with strong exchange effects have been considered for the case of Cr^{3+} ions in phosphate glass.[231] In this situation the spin Hamiltonian contains an additional term due to the coupling of the two $(S_1 = S_2 = \frac{3}{2})$ Cr^{3+} spins. The term which must be added to the spin-Hamiltonian of eq 1 is of the form

$$\frac{1}{2}J[(S + 1) - S_1(S_1 + 1) - S_2(S_2 + 1)]$$

where S denotes the sum $S_1 + S_2$, and J represents the strength of the isotropic exchange interaction. The reader is referred to ref 231 for details.

3. More Complicated Resonance Conditions

When more than one or two interactions are present, the perturbation treatment leading to the resonance con-
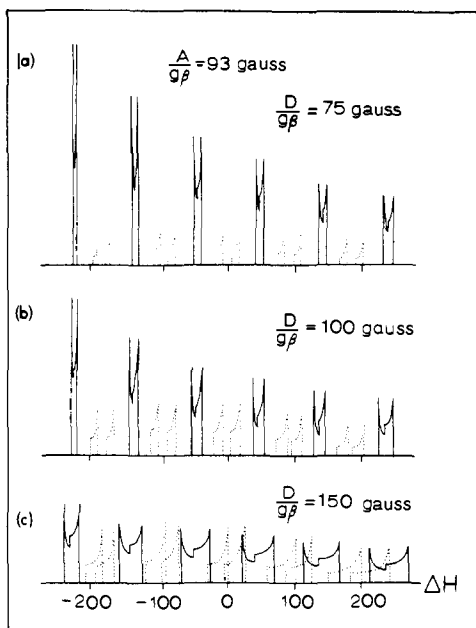
Figure 26. Powder patterns for the $M = -\frac{1}{2} \leftrightarrow \frac{1}{2}$ fine structure transitions including hyperfine effects and assuming axial symmetry. These powder patterns were calculated using third-order perturbation theory.[45] Solid lines refer to $\Delta m = 0$ (allowed) transitions, and dashed lines refer to $\Delta m = \pm 1$ (forbidden) transitions. All intensities are drawn to the same scale. The magnetic field scale is $|H - H_0|$ in gauss. For this example, $A/g\beta = 93$ G and (a) $D/g\beta = 75$ G, (b) $D/g\beta = 100$ G, (c) $D/g\beta = 150$ G (after ref 45).

dition becomes extremely tedious, and the calculation of singularities of the powder spectra becomes prohibitive. However, with the advent of suitable computer techniques,[39,97-103] the resonance condition can be used to calculate the powder spectrum numerically given appropriate spin-Hamiltonian parameters as input data (see section II). For this reason, the very complicated and lengthy resonance condition correct to second order in perturbation theory for a spin-Hamiltonian containing electronic Zeeman, fine-structure, hyperfine, quadrupole, nuclear Zeeman, and magnetic shift interactions is listed in Appendix I. No attempt will be made here to describe or categorize the salient features of this complex situation.

4. Ferromagnetic Resonance

In this section, we digress from the main thrust of the review to discuss the application of powder pattern techniques to ferromagnetic resonance. Until recently ferromagnetic resonance in powders has been the exclusive province of specialists in magnetism. However, the return of lunar material by the Apollo astronauts and the automated "Luna" probes has led to the application of such methods to geochemical problems.[232-236]

The resonance condition for ferromagnetic centers in a single crystal is given by[237]

$$hv = g\beta\{[H_3{}^a + (N_2 + N_2{}^e - N_3)M_3] \times$$
$$[H_3 + (N_1 + N_1{}^e - N_3)M_3]\}^{1/2} \quad (70)$$

where $H_3{}^a$ is the applied magnetic field and M_3 is the magnetization. The demagnetizing factors $N_{1,2,3}$ and $N_{1,2}{}^e$ reflect the shape of the specimen and the crystalline anisotropy energy, respectively. Equation 70 assumes that the ferromagnetic center is small compared to the skin depth of the sample. The magnetization energy as expressed in eq 70 depends on the relative orienta-
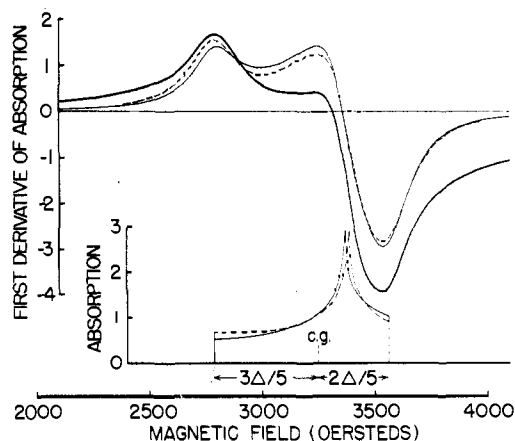

Figure 27. Derivative spectrum of ferromagnetic resonance in vacuum annealed lunar soils (heavy solid line). Lighter weight curves are computer generated derivative spectra and powder patterns. The solid lines were obtained using eq 71. The dashed lines represent some added sophistication as described in ref 239 (after ref 235).

tion of the magnetization and the crystal axes as well as on the shape of the specimen.

For a spherical specimen with small crystalline anisotropy energy ($N_1 = N_2 = N_3 = 4\pi/3$ and $N_{1,2}{}^e < H_3{}^a$) and cubic crystal structure, the angular dependence of the resonance field becomes[213,238,239]

$$H(\theta',\varphi') = H_0 - \frac{2K_1}{M_S}[1 - 5(\cos^2\theta' \times$$
$$\sin^2\theta' + \sin^4\theta' \sin^2\varphi' \cos^2\varphi')] \quad (71)$$

where $2K_1/M_S$ is the first-order anisotropy field and θ' and ϕ' are the polar and azimuthal angles of the crystal axes (cube edges) with respect to the applied magnetic field. Treatments of the case of uniaxial anisotropy are also available.[236,240]

An illustrative example of the use of eq 71 is provided by the "characteristic" ferromagnetic resonance signal observed in lunar soils.[232-236] Figure 27 shows a derivative signal found to be typical of vacuum annealed lunar fines (heavy line) compared to a computer generated trace employing eq 71. The quantity Δ of Figure 27 is $(5/3)(2K_1/M_S)$. Detailed investigations of this type of resonance are currently being pursued to determine whether the response of Figure 27 is due to metallic iron or to a "magnetite-like" phase present in lunar soils.[234-236] This question is of particular interest because ferrites like magnetite are relatively oxidized minerals, and their existence on the moon would require conditions somewhat less reducing at the time of formation than presently prevails on the lunar surface.

C. Matrix Diagonalization

When two or more terms in the spin-Hamiltonian are of comparable magnitude, the only accurate method of determining the powder pattern is by diagonalizing the entire matrix for each random orientation of the spin with respect to the applied magnetic field and then summing over the contributions made by each of these orientations. This procedure, which requires the use of computer techniques, has been employed by several authors[80-83,98-102] (see section II) both to categorize the resonance fields along the three principal axes of the tensors[80-83] and to calculate complete powder spectra.[98-102]

The most complete and detailed calculations utilizing matrix diagonalization techniques concern the fine-structure and electronic Zeeman interactions for spin $I = \frac{5}{2}$.[80-83] We restrict our attention in this section to a sum-
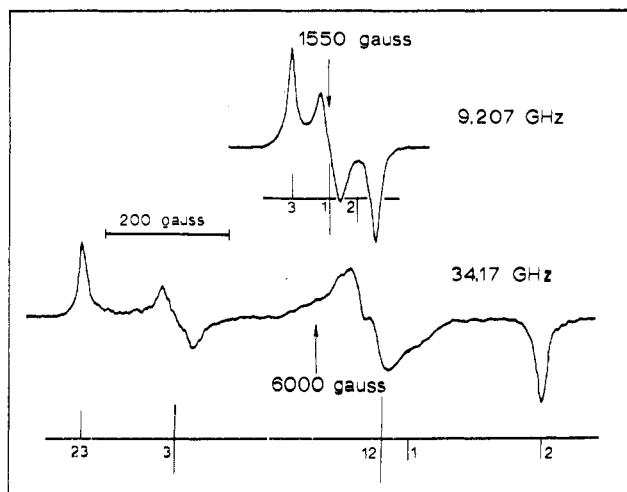
Figure 28. Derivative spectra of Fe^{3+} in powdered $NH_4CoEDTA$ at 9.207 and 34.17 GHz. Lines marked 1, 2, 3 or 12, 23 were obtained with the magnetic field parallel to the corresponding principal axes or principal planes assuming $|D| = 0.83$ cm^{-1} and $E/D = 0.31$. See Appendix III and especially Figure 42 for details (after ref 83).

mary of these results which are applicable to Fe^{3+} ions and to Mn^{2+} ions neglecting hyperfine effects. Three very similar treatments by Barry,[81] Dowsing and Gibson,[82] and Aäsa[83] have cataloged the allowed transitions ($M - 1 \leftrightarrow M$) along the three principal axes of the crystal field (fine-structure tensor) by plotting the reduced crystal field strength $D/h\nu$ (or the inverse of this quantity) vs. the reduced resonance energy $g'\beta H/g_0\beta H$ (or the inverse) for various values of the asymmetry ratio E/D. The "effective g value" g' is given by the equation $h\nu = g'\beta H$, where H is the resonance field in the presence of isotropic electronic Zeeman and fine-structure effects and where ν is the applied frequency. In this fashion Aäsa[83] and Dowsing, et al.,[241] have also cataloged the extra divergences which sometimes appear in powder spectra.

Appendix III presents the matrix diagonalization results in graphical detail (see Figures 32–42) following the notation of Aäsa. The six energy levels are always labeled 1 through 6 in order of increasing energy. Logarithmic graphs of $h\nu/D$ vs. g_0/g' are shown in Figures 32–42 of Appendix III.

An example of the use of matrix diagonalization techniques to evaluate the spin-Hamiltonian parameters for Fe^{3+} ions ($S = \frac{5}{2}$) in powdered ammonium ethylenediaminetetraacetatocobaltate(III) doped with Fe^{3+} (henceforth abbreviated $NH_4CoEDTA$)[83] is presented in Figure 28. The upper portion of the figure presents the derivative curve of the central transition ($3 \leftrightarrow 4$) at X-band. The lines labeled 1, 2, 3 indicate the positions of the ordinary singularities which occur along one of the principal axes of the fine-structure tensor using the parameters listed in the caption. The lower portion of the figure indicates the situation at Ka-band. Extra divergences labeled 23 and 12 also contribute at this frequency. The noise in the spectrum at Ka-band is due to finite crystallite size and can be effectively reproduced in computer simulations (see ref 39, Figure 1).

Esr spectra of Mn^{2+} ($S = \frac{5}{2}$) are further complicated by hyperfine effects which effectively split each fine-structure feature into six nearly equally spaced components ($I = \frac{5}{2}$ for ^{55}Mn). Figure 29a illustrates the derivative spectrum observed in Mn^{2+}-doped $SrO \cdot 3B_2O_2$ polycrystalline powder.[84] The three ordinary singularities for all five allowed fine-structure transitions are indicated by vertical lines whose heights represent the relative transi-

tion probabilities. Extra singularities are not indicated. The splitting of each fine structure feature into six nearly equally spaced hyperfine components is indicated for two representative features by dashed lines.

In Figure 29b the same spin-Hamiltonian parameters are used to generate a derivative using the perturbation techniques described in previous sections. Discrepancies between the computer-generated and experimental spectra result from the inadequacy of second-order perturbation theory for describing the fine-structure and hyperfine interactions and from the influence of forbidden transitions. Figure 29 is a good illustration of the combined use of both perturbation and matrix diagonalization techniques for evaluating spin-Hamiltonian parameters. Additional examples of the use of matrix diagonalization techniques are available elsewhere; see ref 39, 80–84, 98–102, 241–243.

D. Special Experimental Techniques

Although special esr and nmr techniques often produce additional complications when applied to powdered samples, in general they do not significantly alter the analysis of the resulting spectra. Double resonance techniques such as electron–nuclear double resonance (endor)[244] and electron–electron double resonance (eldor)[245] can usually be analyzed according to the procedures outlined in previous sections. Similarly, experiments involving irradiation and bleaching in situ can be treated using the techniques already described.

As an example of a special technique where additional complications arise, we consider the effect of dynamic nuclear polarization (dnp) produced by an anisotropic esr center in a polycrystalline powder on the nmr spectrum.[246-247] Dynamic nuclear polarization occurs when the electronic spins are not in equilibrium with the lattice because they are being driven by a microwave field at the electronic Larmor frequency.[7] When a polycrystalline material contains an isotropic nmr spectrum, then dnp produced by an anisotropic esr center yields an enhanced or quenched nmr signal without producing any change in shape.[247] When the nmr spectrum is anisotropic, then the lineshape is enhanced in some regions of magnetic field corresponding to certain crystallite orientations and quenched in others. The detailed nmr lineshape in this case depends on the relative magnetic field positions of the nmr and esr resonance conditions, both of which are functions of the orientation of the individual crystallites in the powder.[248] Detailed calculations of the resulting powder spectra have not been performed although qualitative treatments are available.[246,247]

Additional complications also arise when the esr spectra are influenced by molecular rotation or diffusion as described in section III.G. Such effects are most often treated by Monte Carlo computer simulations[108] which are beyond the scope of the present review. When either molecular rotation or diffusion is present, the static broadening which generates the powder pattern is partially averaged out, and the resulting absorption spectrum approaches a single line governed by the average of the traceless components of the interaction tensors. The degree of narrowing depends on the rate of rotation or diffusion. The reader is referred to the section on rotating samples (section III.H) above and to additional references on motional narrowing of magnetic resonance lines (ref 7, 34, 87, 108, 178–180).

V. Strained, Disordered, and Glassy Materials

The foregoing sections have described the effect on magnetic resonance spectra of the random orientations
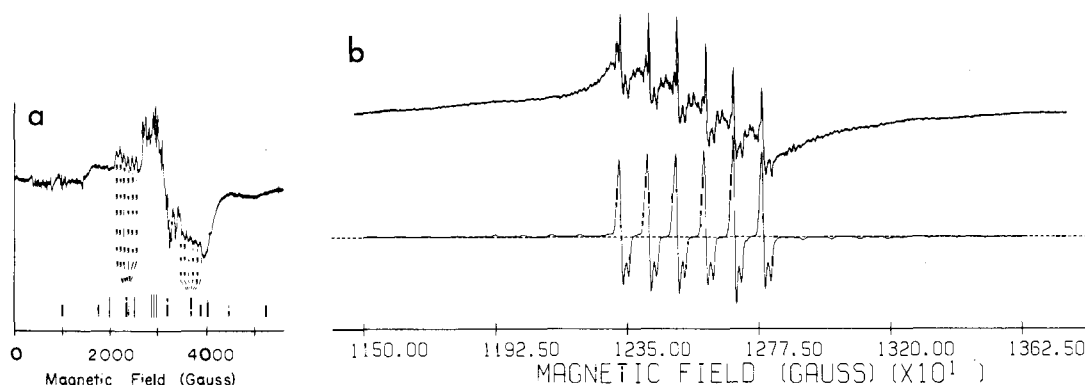
Figure 29. Esr spectra of Mn^{2+}-doped $SrO \cdot 3B_2O_3$ powder. (a) Experimental spectrum at 9 GHz. The solid lines indicate the positions of singularities in the powder pattern assuming no hyperfine interaction. The height of each line is proportional to the transition probability for the singularity. Dashed lines indicate the six hyperfine lines for two representative singularities. (b) Experimental (top) and computer-evaluated (bottom) spectra at 35 GHz. The broad underlying intensity in the experimental spectrum which is not reproduced in the computer-evaluated trace is due to distortions of the primary Mn^{2+} site in this strained material. Such effects are discussed in the next section (after ref 84).

of nuclear or paramagnetic sites in polycrystalline materials. The concept of a powder pattern was introduced to define the envelope of the absorption of microwave or rf power by a polycrystalline or powdered material. For such materials, a powder pattern represents the sum of absorptions due to an ensemble of sites whose principal axes are randomly oriented with respect to the applied magnetic field.

In a disordered or glassy material an additional complication arises due to the basic randomness of the structure itself. In these materials, there often exists a continuously random variation in the local environments surrounding any particular nuclear or paramagnetic site.[249] This variation of local environments can result in a continuous variation of the Hamiltonian parameters describing the magnetic resonance spectra of these sites. While the absorption in a powdered crystalline material can be accurately represented by a randomly oriented ensemble of otherwise identical sites, the absorption in a glassy or disordered solid must often be characterized by an additional ensemble of sites with differing local environments. The assumption which is often made in constructing a *powder pattern* for glassy or disordered materials is that these two ensembles are complete and separable. That is, there exists an identical ensemble of sites with random variations in local environments for every particular orientation, and, conversely, there exists an identical ensemble of randomly oriented sites for every particular local environment. With this working assumption, the sum over random orientations (called a powder pattern in the first four sections of this review) may be interchanged with the sum over random variations in local environments.[39,103]

Magnetic resonance spectra in glasses have been calculated by first performing the sum over variations in local environments,[104] although it can be shown that a great economy in computing time results by performing the angular sum first.[39,103] Computer simulation techniques are essential to the evaluation of magnetic resonance spectra observed in glasses and disordered materials because closed mathematical expressions are not generally possible to describe the more complicated averages over both orientation and local environment. As in the case of computer evaluation of powder patterns described in section II, one uses a finite number of sites possessing discrete Hamiltonian parameters to approximate the continuously random variation of local environments.

In favorable situations only some of the Hamiltonian parameters (and thus only some of the singular points of

the powder spectrum) are sensitive to the existing variations in local environments. In the most favorable of situations the variations in Hamiltonian parameters can be calculated from an assumed model of the nuclear or paramagnetic site. For example, Imagawa[250] has obtained semiquantitative fits to the Cu^{2+} spectra observed in various oxide glasses by considering a model for the Cu^{2+} center which assumes that the dominant fluctuations in the local environment involve only one of the copper ligand orbitals. Similarly, Griscom[251] has fitted the esr spectra of halogen atoms in oxide glasses assuming a statistical (Gaussian) distribution in the splitting of the orbital degeneracy Δ between the $3p_z$ and the $3p_x$, $3p_y$ orbitals which define the ground state of a chlorine atom in a rigid matrix. It is interesting to note that this Gaussian distribution in Δ leads to a skewed distribution in $g_\perp$, a situation which has been encountered more than once in the esr spectra of glassy materials.[251,252] The reader is referred to ref 251 for details. Similar approaches which take into account the statistical fluctuations in environment have been suggested to explain Ti^{3+} and Mn^{2+} esr in oxide glasses (ref 80, 84, 253), ^{93}Nb, ^{51}V, and ^{11}B nmr quadrupolar spectra in disordered polycrystalline and in glassy materials (ref 104, 139, 165, 254), radiation-damage esr centers in oxide glasses (ref 39, 101, 133, 213, 214, 251, 252, 255–257), and extensively delocalized esr centers in boric acid glasses (ref 212).

Recently Peterson and Kurkjian[253] have proposed an approach in which one defines a random vector, whose components are all of the Hamiltonian parameters. In this procedure, the powder spectrum is evaluated using basic techniques of probability theory. Although perhaps more attractive formally, this approach is exactly equivalent to the more *ad hoc* treatments of several other authors.[39,101,252] In all cases, one requires a specific model to relate the distributions of Hamiltonian parameters to distributions of more fundamental physical properties, such as changes in bonding character.

A general review of all the nmr and esr investigations in glasses is beyond the scope of the present article; however, an excellent summary through 1968 is available in the article of Wong and Angell.[258] We confine our discussion here to a few specific examples which illustrate the additional complications arising in the analysis of magnetic resonance spectra in noncrystalline materials. One basic principle has proved to be extremely useful in evaluating the magnetic resonance spectra of glasses, namely, that the best starting point for fitting a glass spectrum is the spectrum observed in the corresponding
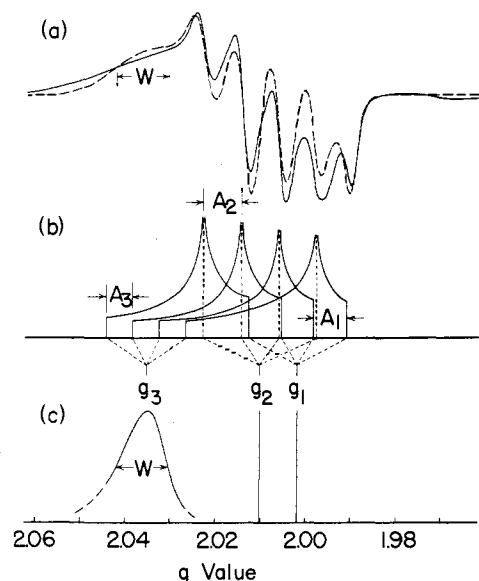
Figure 30. (a) Experimental (solid line) and computer-evaluated (dashed line) derivative spectra of the esr spectrum observed in X-irradiated 20% K_2O–80% B_2O_3 glass. (b) Powder patterns of most probable site in distribution. (c) Distribution function for the spin-Hamiltonian parameter g_3 as described in the text. Details available in ref 252 and 256 (after ref 256).

crystalline compound, when one exists. The success of this procedure is well illustrated by the [11]B nmr spectra observed in the alkali–borate glass system $(xMe_2O \cdot (1 - x)B_2O_3$, where Me is an alkali metal) in which three distinct boron sites are observed in three crystalline materials of the system. The relative prominence of each site in any given glass composition can be determined using computer simulation techniques.[39,214] The reader is referred to the literature for details.[39,132,133,214]

In the above illustration, the distribution of local environments surrounding each of the three crystal-like sites is relatively unimportant, although such distributions have been investigated in simple glass compositions such as B_2O_3 (no alkali oxide content).[133] In this material, Kriz[133] has fitted the [11]B nmr spectra at both 16 and 8 MHz well within the noise on the experimental derivative traces by assuming a Gaussian distribution of quadrupole coupling constants of half-width $\sim$0.1 MHz centered at 2.66 MHz (the crystalline value). The asymmetry parameter η was assumed to be 0.11 for all sites in the ensemble. Such a distribution function, although not unique,[133] is a first step toward understanding the nature of the boron site distortions in glassy B_2O_3.

The esr hole centers observed in irradiated alkali–borate and alkali–silicate glasses are examples where statistical distributions of local environments are central to the understanding of the observed spectra. As in the case of the [11]B nmr spectra in the alkali–borate glass system, three distinct hole centers, which occur in three crystalline compounds of the system, also occur in the glasses. The relative prominence of each site in any given glass composition can again be determined using computer simulation techniques.[214] In Figure 30a, the esr derivative spectrum occurring in irradiated 20 mol % K_2O–80 mol % B_2O_3 glass is displayed (solid line). The powder patterns for the esr center observed in irradiated polycrystalline $Me_2O \cdot 3B_2O_3$ consist of four components generated by the hyperfine interaction with a boron nucleus of $I = \frac{3}{2}$ (see section IV.B) and are shown in Figure 30b ($g_1 = 2.0020$, $g_2 = 2.0103$, $g_3 = 2.035$, $A_1 = 12.2$ G, $A_2 = 14.1$ G, $A_3 = 7$ G). In the vitreous material, this primary crystalline site becomes a randomly distorted ensemble, which is manifested in a distribution of g_3
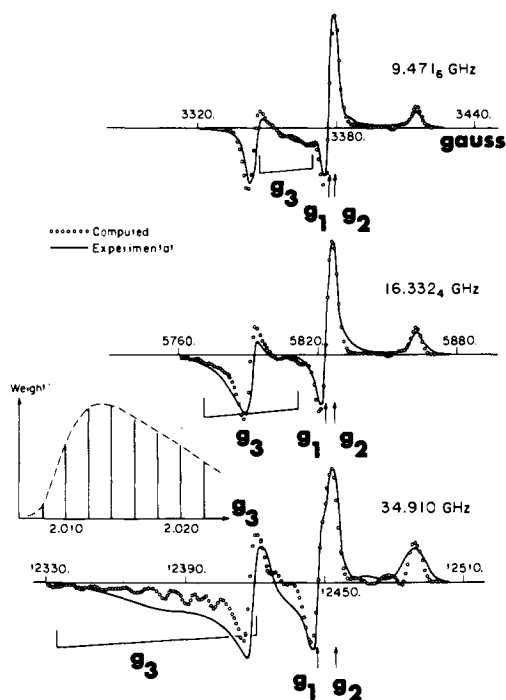

Figure 31. Experimental (solid lines) and computer-evaluated (open circles) esr derivative spectra of nitrogen-related hole center in X-irradiated sodium silicate glasses at 9, 16, and 35 GHz. The three singularities in the powder pattern neglecting hyperfine effects $H(g_i)$ are denoted as g_i in this figure. The inset denotes the assumed distribution function in g_3 as described in the text (after ref 101).

values as indicated in Figure 30c. With the ensemble of g_3 values of Figure 30c, one obtains the dashed derivative trace of Figure 30a, which is a good representation of the experimental derivative trace. In addition, the identical distribution function also fits the spectrum observed at Ka band (35 GHz).[252] The relationship of this empirical distribution of g_3 to more fundamental physical parameters is somewhat uncertain at present, although several possibilities have been suggested (see ref 213, 252, 256, 259, 260).

As a final example, we consider the esr spectrum of a nitrogen related hole center observed in irradiated sodium silicate glasses.[101] In this example, which is illustrated in Figure 31, there is also an empirically determined distribution of g_3 values as shown in the inset of the figure. Solid lines represent experimental derivative spectra and open circles show computer-evaluated spectra in Figure 31. The mean value spin-Hamiltonian parameters ($g_1 = 2.0039$; $g_2 = 2.0026$; $g_3 = 2.014$; $A_1 = A_3 = 2$ G; $A_2 = 36$ G) indicate a hyperfine interaction with a nitrogen atom similar to the esr centers observed in NH_2, NF_2, and $N(SO_3)_2$.[101] Note that the grid size of the g_3 distribution function is too coarse to eliminate all structure at the highest frequency, but that the general fit is quite accurate at all three frequencies.

Again, in this example the relationship of the g_3-distribution function to more fundamental structural parameters is as yet undetermined. However, the qualitative similarities of the spin-Hamiltonian parameters and g_3-distribution functions in the boron and nitrogen hole centers discussed in these two examples are intriguing.

We end this section with a few words of caution. The evaluation of magnetic resonance spectra in disordered and vitreous materials is a relatively new problem which remains somewhat undefined. Since the understanding of these spectra requires computer evaluation of complicated integrals, one can get lost in the myriad of computational details and produce fits to experimental spectra

which have no structural significance. The first step in understanding the structure and the "defect centers" of disordered and glassy materials as probed by magnetic resonance techniques is the discovery of a simple physical model which predicts the qualitative features of the spectrum including the mean-value Hamiltonian parameters and the general features of the distribution functions. In fitting complicated spectra in glassy or disordered materials one must keep in mind the importance of simple physical models which relate the magnetic resonance spectral parameters to structural properties of the materials.

VI. Future Prospects

Although the study of magnetic resonance in powdered materials will never be a substitute for detailed investigations of single crystals, there are several areas where powder techniques should become more useful in the future. The use of powders to determine Hamiltonian parameters quickly and routinely in cases where single-crystal accuracy is not important should increase as the techniques for analyzing powders become more refined. Increased use of signal averaging techniques will make computer simulation of powder spectra, which would otherwise be weak or overmodulated, more feasible. Point-by-point measurements of powder nmr spectra by pulsed techniques should greatly expand the types of materials which can be studied, such as those in which the nuclei have large quadrupole coupling constants. It is anticipated that the evaluation of magnetic resonance spectra in glasses and disordered solids will be placed on a firmer foundation in the near future with the result that statistical variations of Hamiltonian parameters can be related to variations of more fundamental structural parameters. New systems in which magnetic resonance of powdered samples will most likely prove useful include metals where the Knight shift is not axial, organic (in addition to hydrocarbons) and inorganic polymers, partially crystalline materials, and many systems of biological importance including the general phenomenon of "spin labels" which monitors the motion of biological molecules.

VII. Appendix I. Magnetic Resonance Perturbation Calculations

The spin-Hamiltonian for an electron of spin S in the presence of nuclear hyperfine, nuclear Zeeman, and nuclear quadrupole interactions is given by

$$\mathcal{K} = \mathcal{K}_z + \mathcal{K}_{fs} + \mathcal{K}_{nfs} + \mathcal{K}_Q + \mathcal{K}_{nz} \quad (A\text{-}1)$$

The various terms in the equation represent the electronic Zeeman, electronic fine structure, nuclear hyperfine structure, nuclear quadrupole, and nuclear Zeeman contributions, respectively. In perturbation theory, it is assumed that the electronic Zeeman term is the largest, with all others being small enough so that perturbation theory can be used.

Swalen and Gladney[34] have converted the above Hamiltonian into a form involving diagonal and off-diagonal electron and nuclear spin operators and the Euler angles θ and ϕ. The electron Zeeman term is

$$\mathcal{K}_z = g\beta H S_z \quad (A\text{-}2)$$

where

$$g = \sqrt{(g_1{}^2 \sin^2 \varphi + g_2{}^2 \cos^2 \varphi) \sin^2 \theta + g_3{}^2 \cos^2 \theta}$$

$$(A\text{-}3)$$

with g_1, g_2, and g_3 as the three principal values of the g tensor. The spin operator S_z is diagonal. It does not necessarily correspond to any of the three principal axes of the g tensor. The fine structure term reduces to eq A-4 where S_+ and S_- are raising and lowering electron spin operators.

$$\mathcal{K}_{fs} = \frac{1}{2}\left[\frac{D}{3}\left(\frac{3g_3{}^2 \cos^2 \theta}{g^2} - 1\right) + \right.$$
$$\left. E \sin^2 \theta \frac{g_1{}^2 \sin^2 \varphi - g_2{}^2 \cos^2 \varphi}{g^2}\right][3S_z{}^2 - S(S+1)] +$$
$$\frac{1}{4}\left[D\left(\frac{g_1{}^2 \cos^2 \theta}{g^2} - 1\right) - \right.$$
$$\left. E\left(1 - \frac{g_3{}^2 \cos^2 \theta}{g^2}\right)\frac{g_1{}^2 \sin^2 \varphi - g_2{}^2 \cos^2 \varphi}{g_1{}^2 \sin^2 \varphi + g_2{}^2 \cos^2 \varphi}\right](S_+{}^2 + S_-{}^2) +$$
$$iE\frac{g_1 g_2 g_3}{g}\frac{\cos\theta \sin\varphi \cos\varphi}{g_1{}^2 \sin^2 \varphi + g_2{}^2 \cos^2 \varphi}(S_+{}^2 - S_-{}^2) +$$
$$E\frac{g_1 g_2}{g}\frac{\sin\theta \sin\varphi \cos\varphi}{\sqrt{g_1{}^2 \sin^2 \varphi + g_2{}^2 \cos^2 \varphi}}(S_+ S_z + S_z S_+ +$$
$$S_- S_z + S_z S_-) - \frac{i}{2}\left(D - \right.$$
$$\left. E\frac{g_1{}^2 \sin^2 \varphi - g_2{}^2 \cos^2 \varphi}{g_1{}^2 \sin^2 \varphi + g_2{}^2 \cos^2 \varphi}\right)\frac{g_3\sqrt{g_1{}^2 \sin^2 \varphi + g_2{}^2 \cos^2 \varphi}}{g^2} \times$$
$$\sin\theta \cos\theta (S_+ S_z + S_z S_+ - S_- S_z - S_z S_-) \quad (A\text{-}4)$$

The nuclear hyperfine interaction Hamiltonian becomes

$$\mathcal{K}_{hfs} = AS_z I_z + \Gamma_1 I_+ S_+ + \Gamma_1{}^* I_- S_- +$$
$$\Gamma_2 I_- S_+ + \Gamma_2{}^* I_+ S_- + \Gamma_3 S_+ I_z + \Gamma_3{}^* S_- I_z \quad (A\text{-}5)$$

where

$$\Gamma_1 \equiv \frac{A_1 A_2}{4B} - \frac{A_3 B}{4A} -$$
$$i\frac{g_1 g_2 g_3 A_3 (A_2{}^2 - A_1{}^2) \cos\theta \sin\varphi \cos\varphi}{4g_a{}^2 gBA}$$

$$\Gamma_2 \equiv \frac{A_1 A_2}{4B} + \frac{A_3 B}{4A} +$$
$$i\frac{g_1 g_2 g_3 A_3 (A_2{}^2 - A_1{}^2) \cos\theta \sin\varphi \cos\varphi}{4g_a{}^2 gBA}$$

$$\Gamma_3 \equiv \frac{g_1 g_2 (A_1{}^2 - A_2{}^2)}{2g_a gA} \sin\theta \sin\varphi \cos\varphi -$$
$$i\frac{g_a g_3 (A_3{}^2 - B^2)}{2g^2 A} \sin\theta \cos\theta$$

$$A = \frac{1}{g}\sqrt{g_a{}^2 B^2 \sin^2 \theta + g_3{}^2 A_3{}^2 \cos^2 \theta}$$

$$g_a{}^2 = g_1{}^2 \sin^2 \varphi + g_2{}^2 \cos^2 \varphi$$

$$B = \frac{1}{g_a}\sqrt{g_1{}^2A_1{}^2\sin^2\varphi + g_2{}^2A_2{}^2\cos^2\varphi}$$

This Hamiltonian is written so that the zero-order wave functions are diagonal in S_z and I_z and off-diagonal in S_+, S_-, I_+, and I_-.

The nuclear quadrupole interaction Hamiltonian is

$$\mathcal{H}_Q = Q_1(3I_z{}^2 - I(I + 1)) + Q_2I_+{}^2 + Q_2{}^*I_-{}^2 + \\ Q_3(I_+I_z + I_zI_+) + Q_3{}^*(I_-I_z + I_zI_-) \quad (A\text{-}6)$$

where

$$Q_1 \equiv \frac{h\nu_Q g_3{}^2A_3{}^2\cos^2\theta}{4A^2g^2} - \frac{h\nu_Q}{12} + \\ \frac{\eta h\nu_Q}{12A^2g^2}[g_1{}^2A_1{}^2\sin^2\varphi - g_2{}^2A_2{}^2\cos^2\varphi]\sin^2\theta$$

$$Q_2 \equiv -\frac{h\nu_Q g_a{}^2B^2\sin^2\theta}{8A^2g^2} - \frac{\eta h\nu_Q}{24}\left[1 + \right.\\ \left.\frac{g_3{}^2A_3{}^2\cos^2\theta}{g^2A^2}\right]\left[\frac{g_1{}^2A_1{}^2\sin^2\varphi - g_2{}^2A_2{}^2\cos^2\varphi}{g_a{}^2B^2}\right] + \\ i\eta h\nu_Q \frac{g_1g_2g_3A_1A_2A_3}{6g_a{}^2gAB^2}\cos\theta\sin\varphi\cos\varphi$$

$$Q_3 \equiv \frac{\eta h\nu_Q g_1g_2A_1A_2\sin\theta\sin\varphi\cos\varphi}{6g_agBA} - \\ \frac{ih\nu_Q g_ag_3A_3B\sin\theta\cos\theta}{4g^2A^2} + i\frac{\eta h\nu_Q g_3A_3\sin\theta\cos\theta}{12g_aBA^2g^2} \times \\ [g_1{}^2A_1{}^2\sin^2\varphi - g_2{}^2A_2{}^2\cos^2\varphi]$$

Finally, the nuclear Zeeman Hamiltonian is given

$$\mathcal{H}_{nz} = -\gamma\hbar H\left\{I_x\frac{g_2A_2 - g_1A_1}{g_aB}\sin\theta\sin\varphi\cos\varphi + \right.\\ I_y\left(1 - \frac{g_1A_1\sin^2\varphi - g_2A_2\cos^2\varphi}{g_agBA}g_3A_3\right)\sin\theta\cos\theta + \\ \left.I_z\left(\frac{g_1A_1\sin^2\varphi + g_2A_2\cos^2\varphi}{gA}\sin^2\theta + \frac{g_3A_3}{gA}\cos^2\theta\right)\right\} \\ (A\text{-}7)$$

In the perturbation calculation of the resonance condition, the zero-order part of the Hamiltonian is taken to be that part which is diagonal in both S and I. The rest is taken to be a perturbation. This allows the use of ordinary nondegenerate perturbation theory.

By the use of standard nondegenerate perturbation theory, it can be shown that the resonance condition for the $M - 1 \leftrightarrow M$ allowed esr transition is, correct to second order, as shown in eq A-8. This equation is derived under the assumption that all of the interaction tensors have the same principal axis system.

It is very rare that all of the interactions discussed above will be present. Usually one or more of the interactions is small enough so that it can be ignored in eq A-8. For example, if only fine-structure effects are present, eq A-8 reduces to eq A-9. Very often the effects of g-tensor anisotropy are small enough that they can be ignored in the fine-structure terms of eq A-9. Equation A-9 then reduces to (A-10). In many cases, only g-tensor anisotropy and hyperfine effects are important. In this case, eq A-8 reduces to (for $S = \frac{1}{2}$) (A-11). Just as in the case of the fine-structure interaction, the effects of g-tensor anisotropy are often negligible in the hyperfine terms. Then eq A-11 reduces to (for $S = \frac{1}{2}$) (A-12).

Finally, for reference, we list the resonance condition including terms to second order in hyperfine, nuclear quadrupole, and nuclear Zeeman effects (eq A-13). It is assumed that fine-structure effects are zero and $S = \frac{1}{2}$.

One will note that eq A-8 through A-13 contain the magnetic field H in several terms, both in the numerator

$$h\nu = g\beta H + \frac{1}{2}\left[\frac{D}{3}\left(3\frac{g_3{}^2}{g^2}\cos^2\theta - 1\right) + \right.\\ \left.E\sin^2\theta\frac{g_1{}^2\sin^2\varphi - g_2{}^2\cos^2\varphi}{g^2}\right](2M - 1) + \\ AM + \frac{2S(S + 1) - 6M(M - 1) - 3}{2g\beta H}\left\{\left[\frac{D}{2}\frac{g_a{}^2}{g^2}\sin^2\theta + \right.\right.\\ \left.\frac{E}{2g^2}(g_1{}^2\sin^2\varphi - g_2{}^2\cos^2\varphi)\left(1 + \frac{g_3{}^2}{g^2}\cos^2\theta\right)\right]^2 + \\ \left.E^2\frac{g_1{}^2g_2{}^2g_3{}^2}{g^2g_a{}^4}\cos^2\theta\sin^2 2\varphi\right\} - \\ \frac{4S(S + 1) - 24M(M - 1) - 9}{2g\beta H}\left\{\left[D - \right.\right.\\ \left.E\frac{g_1{}^2\sin^2\varphi - g_2{}^2\cos^2\varphi}{g_a{}^2}\right]^2\frac{g_a{}^2g_3{}^2}{g^4}\sin^2\theta\cos^2\theta + \\ E^2\frac{g_1{}^2g_2{}^2}{g^2g_a{}^2}\sin^2\theta\sin^2 2\varphi\right\} + \frac{m^2\sin^2\theta}{2g\beta H}\left\{\frac{g_1{}^2g_2{}^2}{g_a{}^2g^2}\frac{(A_1{}^2 - A_2{}^2)^2}{A^2}\times \right.\\ \left.\sin^2\varphi\cos^2\varphi + \frac{g_a{}^2g_3{}^2}{g^4}\frac{(A_3{}^2 - B^2)}{A^2}\cos^2\theta\right\} + \\ \frac{[I(I + 1) - m^2]}{4g\beta H}\left\{\frac{A_1{}^2A_2{}^2}{B^2} + \frac{A_3{}^2B^2}{A^2} + \frac{g_1{}^2g_2{}^2g_3{}^2}{4g_a{}^4g^2}\times \right.\\ \left.\frac{A_3{}^2(A_2{}^2 - A_1{}^2)^2}{B^2A^2}\cos^2\theta\sin^2 2\varphi\right\} + \frac{m(2M - 1)}{g\beta H}\frac{A_1A_2A_3}{2A} + \\ \frac{h^2\nu_Q{}^2m}{8M(M - 1)A}[4I(I + 1) - 8m^2 - 1]\left\{\frac{\eta^2}{9}\frac{g_1{}^2g_2{}^2}{g_a{}^2g^2}\frac{A_1{}^2A_2{}^2}{B^2A^2}\times \right.\\ \left.\sin^2\theta\sin^2 2\varphi + \frac{g_3{}^2g_a{}^2}{g^4}\frac{A_3{}^2B^2}{A^4}\sin^2\theta\cos^2\theta\left(1 - \frac{\eta}{3}\times \right.\right.\\ \left.\left.\frac{g_1{}^2A_1{}^2\sin^2\varphi - g_2{}^2A_2{}^2\cos^2\varphi}{g_a{}^2B^2}\right)\right\} - \\ \frac{h^2\nu_Q{}^2m[2I(I + 1) - 2m^2 - 1]}{32AM(M - 1)}\left\{\left[\frac{g_a{}^2B^2}{g^2A^2}\sin^2\theta + \frac{\eta}{3}\left(1 + \right.\right.\right.\\ \left.\left.\frac{g_3{}^2A_3{}^2}{g^2A^2}\cos^2\theta\right)\left(\frac{g_1{}^2A_1{}^2\sin^2\varphi - g_2{}^2A_2{}^2\cos^2\varphi}{g_a{}^2B^2}\right)\right] + \\ \left.\frac{16}{9}\eta^2\frac{g_1{}^2g_2{}^2g_3{}^2A_1{}^2A_2{}^2A_3{}^2}{g_a{}^4g^2A^2B^4}\cos^2\theta\sin^2\varphi\cos^2\varphi\right\} + \\ \frac{\gamma^2\hbar^2H^2}{2M(M - 1)A}\left\{\left(\frac{g_2A_2 - g_1A_1}{g_aB}\right)^2\sin^2\theta\sin^2\varphi\cos^2\varphi + \right.\\ \left.\left(1 - \frac{g_1A_1\sin^2\varphi + g_2A_2\cos^2\varphi}{g_agBA}g_3A_3\right)^2\sin^2\theta\cos^2\theta\right\} + \\ \frac{m(2M - 1)A}{g\beta H}\left\{\frac{g_1{}^2g_2{}^2}{2g_a{}^2g^2}\frac{(A_1{}^2 - A_2{}^2)}{A^2}E\sin^2\theta\sin^2\varphi\cos^2\varphi - \right.\\ \frac{1}{4}\frac{g_3{}^2g_a{}^2}{g^4}\frac{A_3{}^2 - B^2}{A^2}\left(D - E\frac{g_1{}^2\sin^2\varphi - g_2{}^2\cos^2\varphi}{g_a{}^2}\right)\times \\ \left.\sin^2\theta\cos^2\theta\right\} - \frac{\gamma h^2\nu_Q H[I(I + 1) - 3m^2]}{8\pi M(M - 1)A}\left\{\frac{2}{3}\eta\times \right.\\ \frac{g_1g_2A_1A_2(g_2A_2 - g_1A_1)}{g_a{}^2gAB^2}\sin^2\theta\sin^2\varphi\cos^2\varphi + \\ \frac{1}{8}\frac{g_3g_a}{g^2}\frac{A_3B}{A^2}\sin^2\theta\cos^2\theta\left(1 - \right.\\ \frac{g_1A_1\sin^2\varphi + g_2A_2\cos^2\varphi}{g_agBA}g_3A_3\right)\left(1 - \frac{\eta}{3}\times \right.\\ \left.\left.\frac{g_1{}^2A_1{}^2\sin^2\varphi - g_2{}^2A_2{}^2\cos^2\varphi}{g_a{}^2B^2}\right)\right\} \quad (A\text{-}8)$$

(Zeeman terms) and in the denominator (some second-order hyperfine terms). In order to solve the resonance condition for magnetic field, the approximation usually made is to ignore the angular variation of H in the hyperfine terms and set $H = H_0 = h\nu_0/g_0\beta$. With this approximation, the resonance conditions of eq A-8 through A-13

$$h\nu = g\beta H + \frac{1}{2}\left[\frac{D}{3}\left(\frac{3g_3^2}{g^2}\cos^2\theta - 1\right) + \right.$$

$$\left. E\sin^2\theta\frac{g_1^2\sin^2\varphi - g_2^2\cos^2\varphi}{g^2}\right](2M-1) +$$

$$\frac{2S(S+1) - 6M(M-1) - 3}{2g\beta H}\left\{\left[\frac{D}{2}\frac{g_a^2}{g^2}\sin^2\theta + \right.\right.$$

$$\frac{E}{2g^2}(g_1^2\sin^2\varphi - g_2^2\cos^2\varphi)\left(1 + \frac{g_3^2}{g^2}\cos^2\theta\right)\right]^2 +$$

$$\left. E^2\frac{g_1^2g_2^2g_3^2}{g^2g_a^4}\cos^2\theta\sin^2 2\varphi\right\} -$$

$$\frac{4S(S+1) - 24M(M-1) - 9}{2g\beta H}\left\{\left[D - \right.\right.$$

$$\left. E\frac{g_1^2\sin^2\varphi - g_2^2\cos^2\varphi}{g_a^2}\right]^2\frac{g_a^2g_3^2}{g^4}\sin^2\theta\cos^2\theta + $$

$$\left. E^2\frac{g_1^2g_2^2}{g^2g_a^2}\sin^2\theta\sin^2 2\varphi\right\} \quad \text{(A-9)}$$

$$h\nu = g\beta H + \frac{1}{2}\left[\frac{D}{3}(3\cos^2\theta - 1) - E\sin^2\theta\cos^2 2\varphi\right] \times$$

$$(2M-1) + \frac{1}{2(g\beta H)}\{D^2\sin^2\theta[(\alpha(M) + \beta(M))\cos^2\theta -$$

$$\beta(M)] + 2ED\sin^2\theta\cos 2\varphi[(\alpha(M) + \beta(M))\cos^2\theta +$$

$$\beta(M)] + E^2[\alpha(M) + (\alpha(M) + 4\beta(M))\cos^2\theta -$$

$$(\alpha(M) + \beta(M))\sin^4\theta\cos^2 2\varphi]\} \quad \text{(A-10)}$$

$$\alpha(M) = 24M(M-1) - 4S(S+1) + 9$$

$$\beta(M) = \frac{1}{4}[6M(M-1) - 2S(S+1) + 3]$$

$$h\nu = g\beta H + Am + \frac{m^2\sin^2\theta}{2g\beta H}\left\{\frac{g_1^2g_2^2}{g_a^2g^2}\frac{(A_1^2 - A_2^2)}{A^2}\sin^2\varphi \times\right.$$

$$\left.\cos^2\varphi + \frac{g_a^2g_3^2}{g^4}\frac{(A_3^2 - B^2)^2}{A^2}\cos^2\theta\right\} +$$

$$\frac{[I(I+1) - m^2]}{4g\beta H}\left\{\frac{A_1^2A_2^2}{B^2} + \frac{A_3^2B^2}{A^2} + \frac{g_1^2g_2^2g_3^2}{4g_a^4g^2}\times\right.$$

$$\left.\frac{A_3^2(A_2^2 - A_1^2)^2}{B^2A^2}\cos^2\theta\sin^2 2\varphi\right\} \quad \text{(A-11)}$$

$$h\nu = g\beta H + Am + \frac{m^2\sin^2\theta}{2g\beta H}\left\{\frac{(A_1^2 - A_2^2)^2}{A^2}\sin^2\varphi \times\right.$$

$$\left.\cos^2\varphi + \frac{(A_3^2 - B^2)^2}{A^2}\cos^2\theta\right\} + \frac{[I(I+1) - m^2]}{4g\beta H} \times$$

$$\left\{\frac{A_1^2A_2^2}{B^2} + \frac{A_3^2B^2}{A^2} + \frac{1}{4}\frac{A_3^2(A_2^2 - A_1^2)^2}{B^2A^2}\cos^2\theta\sin^2 2\varphi\right\}$$

$$\text{(A-12)}$$

can be easily solved for H. In practice, such an approximation is accurate provided the anisotropy in the g tensor is small. When this anisotropy is large, a complicated quadratic equation in H must be solved to obtain the resonance condition as a function of H, and the variation of transition probability with angle (to be discussed below) must be included.

Equation A-8 was derived for the case of electron spin resonance. It can, however, be readily converted into a nuclear magnetic resonance expression by making the replacements

$$D \to \nu_Q/2 \qquad\qquad g_i \to -(\gamma\hbar/\beta)(1 - \sigma_i)$$
$$E \to (\eta/6)\nu_Q \qquad\qquad (i = 1, 2, 3).$$

$$h\nu = g\beta H + Am + \frac{m^2\sin^2\theta}{2g\beta H}\left\{\frac{g_1^2g_2^2}{g_a^2g^2}\frac{(A_1^2 - A_2^2)^2}{A^2}\times\right.$$

$$\left.\sin^2\varphi\cos^2\varphi + \frac{g_a^2g_3^2}{g^4}\frac{(A_3^2 - B^2)^2}{A^2}\cos^2\theta\right\} +$$

$$\frac{[I(I+1) - m^2]}{4g\beta H}\left\{\frac{A_1^2A_2^2}{B^2} + \frac{A_3^2B^2}{A^2} + \frac{g_1^2g_2^2g_3^2}{4g_a^4g^2}\times\right.$$

$$\left.\frac{A_3^2(A_2^2 - A_1^2)^2}{B^2A^2}\cos^2\theta\sin^2 2\varphi\right\} -$$

$$\frac{h^2\nu_Q^2m[4I(I+1) - 8m^2 - 1]}{2A}\left\{\frac{\eta^2}{9}\frac{g_1^2g_2^2}{g_a^2g^2}\frac{A_1^2A_2^2}{B^2A^2}\times\right.$$

$$\sin^2\theta\sin^2 2\varphi + \frac{g_3^2g_a^2}{g^4}\frac{A_3^2B^2}{A^4}\left(1 - \frac{\eta}{3}\times\right.$$

$$\left.\left.\frac{g_1^2A_1^2\sin^2\varphi - g_2^2A_2^2\cos^2\varphi}{g_a^2B^2}\right)^2\sin^2\theta\cos^2\theta\right\} +$$

$$\frac{h^2\nu_Q^2m[2I(I+1) - 2m^2 - 1]}{8A}\left\{\left[\frac{g_a^2B^2}{g^2A^2}\sin^2\theta + \frac{\eta}{3}\left(1 + \right.\right.\right.$$

$$\left.\left.\left.\frac{g_3^2A_3^2}{g^2A^2}\cos^2\theta\right)\left(\frac{g_1^2A_1^2\sin^2\varphi - g_2^2A_2^2\cos^2\varphi}{g_a^2B^2}\right)\right] + \right.$$

$$\left.\frac{16}{9}\eta^2\frac{g_1g_2g_3}{g_a^4g^2}\frac{A_1^2A_2^2A_3^2}{A^2B^4}\cos^2\theta\sin^2\varphi\cos^2\varphi\right\} -$$

$$2\frac{\gamma^2\hbar^2H^2}{A}\left\{\left(\frac{g_2A_2 - g_1A_1}{g_aB}\right)^2\sin^2\theta\sin^2\varphi\cos^2\varphi + \right.$$

$$\left.\left(1 - \frac{g_1A_1\sin^2\varphi + g_2A_2\cos^2\varphi}{g_agBA}g_3A_3\right)^2\sin^2\theta\cos^2\theta\right\} +$$

$$\frac{\gamma\hbar^2\nu_QH}{2\pi A}[I(I+1) - 3m^2]\left\{\frac{2}{3}\eta\frac{g_1g_2A_1A_2(g_2A_2 - g_1A_1)}{g_a^2gAB^2}\times\right.$$

$$\sin^2\theta\sin^2\varphi\cos^2\varphi + \frac{1}{8}\frac{g_3g_a}{g^2}\frac{A_3B}{A^2}\left(1 - \right.$$

$$\left.\frac{g_1A_1\sin^2\varphi + g_2A_2\cos^2\varphi}{g_agBA}g_3A_3\right)\left(1 - \frac{\eta}{3}\times\right.$$

$$\left.\left.\frac{g_1^2A_1^2\sin^2\varphi - g_2^2A_2^2\cos^2\varphi}{g_a^2B^2}\right)\sin^2\theta\cos^2\theta\right\} \quad \text{(A-13)}$$

and by discarding the nuclear quadrupole, hyperfine, and nuclear Zeeman terms (since they have no nmr analogies). Also, the electron spin quantum numbers S and M must be replaced by the nuclear spin quantum numbers I and m. Then, the nmr resonance condition is, correct to terms of second order in the nuclear quadrupole interaction, as shown in eq A-14, where $\alpha(m)$ and $\beta(m)$ are ob-

$$h\nu = \gamma\hbar H[(1 - \sigma_1)^2\sin^2\theta\sin^2\varphi +$$

$$(1 - \sigma_2)^2\sin^2\theta\cos^2\varphi + (1 - \sigma_3)^2\cos^2\theta]^{1/2} -$$

$$\frac{1}{2}(m - \frac{1}{2})\nu_Q[3\cos^2\theta - 1 - \eta\sin^2\theta\cos 2\varphi] +$$

$$\frac{\nu_Q^2}{12\gamma\hbar H}\left\{\frac{3}{2}\sin^2\theta[(\alpha(m) + \beta(m))\cos^2\theta - \beta(m)] + \right.$$

$$\eta\cos 2\varphi\sin^2\theta[(\alpha(m) + \beta(m))\cos^2\theta + \beta(m)] +$$

$$\frac{\eta^2}{6}[\alpha(m) - (\alpha(m) + 4\beta(m))\cos^2\theta - (\alpha(m) +$$

$$\beta(m))\cos^2 2\varphi\sin^4\theta]\right\} \quad \text{(A-14)}$$

tained from eq A-10 above with S, m replaced by I, m, respectively. In this expression, the effects of magnetic shift anisotropy have been ignored in the quadrupolar term.

The magnetic shift term of eq 2 is usually approximated by expanding the square root since the quantities σ_1, σ_2, σ_3 are always much less than unity. In this approximation the first term of eq A-14 becomes $\gamma \hbar H\{(1 - \sigma_1) \cdot \sin^2 \theta \sin^2 \varphi + (1 - \sigma_2) \sin^2 \theta \cos^2 \varphi + (1 - \sigma_3) \cos^2 \theta\}$. The Knight shift K is normally defined as the negative of the quantity σ of eq A-14 while the chemical and paramagnetic shifts are usually defined as equal to σ.

In electron spin resonance, there are cases in which fine-structure effects are so large that they dominate all other effects. In such a case, $\mathcal{K}_{fs}$ will be the largest term in eq A-1, with all of the others being much smaller. In this case, H_{fs} must be diagonalized first, and the other terms are handled by the use of perturbation theory.[7,40] The fine-structure Hamiltonian is

$$\mathcal{K}_{fs} = D[S_z^2 - \tfrac{1}{3}S(S + 1)] + E(S_x^2 - S_y^2) \quad \text{(A-15)}$$

where the electron spin operators refer to the principal axis system of the fine structure tensor. In most cases of interest, the only perturbing term that need be considered is the electronic Zeeman term, which can be written as

$$\mathcal{K}_z = \beta H(g_1 \sin \theta \sin \varphi \, S_x + g_2 \sin \theta \cos \varphi \, S_y +$$
$$g_3 \cos \theta \, S_z) \quad \text{(A-16)}$$

An important difference between eq A-15 and A-16 and their counterparts in eq A-4 and A-2, respectively, is that here the electron spin operators are referred to the principal axes of the fine-structure tensor. In the earlier perturbation expressions, the spin operators were chosen so that the electronic Zeeman Hamiltonian was diagonal. An interesting nmr example of the situation described by eq A-15 and A-16 concerns nmr in the strong quadrupole regime where transitions are observed in powdered samples at approximately two and three times the Larmor frequency.[261]

The zero-order problem (involving only fine structure effects) can be solved exactly only for certain special cases. The following results can be converted to nmr notation by making the substitutions expressed in eq 5, but they are in the province of nuclear quadrupole resonance (nqr) and beyond the scope of this review.[40] One special case which can be solved exactly is the approximation of axial symmetry in both the g tensor and the fine-structure Hamiltonians. This is obtained by setting $E = 0$ in eq A-15 and $g_1 = g_2 = g_\perp$ in eq A-16. The eigenvalues of eq A-15 have the values

$$E_M = D[M^2 - \tfrac{1}{3}S(S + 1)] \quad \text{(A-17)}$$

Note that the energy levels are doubly degenerate, i.e., $E_M = E_{-M}$. The selection rule for allowed transitions is $\Delta M = 1$, so the allowed transitions obey the resonance condition

$$h\nu = D[2|M| - 1] \quad \text{(A-18)}$$

There are $S - \tfrac{1}{2}$ distinct transition frequencies for half-integral spins, and S of them for integral spins.

When the Zeeman perturbation is present, the spectra are shifted and split. There are two cases of interest, depending on whether the spin is integral or half-integral. For integral spins, first-order degenerate perturbation theory gives the resonance condition

$$h\nu = D[2|M| - 1] + \frac{M}{|M|} g_3 \beta H \cos \theta \quad \text{(A-19)}$$

The intensity of this transition is independent of the orientation of the oscillating field relative to the axis of symmetry. When the spin S is half-integral, the resonance condition for the $M - 1 \leftrightarrow M$ transition is the same as eq A-19 so long as the $M = \pm\tfrac{1}{2}$ states are not involved. The $\pm\tfrac{3}{2} \leftrightarrow \pm\tfrac{1}{2}$ transitions give rise to four resonance lines, with the resonance conditions

$$h\nu = 2D + \frac{3g_3 + f(\theta)}{2} \beta H \cos \theta$$

$$h\nu = 2D + \frac{3g_3 - f(\theta)}{2} \beta H \cos \theta$$

$$h\nu = 2D - \frac{3g_3 - f(\theta)}{2} \beta H \cos \theta$$ (A-20)

$$h\nu = 2D - \frac{3g_3 + f(\theta)}{2} \beta H \cos \theta$$

where

$$f(\theta) = \sqrt{g_3^2 + g_\perp^2(S + \tfrac{1}{2})^2 \tan^2 \theta} \quad \text{(A-21)}$$

The central transition $(-\tfrac{1}{2} \leftrightarrow +\tfrac{1}{2})$ has the resonance condition

$$h\nu = f(\theta) \, \beta H \cos \theta \quad \text{(A-22)}$$

The intensities of these lines are functions of the orientation of the oscillating magnetic field relative to the symmetry axis.

Another problem that has been considered is the situation in which $D = 0$ in eq A-15.[41] The zero-field energy levels when $S = \tfrac{5}{2}$ are the three twofold-degenerate levels

$$W_0 = 0$$

$$W_+ = 2\sqrt{7}E \quad \text{(A-23)}$$

$$W_- = 2\sqrt{7}E$$

The addition of the Zeeman perturbation removes the degeneracy and splits the doublets. The transitions of interest will occur between the two members of the doublets, with the resonance conditions

$$h\nu = (15/7)g\beta H$$

$$h\nu = (3/7)g\beta H\sqrt{64 - 63 \cos^2 \theta \mp 24 \sqrt{7} \sin^2 \theta \cos 2\varphi}$$
(A-24)

In this expression, it is assumed that the g tensor is isotropic, and that all matrix elements between members of different doublets are ignored. Note that the resonance condition for the W_0 doublet is independent of the orientation. The intensities of these transitions depend on the angle between the oscillating field and the principal axes of the fine structure tensor.

The situation in which both D and E are nonzero has been considered, but the problem is complicated by the fact that the zero-field Hamiltonian (eq A-15) cannot be diagonalized in the general case of arbitrary spin S. Certain special cases, however, have been considered by Bowers and Owen.[18] Wickman, Klein, and Shirley[242] have diagonalized the fine-structure Hamiltonian within an $S = \tfrac{5}{2}$ manifold by computer techniques, and have used the resulting wave functions in a first-order perturbation calculation of the effects of the Zeeman interaction, assuming the g tensor to be isotropic.

In general the transition probability of magnetic resonance spectra depends on the orientation of the oscillating magnetic field relative to the principal axes of the interaction tensors. If g-tensor anisotropy is small, and if other effects are negligible, it is a good approximation to ignore the orientational dependence of the transition

probability. However, if g-tensor anisotropy is large, this orientational dependence can be important. Bleaney[71] has shown that the transition probability for the case of an axially symmetric g tensor is proportional to

$$I \propto \frac{g_{\parallel}^2 g_{\perp}^2}{g^2} \sin^2 \psi + g_{\perp}^2 \cos^2 \psi \qquad \text{(A-25)}$$

where the angle ψ is defined in Figure 1. This expression is also accurate, to a first approximation, in the presence of axial hyperfine effects.[72] This calculation has been extended to the case of full g-tensor anisotropy by Isomoto, Watari, and Kotani,[73] who obtained

$$I \propto (\cos \psi \cos \varphi - \cos \theta \sin \varphi \sin \psi)^2 g_1^2 +$$

$$g_2^2 (\cos \psi \sin \varphi + \cos \theta \cos \varphi \sin \psi)^2 + \sin^2 \theta \sin^2 \psi \, g_3^2 -$$

$$\frac{1}{g^2} [\sin \theta \sin \varphi \, (\cos \psi \cos \varphi - \cos \theta \sin \varphi \sin \psi) \, g_1^2 -$$

$$\sin \theta \cos \varphi \, (\cos \psi \sin \varphi + \cos \theta \sin \psi) g_2^2 +$$

$$\sin \theta \cos \theta \sin \psi \, g_3^2]^2 \qquad \text{(A-26)}$$

In both of these expressions, it is assumed that the oscillating field H_1 is polarized in a plane perpendicular to that of the static field H_0.

Bleaney[71] also considered the situation where H_1 was not perpendicular to H_0. Kneubühl and Natterer have also investigated the transition probability for full g anisotropy and have included the effects of the fine-structure interaction and the variation of the angle of H_0 with respect to H_1.[230] The reader is referred to ref 230 for these more complicated results.

VIII. Appendix II. Instrumental Broadening of Powder Absorption and Dispersion Spectra

In this appendix, corrections for various instrumental effects such as modulation broadening[262-267] or magnetic field inhomogeneity[268] are discussed. A technique for obtaining a replica of the absorption spectrum (not its derivative) in the derivative of the dispersion mode is also described.[269,270]

Most magnetic resonance measurements are performed by superimposing on the slowly varying dc field a small magnetic field which is modulated at a frequency ν_m, and the change in rf or microwave power at the frequency ν_m is then detected.[271] In the limit of infinitesimal modulation amplitude, the detected output is proportional to the derivative of the absorption signal. In practice, finite modulation amplitudes are required, and some distortion of the observed signal results.

Corrections for finite modulation amplitude, which apply when the modulation amplitude is small compared to the line width, have been calculated using either a Taylor series expansion[266] or an average over the modulation amplitude.[263] Corrections when the modulation frequency is no longer negligible with respect to the linewidth expressed as a frequency have also been computed.[262] A more general approach to the problem involves the definition of a convolution function,[264,265] similar in form to the Gaussian and Lorentzian functions of eq 6-8, which takes account of the instrumental response. The experimentally observed lineshape $h(x)$ is given by a convolution of the true lineshape for infinitesimal modulation amplitude and frequency $S(y)$ and the appropriate convolution function $F(x - y)$.

$$h(x) = \int_{-\infty}^{\infty} S(y) \, F(x - y) \, dy$$

For finite magnetic field modulation amplitude H_m, the variables in the above integral can be redefined so that the integral only exists from $x - H_m$ to $x + H_m$. One method for evaluating $S(y)$ involves an unfolding procedure due to Stokes[272] where F and h are each expanded in a Fourier series with identical periods chosen so that $h(x)$ is essentially zero outside of this interval. Using this procedure, the true lineshape $S(y)$ can be expressed as a Fourier expansion involving the expansion coefficients of $h(x)$ and $F(x - y)$.[265] From an experimental determination of F, one can then determine S as illustrated in ref 265. However, since the Fourier series must in practice be cut off after a finite number of terms, spurious oscillations in the wings of $S(y)$ occur. A more efficient technique which helps to eliminate this difficulty involves approximating the function $S(y)$ as $F(y)$ plus a correction term or a rapidly convergent series of correction terms.[264] This method, which does not express $S(y)$ as a completely resynthesized curve but rather as a correction on an assumed curve, is discussed further in ref 264. Correction curves for sinusoidal, modulation-broadened, pure Lorentzian absorption and dispersion curves are also available.[267]

Under certain conditions, an nmr high-power-dispersion, derivative signal (real part of the rf susceptibility which is varying at the modulation frequency ω_m) may be proportional to the absorption itself (imaginary part of the rf susceptibility). These conditions include: (1) $T_1 \gg T_2$, where T_1 and T_2 are the spin–lattice (longitudinal) and spin–spin (transverse) relaxation times, respectively; (2) $H_m < \Delta H$, where H_m is the magnitude of the magnetic field modulation and ΔH is the line width of the resonance; (3) $H_1 A(H_0) < 1$, where H_1 is the magnitude of the rf field and $A(H_0)$ is the magnitude of the absorption at the resonance field H_0; (4) $dH_0/dT < H_1/T_1$, the condition for slow passage; (5) either $\omega_m T_1 \gg 1$ or $H_1 A(H_0) < \omega_m T_1 < 1$.

The high-power dispersion mode, nmr derivative response will be proportional to the absorption spectrum only if all five of the above conditions are satisfied. In many cases, the dispersion derivative signal will look similar to an absorption spectrum when some of the five conditions are unsatisfied or marginally satisfied, but the lineshape will not be an accurate representation of the true absorption. Since it is sometimes difficult to determine if all the necessary conditions have been met in a given experimental spectrum, one must exercise great caution in using this method if the true absorption spectrum is desired.

IX. Appendix III. Catalog of Singularities of S = $\frac{5}{2}$ Powder Patterns

In this appendix, we adopt the notation of Aäsa[83] to catalog the allowed transitions $(M - 1 \leftrightarrow M)$ along the three principal axes of the crystal field, or fine-structure, tensor. The six energy levels are labeled 1 through 6 in order of increasing energy regardless of the M values to which they correspond. When two levels cross, they exchange labels. Extra divergences which sometimes occur for transitions in principal planes of the crystal field tensor are also cataloged. Logarithmic graphs of the inverse of reduced crystal field strength $h\nu/D$ as a function of the inverse of reduced resonance energy g_0/g' are presented in Figures 32 to 42.

Figures 32 and 33 for the 1 $\leftrightarrow$ 2 and 5 $\leftrightarrow$ 6 allowed transitions include E/D ratios of 0, 3/20, 1/4, 1/3. The 2 $\leftrightarrow$ 3 transitions for E/D = 0, 3/20, 1/3 are shown in Figures 34-36, respectively. Figures 36-38 show the 4 $\leftrightarrow$ 5 allowed transitions for E/D = 1/3, 3/20, 0, respectively.

Figure 32. Positions of esr powder pattern singularities obtained from the 1 ↔ 2 transition with $S = \frac{5}{2}$ for $E/D = 0, 3/20, 1/4, 1/3$ as explained in the text. Lines marked 1, 2, and 3 refer to transitions obtained when the magnetic field is parallel to the corresponding principal axes of the fine structure tensor. Relative transition probabilities are given by the figures in parentheses (after ref 83).

Figure 33. Positions of esr powder pattern singularities obtained from the 5 ↔ 6 transition with $S = \frac{5}{2}$ for $E/D = 0, 3/20, 1/4, 1/3$ as explained in the text (after ref 83).

Figure 34. Positions of esr powder pattern singularities obtained from the 2 ↔ 3 transition with $S = \frac{5}{2}$ for $E/D = 0$ as explained in the text (after ref 83).

Finally, Figures 39–42 display the 3 ↔ 4 transitions for $E/D = 0, 3/20, 1/4, 1/3$, in that order. The inverse reduced resonance energies of resonance lines g_0/g' at a

Figure 35. Position of esr powder pattern singularities obtained from the 2 ↔ 3 transition with $S = \frac{5}{2}$ for $E/D = 3/20$ as explained in the text (after ref 83).

Figure 36. Positions of esr powder pattern singularities obtained from the 2 ↔ 3 and 4 ↔ 5 transitions with $S = \frac{5}{2}$ for $E/D = 1/3$ as explained in the text. The curves labeled with axis numbers refer to the 2 ↔ 3 transition. The appropriate axis numbers for the 4 ↔ 5 transition can be obtained by interchanging 2 and 3, leaving 1 unchanged (after ref 83).

Figure 37. Positions of esr powder pattern singularities obtained from the 4 ↔ 5 transition with $S = \frac{5}{2}$ for $E/D = 3/20$ as explained in the text (after ref 83).

given reduced frequency $h\nu/D$ are given by the intersection of a horizontal line with the curves of Figures 32–42.

The relative transition probabilities are given in parentheses in Figures 32–42 but only at points where there is a rapid change in the probability or where its value is exceptionally large or small. Curves marked 1, 2, 3 refer to resonance fields parallel to the 1, 2, and 3 principal axes

Figure 38. Positions of esr powder pattern singularities obtained from the 4 ↔ 5 transition with $S = \frac{5}{2}$ for $E/D = 0$ as explained in the text (after ref 83).

Figure 41. Positions of esr powder pattern singularities obtained from the 3 ↔ 4 transition with $S = \frac{5}{2}$ for $E/D = 1/4$ as described in the text (after ref 83).

Figure 39. Positions of esr powder pattern singularities obtained from the 3 ↔ 4 transition with $S = \frac{5}{2}$ for $E/D = 0$ as explained in the text (after ref 83).

Figure 42. Positions of esr powder pattern singularities obtained from the 3 ↔ 4 transition with $S = \frac{5}{2}$ for $E/D = 1/3$ as described in the text (after ref 83).

1, 2, or 3 axes. In particular, an extra singularity of the form 12 or 13 occurs in Figure 42 near $g_0/g' = 0.5$ for $h\nu/D < 2$. For $h\nu/D \gg 1$, the matrix diagonalization solutions approach those in section IV.B where the fine structure is treated to second order in perturbation theory (Figure 24 and eq 65–69 with $S = \frac{5}{2}$).

X. Addendum

One caution, which was omitted from the text of the review, should be mentioned. In comparing the expressions presented in this work with those appearing in the original articles cited, the coordinate system employed must be taken into account. This review employs Euler angles of rotation as described in Goldstein,[33] while often in the literature the variables cos $\theta = \mu$ and φ refer to polar and azimuthal angles.

Several improvements and extensions of the analyses presented in this review have recently appeared. The impending use of glass fibers as optical wave guides has stimulated new interest in the esr spectra of radiation-damaged glasses.[273-275] In particular, the distributions of spin-Hamiltonian parameters, which are introduced in the analysis of magnetic spectra of glasses to account for variations in local environment, have been defined in two interesting cases. In the first case, the ^{29}Si hyperfine structure ($I = \frac{1}{2}$) associated with an e' center in glassy SiO_2 has been simulated numerically.[274] This simulation is interesting because the distribution of hyperfine coupling constants clearly reflects the presence of the second-order terms. As may be seen from eq 63 or

Figure 40. Positions of esr powder pattern singularities obtained from the 3 ↔ 4 transition with $S = \frac{5}{2}$ for $E/D = 3/20$ as described in the text (after ref 83).

as explained in the text. Curves labeled 12, 13, 23 refer to extra powder singularities which occur when the magnetic field H lies in the corresponding planes.

Figures 32 and 33 show that no extra singularities occur in the 1 ↔ 2 and 5 ↔ 6 transitions for all values of D and E/D. The other transitions yield extra singularities whose number and position depend on the ratio $h\nu/D$. Not all extra singularities are noted in Figures 34–42, especially if they overlap ordinary singularities along the

A-11, the second-order hyperfine shift either adds to, or subtracts from, the first-order shift, depending on the sign of m. It is this asymmetry in the second-order terms which provides agreement with the experimental spectrum.

In the second case, the Pb^{3+} centers in irradiated lead silicate glasses have been identified, and the spectrum has been fit using computer simulation techniques.[275] This spectrum is particularly interesting because it involves a hyperfine interaction which is larger (~ 13 kG) than that which may be treated using the perturbation theory of section IV.B.1. To simulate the spectrum a numerical diagonalization of the matrix was performed on a 20×20 point grid in μ, φ-space. Pb^{3+} is spin $\frac{1}{2}$, but only the high-field hyperfine line is observable at X-band because of the large value of the hyperfine coupling constant.

Some progress has been made in calculations of empirically determined distributions of nmr Hamiltonian parameters in glassy materials. Although the numerical computation procedures and the Hamiltonian parameter distributions applied by different authors to the problem of boron sites in borate glasses are quite similar, the conclusions concerning local bond angle and bond length distortions are very different.[276-278]

An analysis of the Gd^{3+} fine structure ($S = \frac{7}{2}$) in powdered materials has been performed by Nicklin, et al.[279] This work is an analog for $S = \frac{7}{2}$ of the material presented in section IV.C and in Appendix III where the case of $S = \frac{5}{2}$ is described.

Finally, several contributions were inadvertently omitted from the text of the review. These include (1) a discussion of combined magnetic shift and quadrupolar effects[280] in powdered $ScMn_2$; (2) a simulation of dipole–dipole effects[281] in $NaBr \cdot 2H_2O$; (3) a numerical calculation of the axial magnetic shift (or axial g-tension) powder pattern with Gaussian broadening;[282] (4) a numerical procedure for calculating second moments of Gaussian and Lorentzian broadened lines by restricting the range of the dependent variable (ν or H) in both the theoretical expression and the experimental spectrum;[283] (5) and a graphical analysis of the superposition of two Gaussian, isotropic resonance lines or of one Gaussian and one Lorentzian line.[284]

XI. References

(1) G. E. Pake, J. Chem. Phys., 16, 327 (1948).
(2) S. Gade, Phys. Rev., 187, 419 (1969).
(3) G. Burns and B. A. Scott, Phys. Rev. Lett., 23, 1191 (1970).
(4) A. Carrington and A. D. McLachlan, "Introduction to Magnetic Resonance," Harper and Row, New York, N. Y., 1962.
(5) C. P. Slichter, "Principles of Magnetic Resonance," Harper and Row, New York, N. Y., 1963.
(6) N. Bloembergen, "Nuclear Magnetic Relaxation," W. A. Benjamin, New York, N. Y., 1962.
(7) A. Abragam, "The Principles of Nuclear Magnetism," Clarendon Press, Oxford, 1961.
(8) J. D. Roberts, "Nuclear Magnetic Resonance," McGraw-Hill, New York, N. Y., 1959.
(9) E. R. Andrew, "Nuclear Magnetic Resonance," Cambridge University Press, London, 1955.
(10) G. E. Pake in "Solid State Physics," Vol. 2, F. Seitz and D. Turnbull, Ed., Academic Press, New York, N. Y., pp 1-91.
(11) G. E. Pake, Amer. J. Phys., 18, 438, 473 (1950).
(12) R. S. Alger, "Electron Paramagnetic Resonance," Interscience, New York, N. Y., 1968.
(13) H. M. Assenheim, "Introduction to Electron Spin Resonance," Plenum Press, New York, N. Y., 1967.
(14) M. Bersohn and J. C. Baird, "An Introduction to Electron Paramagnetic Resonance," W. A. Benjamin, New York, N. Y., 1966.
(15) G. E. Pake, "Paramagnetic Resonance," W. A. Benjamin, New York, N. Y., 1962.
(16) C. P. Poole, "Electron Spin Resonance," Interscience, New York, N. Y., 1967.
(17) W. Low in "Solid State Physics," Suppl. 2, F. Seitz and D. Turnbull, Ed., Academic Press, New York, N. Y., 1960.

(18) K. D. Bowers and J. Owen, Rep. Progr. Phys., 18, 304 (1955).
(19) B. Bleaney and K. W. H. Stevens, Rep. Progr. Phys., 16, 108 (1953).
(20) B. Bleaney, Phil. Mag., 42, 441 (1951).
(21) A. Abragam and M. H. L. Pryce, Proc. Roy. Soc., Ser. A, 205, 135 (1951).
(22) A. Abragam and M. H. L. Pryce, Proc. Roy. Soc., Ser. A, 206, 164 (1951).
(23) A. Abragam and M. H. L. Pryce, Proc. Roy. Soc., Ser. A, 206, 173 (1951).
(24) W. E. Lamb, Phys. Rev., 60, 817 (1941).
(25) N. F. Ramsey, Phys. Rev., 86, 243 (1952).
(26) N. Karplus and T. P. Das, J. Chem. Phys., 34, 1683 (1961).
(27) E. D. Jones, Phys. Rev., 151, 315 (1966).
(28) B. Bleaney, Phys. Rev., 104, 1190 (1956).
(29) T. Moriya, Progr. Theor. Phys., 16, 641 (1956).
(30) R. G. Shulman, Phys. Rev. Lett., 2, 459 (1959).
(31) W. D. Knight, Phys. Rev., 76, 1259 (1949).
(32) C. H. Townes, C. Herring, and W. D. Knight, Phys. Rev., 77, 852 (1950).
(33) H. Goldstein, "Classical Mechanics," Addison-Wesley, Reading, Mass., 1950, pp 107-109.
(34) J. D. Swalen and H. M. Gladney, IBM J. Res. Develop., 8, 515 (1964).
(35) M. H. Cohen and F. Reif in "Solid State Physics," Vol. 5, F. Seitz and D. Turnbull, Ed., Academic Press, New York, N. Y., 1957.
(36) G. H. Stauss, J. Chem. Phys., 40, 1988 (1964).
(37) K. Narita, J. Umeda, and H. Kusumoto, J. Chem. Phys., 44, 2719 (1966).
(38) G. M. Volkoff, Can. J. Phys., 31, 820 (1953).
(39) P. C. Taylor and P. J. Bray, J. Magn. Res., 2, 305 (1970).
(40) T. P. Das and E. L. Hahn, "Solid State Physics," Suppl. 1, F. Seitz and D. Turnbull, Ed., Academic Press, New York, N. Y., 1958.
(41) T. Castner, G. S. Newell, W. C. Holton, and C. P. Slichter, J. Chem. Phys., 32, 668 (1960).
(42) W. H. Jones, Jr., T. P. Graham, and R. G. Barnes, Phys. Rev., 132, 1898 (1963).
(43) J. F. Baugher, P. C. Taylor, T. Oja, and P. J. Bray, J. Chem. Phys., 50, 4914 (1969).
(44) V. M. Vinokorov, M. M. Zaripov, and V. G. Stepanov, Sov. Phys.-Solid State, 6, 866 (1964).
(45) H. W. de Wijn and R. F. van Balderen, J. Chem. Phys., 46, 1381 (1967).
(46) F. Wolf, D. Kline, and H. S. Story, J. Chem. Phys., 53, 3538 (1970).
(47) G. Burns, J. Appl. Phys., 32, 2048 (1961).
(48) J. E. Adams, L. Berry, and R. R. Hewitt, Phys. Rev., 143, 164 (1966).
(49) R. Bersohn, J. Chem. Phys., 20, 1505 (1952).
(50) J. F. Baugher and P. C. Taylor, unpublished research.
(51) D. J. E. Ingram, "Spectroscopy at Radio and Microwave Frequencies," Butterworths, London, 1967.
(52) E. Wasserman, L. C. Snyder, and W. A. Yager, J. Chem. Phys., 41, 1763 (1964).
(53) C. A. Hutchison and B. W. Mangum, J. Chem. Phys., 29, 952 (1958).
(54) I. Chen, C. Kikuchi, and H. Watanabe, J. Chem. Phys., 42, 189 (1965).
(55) I. Chen, C. Kikuchi, and H. Watanabe, J. Chem. Phys., 50, 2237 (1969).
(56) J. S. Griffith, "The Theory of Transition Metal Ions," Cambridge University Press, London, 1961.
(57) V. M. Vinokorov, M. M. Zaripov, and V. G. Stepanov, Sov. Phys.-Solid State, 6, 870 (1964).
(58) V. J. Folen, Phys. Rev., 125, 1581 (1962).
(59) P. B. Dorain, Phys. Rev., 112, 1058 (1958).
(60) L. M. Matarrese and C. Kikuchi, J. Phys. Chem. Solids, 1, 117 (1956).
(61) T. P. P. Hall, W. Hayes, and F. I. B. Williams, Proc. Phys. Soc. (London), 78, 883 (1961).
(62) W. Low, Phys. Rev., 105, 793 (1957).
(63) J. Lambe and C. Kikuchi, Phys. Rev., 119, 1256 (1960).
(64) S. P. Keller, I. L. Gelles, and W. V. Smith, Phys. Rev., 110, 850 (1958).
(65) E. R. Andrew and R. Bersohn, J. Chem. Phys., 18, 159 (1950).
(66) P. A. Casabella, J. Chem. Phys., 41, 3793 (1964).
(67) P. A. Casabella, and T. Oja, J. Chem. Phys., 50, 4814 (1969).
(68) H. M. Kriz and P. C. Taylor, J. Chem. Phys., 55, 2601 (1971).
(69) D. L. Vanderhart and H. S. Gutowsky, J. Chem. Phys., 49, 261 (1968).
(70) D. L. Vanderhart, H. S. Gutowsky, and T. C. Farrar, J. Chem. Phys., 50, 1058 (1969).
(71) B. Bleaney, Proc. Phys. Soc., London, 75, 621 (1960).
(72) T. Vänngard and R. Aasa, "Paramagnetic Resonance," Vol. 2, W. Low, Ed., Academic Press, New York, N. Y., 1963, p 509.
(73) A. Isomoto, H. Watari, and M. Kotani, J. Phys. Soc. Jap., 29, 1571 (1970).
(74) J. H. Van Vleck, Phys. Rev., 74, 1168 (1948).
(75) F. Bloch, Phys. Rev., 70, 460 (1946).
(76) N. Bloembergen and R. J. Rowland, Phys. Rev., 97, 1679 (1955).
(77) D. G. Hughes and D. K. C. MacDonald, Proc. Phys. Soc., London, 78, 75 (1961).
(78) W. Meisel, Phys. Status Solidi, (b) 43, K129 (1971).
(79) G. Elste, Z. Astrophys., 33, 39 (1953).
(80) D. L. Griscom and R. E. Griscom, J. Chem. Phys., 47, 2711 (1967).

(81) T. I. Barry, National Laboratory Report, Teddington, Middlesex, England, June 1967, unpublished.
(82) R. D. Dowsing and J. F. Gibson, J. Chem. Phys., 50, 294 (1969).
(83) R. Aäsa, J. Chem. Phys., 52, 3919 (1970).
(84) P. C. Taylor and P. J. Bray, J. Phys. Chem. Solids, 33, 43 (1972).
(85) R. H. Sands, Phys. Rev., 99, 1222 (1955).
(86) J. A. Ibers and J. D. Swalen, Phys. Rev., 127, 1914 (1962).
(87) F. K. Kneubühl, J. Chem. Phys., 33, 1074 (1960).
(88) H. M. McConnell and B. G. McFarland, Quart. Rev. Biophys., 3, 91 (1970).
(89) E. P. Jones and D. L. Williams, Phys. Lett., 1, 109 (1962).
(90) J. Marruani, Chem. Phys. Lett., 7, 29 (1970).
(91) F. Borsa and R. G. Barnes, J. Phys. Chem. Solids, 25, 1305 (1964).
(92) H. R. Gersmann and J. D. Swalen, J. Chem. Phys., 36, 3221 (1962).
(93) P. Kottis and R. Lefebvre, J. Chem. Phys., 41, 379 (1964).
(94) J. A. R. Coope, Chem. Phys. Lett., 3, 589 (1969).
(95) I. Chen, M. Abkowitz, and J. H. Sharp, J. Chem. Phys., 50, 2237 (1969).
(96) D. L. Griscom, P. C. Taylor, and P. J. Bray, J. Chem. Phys., 50, 977 (1969).
(97) J. Maruani, Mol. Phys., 18, 165 (1970).
(98) R. Lefebvre and J. Maruani, J. Chem. Phys., 42, 1480 (1965).
(99) R. Lefebvre and J. Maruani, J. Chem. Phys., 42, 1496 (1965).
(100) M. Kopp and J. H. Mackey, J. Comput. Phys., 3, 539 (1969).
(101) J. H. Mackey, M. Kopp, E. C. Tynan, and T. F. Yen, "Electron Spin Resonance of Metal Complexes," Plenum Press, New York, N. Y., 1969, p 33.
(102) J. Maruani in "Electron Magnetic Resonance and Solid Dielectrics," R. Servant and A. Charru, Ed., North Holland Publishing Co., Amsterdam, 1964, pp 303–307.
(103) P. C. Taylor and P. J. Bray, "Lineshape Program Manual," Brown University, R. I., 1968, unpublished. This manual is available from the authors on request.
(104) B. R. McCart and R. G. Barnes, J. Chem. Phys., 48, 127 (1968).
(105) J. W. Searl, R. C. Smith, and S. J. Wyard, Proc. Phys. Soc., London, 78, 1174 (1961).
(106) J. W. Searl, R. C. Smith, and S. J. Wyard, Proc. Phys. Soc., London, 74, 491 (1959).
(107) D. G. Hughes and T. J. Rowland, Can. J. Phys., 42, 209 (1964).
(108) M. S. Itzkowitz, J. Chem. Phys., 46, 3048 (1967).
(109) N. Bloembergen and T. J. Rowland, Acta Met., 1, 731 (1953).
(110) J. E. Adams, B. F. Williams, and R. R. Hewitt, Phys. Rev., 151, 238 (1966).
(111) G. Schoffa and G. Bürk, Phys. Status Solidi, 8, 557 (1965).
(112) J. A. Weil and H. G. Hecht, J. Chem. Phys., 38, 281 (1963).
(113) B. F. Williams and R. R. Hewitt, Phys. Rev., 146, 286 (1966).
(114) P. W. France and H. O. Hooper, J. Phys. Chem. Solids, 31, 2223 (1970).
(115) P. A. Casabella, J. Chem. Phys., 40, 149 (1964).
(116) J. F. Baugher, H. M. Kriz, P. C. Taylor, and P. J. Bray, J. Magn. Res., 3, 415 (1970).
(117) J. F. Baugher, Ph.D. Thesis, Brown University, Providence, R.I., 1968, unpublished (available from University Microfilms No. 70-8689).
(118) B. Pedersen, Acta Chem. Scand., 22, 449 (1968).
(119) J. Bacon, R. J. Gillespie, J. S. Hartman, and U. R. K. Rao, Mol. Phys., 18, 561 (1970).
(120) T. deNeef, D. C. Koninsberger, and P. van der Leeden, Appl. Sci. Res., 22, 251 (1970).
(121) Y. M. Kim, D. E. Reardon, and P. J. Bray, J. Chem. Phys., 48, 3396 (1968).
(122) P. C. Taylor, D. L. Griscom, and P. J. Bray, J. Chem. Phys., 54, 748 (1971).
(123) N. M. Aleksandrov and F. I. Skripov, Sov. Phys.-Usp., 4, 947 (1962).
(124) E. Fukushima, J. Chem. Phys., 55, 2463 (1971).
(125) B. Pedersen, Acta Chem. Scand., 22, 1813 (1968).
(126) H. M. Kriz and P. J. Bray, J. Magn. Res., 4, 69 (1971).
(127) C. Rhee, J. Korean Phys. Soc., 4, 51 (1971).
(128) C. Rhee and P. J. Bray, J. Chem. Phys., 56, 2476 (1972).
(129) H. M. Kriz and P. J. Bray, J. Magn. Res., 4, 16 (1971).
(130) H. M. Kriz and P. J. Bray, J. Magn. Res., 4, 76 (1971).
(131) H. M. Kriz, S. G. Bishop, and P. J. Bray, J. Chem. Phys., 49, 557 (1968).
(132) H. M. Kriz, M. J. Park, and P. J. Bray, Phys. Chem. Glasses, 12, 45 (1971).
(133) H. M. Kriz and P. J. Bray, J. Non.-Cryst. Solids, 6, 27 (1971).
(134) B. A. Scott, G. R. Eulenberger, and R. A. Bernheim, J. Chem. Phys., 48, 263 (1968).
(135) G. W. Ossman and J. W. McGrath, J. Chem. Phys., 49, 783 (1968).
(136) S. L. Segel, J. Chem. Phys., 51, 848 (1969).
(137) R. A. Bennet, H. O. Hooper, and V. Roy, J. Appl. Phys., 40, 2441 (1969).
(138) G. W. Ossman, A. A. Silvidi, and J. W. McGrath, J. Chem. Phys., 52, 509 (1970).
(139) G. E. Peterson, J. R. Carruthers, and A. Carnevale, J. Chem. Phys., 53, 2436 (1970).
(140) H. W. de Wijn, A. M. van Diepen, and K. H. J. Buschow, Phys. Rev. B, 1, 4203 (1970).
(141) A. H. Silver and T. Kushida, J. Chem. Phys., 38, 865 (1963).
(142) E. Fukushima, Acta Crystallogr., Sect. A, 27, 65 (1971).
(143) T. V. Hynes and N. M. Alexander, J. Chem. Phys., 54, 5296 (1971).

(144) J. P. Kopp and R. G. Barnes, J. Chem. Phys., 54, 1840 (1971).
(145) R. G. Barnes, R. B. Creel, and D. R. Torgeson, J. Chem. Phys., 53, 3762 (1970).
(146) R. B. Creel and R. G. Barnes, J. Chem. Phys., 56, 1549 (1972).
(147) R. G. Barnes, D. J. Genin, R. G. Lecander, and D. R. Torgeson, Phys. Rev., 145, 302 (1966). The sign of first-order magnetic shift is incorrect in this reference.
(148) J. F. Hon and P. J. Bray, Phys. Rev., 110, 624 (1958).
(149) S. G. Bishop, P. J. Ring, and P. J. Bray, J. Chem. Phys., 45, 1525 (1966).
(150) G. Burns, Phys. Rev., 127, 1193 (1962).
(151) J. F. Hon, Phys. Rev., 124, 1368 (1961).
(152) A. H. Silver and T. Kushida, J. Chem. Phys., 38, 865 (1963).
(153) A. H. Silver and P. J. Bray, J. Chem. Phys., 32, 288 (1960).
(154) P. J. Bray, J. O. Edwards, J. G. O'Keefe, V. F. Ross, and I. Tatsuzaki, J. Chem. Phys., 35, 435 (1961).
(155) H. W. de Wijn, A. M. Van Diepen, and K. H. J. Buschow, Phys. Rev. B, 1, 4203 (1970).
(156) B. F. Stein and R. H. Walmsley, Phys. Rev., 148, 933 (1966).
(157) C. J. Troup, Phys. Lett., 2, 9 (1962).
(158) D. E. O'Reilly, E. M. Peterson, Z. M. Saffar, and C. E. Scheie, Chem. Phys. Lett., 8, 470 (1971).
(159) R. Blinc, E. Pirkmajer, J. Slivnik, and I. Zupancic, J. Chem. Phys., 45, 1488 (1966).
(160) E. R. Andrew and D. P. Tunstall, Proc. Phys. Soc., London, 81, 986 (1963).
(161) W. Derbyshire, J. P. Stuart, and D. Warner, Mol. Phys., 17, 449 (1969).
(162) C. MacLean and E. L. Mackor, Proc. Phys. Soc., London, 88, 341 (1966).
(163) J. F. Baugher, H. M. Kriz, P. C. Taylor, and P. J. Bray, unpublished, available from the authors on request.
(164) R. G. Barnes, F. Borsa, S. L. Segel, and D. R. Torgeson, Phys. Rev., 137, A1828 (1965).
(165) F. R. Landsberger and P. J. Bray, J. Chem. Phys., 53, 2757 (1970).
(166) R. G. Barnes, W. H. Jones, and T. P. Graham, Phys. Rev. Lett., 6, 221 (1961).
(167) R. R. Hewitt and B. F. Williams, Phys. Rev. Lett., 12, 216 (1964).
(168) W. H. Jones and F. J. Milford, Phys. Rev., 125, 1259 (1962).
(169) L. J. Ancher, G. K. Schoep, E. A. P. Diemer, N. J. Poulis, and E. C. van Reuth, Physica, 49, 307 (1969).
(170) G. C. Carter and J. C. Swartz, J. Phys. Chem. Solids, 32, 2415 (1971).
(171) D. R. Torgeson, R. G. Barnes, and R. B. Creel, J. Chem. Phys., 56, 4178 (1972).
(172) D. L. Radhakishna Setty and B. D. Mungurwadi, Proc. Phys. Soc., London, 90, 495 (1967).
(173) D. R. Torgeson and R. G. Barnes, Phys. Rev., 136, 738 (1964).
(174) F. C. Thatcher and R. R. Hewitt, Phys. Rev. B, 1, 454 (1970).
(175) M. A. Ruderman and C. Kittel, Phys. Rev., 96, 99 (1954).
(176) Y. S. Karimov and I. F. Scheogolev, Soviet Phys. JETP, 14, 772 (1962).
(177) J. F. Baugher and P. J. Bray, Phys. Chem. Glasses, 10, 77 (1969).
(178) N. Bloembergen, E. M. Purcell, and R. V. Pound, Phys. Rev., 73, 679 (1948).
(179) T. B. Cobb and C. S. Johnson, Jr., J. Chem. Phys., 52, 6224 (1970).
(180) H. M. McIntyre and C. S. Johnson, Jr., J. Chem. Phys., 55, 345 (1971).
(181) J. A. Pople, W. G. Schneider, and H. J. Bernstein, "High-Resolution Nuclear Magnetic Resonance," McGraw-Hill, New York, N.Y., 1959.
(182) E. R. Andrew, in "Magnetic Resonance," C. K. Coogan, N. S. Ham, S. N. Stewart, J. R. Pilbrow, and G. V. H. Wilson, Ed., Plenum Press, New York, N.Y.; 1970, p 163.
(183) E. R. Andrew and V. T. Wynn, Proc. Roy. Soc., Ser. A, 291, 257 (1966).
(184) E. R. Andrew, L. F. Farnell, and T. D. Gledhill, Phys. Rev. Lett., 19, 6 (1967).
(185) E. R. Andrew and L. F. Farnell, Mol. Phys., 15, 157 (1968).
(186) E. R. Andrew, Arch. Sci., 12, 103 (1959).
(187) E. R. Andrew and R. G. Eades, Discuss. Faraday Soc., 34, 38 (1962).
(188) E. R. Andrew, L. F. Farnell, M. Firth, T. D. Gledhill, and I. Roberts, J. Magn. Res., 1, 27 (1969).
(189) E. R. Andrew and A. Jasinski, J. Phys. C, 4, 391 (1971).
(190) R. Neiman and D. Kivelson, J. Chem. Phys., 35, 156 (1961).
(191) J. F. Baugher and P. C. Taylor, J. Magn. Resonance, in press.
(192) S. Lee and P. J. Bray, J. Chem. Phys., 39, 2863 (1963).
(193) S. Lee and P. J. Bray, J. Chem. Phys., 40, 2982 (1964).
(194) S. M. Blinder, J. Chem. Phys., 33, 748 (1960).
(195) M. Iwasaki, J. Chem. Phys., 45, 990 (1966).
(196) E. L. Cochran, F. J. Adrian, and V. A. Bowers, J. Chem. Phys., 34, 1161 (1961).
(197) H. Sternlicht, J. Chem. Phys., 33, 1128 (1960).
(198) M. Abkowitz, I. Chen, and J. H. Sharp, J. Chem. Phys., 48, 4561 (1968).
(199) M. Abkowitz and I. Chen, J. Chem. Phys., 54, 811 (1971).
(200) H. J. Gerritsen and H. R. Lewis, Phys. Rev., 119, 1010 (1960).
(201) P. A. Narayana and K. V. L. N. Sastry, J. Chem. Phys., 57, 1805 (1972).
(202) H. G. Hecht and T. S. Johnson, J. Chem. Phys., 46, 23 (1967).
(203) G. Hochstrasser, Phys. Chem. Glasses, 7, 178 (1966).
(204) H. Toyuki and S. Akagi, Phys. Chem. Glasses, 13, 15 (1972).
(205) I. Siegel, Phys. Rev., 134, A193 (1964).

(206) R. J. Faber and M. T. Rogers, *J. Amer. Chem. Soc.*, **81**, 1849 |1959).
(207) D. E. O'Reilly, *J. Chem. Phys.*, **29**, 1188 |1958); *erratum*, **30**, 591 (1959).
(208) J. L. Ragle, *J. Chem. Phys.*, **38**, 2020 (1963).
(209) J. S. Waugh and F. W. Dobbs, *J. Chem. Phys.*, **31**, 1235 (1959).
(210) R. W. Fessenden, *J. Chem. Phys.*, **37**, 747 |1962).
(211) J. Maruani, C. A. McDowell, H. Nakajima, and P. Raghunathan, *Mol. Phys.*, **14**, 349 |1968).
(212) G. S. Owen and G. Vincow, *J. Chem. Phys.*, **54**, 368 |1971).
|213) P. C. Taylor and D. L. Griscom, *J. Chem. Phys.*, **55**, 3610 |1971).
(214) P. C. Taylor and P. J. Bray, *Bull. Amer. Ceram. Soc.*, **51**, 234 (1972).
(215) T. G. Castner and W. Känzig, *J. Phys. Chem. Solids*, **3**, 178 (1957).
(216) D. Schoemaker, *Phys. Rev.*, **149**, 693 |1966).
(217) W. Dreybrodt and D. Silber, *Phys. Status Solidi*, **16**, 215 |1966).
(218) G. L. Bir, *Sov. Phys.-Solid State*, **5**, 1628 (1964); *Fiz. Tverd. Tela*, **5**, 2236 (1963).
(219) S. R. P. Smith, P. V. Auzins, and J. E. Wertz, *Phys. Rev.*, **166**, 222 (1968).
(220) G. J. Wolga and R. Tseng, *Phys. Rev.*, **133**, A1563 |1964).
(221) E. Friedman and W. Low, *Phys. Rev.*, **120**, 408 (1960).
(222) J. Mankowitz and W. Low, *Phys. Rev. B*, **2**, 28 (1970).
(223) S. H. Choh and G. Seidel, *Phys. Rev.*, **164**, 412 |1967).
(224) B. Bleaney and R. S. Rubins, *Proc. Phys. Soc., London*, **77**, 103 (1961); *Corrigendum*, **78**, 778 |1961).
(225) W. A. Yager, E. Wasserman, and R. M. R. Cramer, *J. Chem. Phys.*, **37**, 1148 |1962).
|226) L. E. Mohrmann, Jr., B. B. Garrett, and W. Burton Lewis, *J. Chem. Phys.*, **52**, 535 |1970).
|227) R. J. Landry, J. T. Fournier, and C. G. Young, *J. Chem. Phys.*, **46**, 1285 (1967).
(228) V. S. Grunin and G. A. Pavlova, *Sov. Phys.-Solid State*, **13**, 637 (1971); *Fiz. Tverd. Tela*, **13**, 772 (1971).
(229) B. B. Garrett, K. DeArmond, and H. S. Gutowsky, *J. Chem. Phys.*, **44**, 3393 (1966).
(230) F. K. Kneubühl and B. Natterer, *Helv. Phys. Acta*, **34**, 710 (1961).
(231) J. T. Fournier, R. J. Landry, and R. H. Bartram, *J. Chem. Phys.*, **55**, 2522 (1971).
(232) S. L. Manatt, D. D. Elleman, R. W. Vaughn, S. I. Chan, F. D. Tsay, and W. T. Huntress, Jr., *Science*, **167**, 709 |1970); F. D. Tsay, S. I. Chan, and S. L. Manatt, *Proc. 2nd Lunar Sci. Conf., Geochim. Cosmochim. Acta, Suppl.* **2**, 3, 2512 (1971).
|233) F. D. Tsay, S. I. Chan, and S. L. Manatt, *Geochim. Cosmochim. Acta*, **35**, 865 (1971).
|234) R. A. Weeks, A. Chatelain, J. L. Kolopus, D. Kline, and J. G. Castle, *Science*, **167**, 704 (1970); J. L. Kolopus, D. Kline, A. Chatelain, and R. A. Weeks, *Proc. 2nd Lunar Sci. Conf., Geochim. Cosmochim. Acta, Suppl.* **2**, 3, 2501 |1971); R. A. Weeks, *Proc. 4th Lunar Sci. Conf., Geochim. Cosmochim. Acta, Suppl.* **4**, 3, 2763 (1973).
(235) D. L. Griscom, E. J. Friebele, and C. L. Marquardt, *Proc. 4th Lunar Sci. Conf., Geochim. Cosmochim. Acta, Suppl.* **4**, 3, 2709 |1973).
(236) D. L. Griscom, *Geochim. Cosmochim. Acta*, **38**, 1509 |1974).
(237) C. Kittel, *Phys. Rev.*, **73**, 155 (1948).
(238) K. J. Standley and K. W. H. Stevens, *Proc. Phys. Soc., London, Sect. B*, **69**, 993 |1956).
|239) E. Schlömann, *J. Phys. Chem. Solids*, **6**, 257 |1958).
(240) E. Schlömann and R. V. Jones, *J. Appl. Phys., Suppl.*, **30**, 117S (1959).
(241) R. D. Dowsing, B. Nieuwenhuijse, and J. Reedijk, *Inorg. Chim. Acta*, **5**, 301 |1971).
|242) H. H. Wickman, M. P. Klein, and D. A. Shirley, *J. Chem. Phys.*, **42**, 2113 (1965).
|243) H. T. Witteveen and J. Reedijk, *Solid State Commun.*, **12**, 397 |1973).
(244) G. Feher and E. A. Gere, *Phys. Rev.*, **103**, 501 (1956).
|245) J. S. Hyde, R. C. Sneed, and G. H. Rist, *J. Chem. Phys.*, **51**, 1404 |1969).
|246) J. Richardson, V. P. Jacobsmeyer, and S. Lee, *J. Chem. Phys.*, **48**, 2115 |1968).
|247) H. H. Niebuhr and S. Lee, *Phys. Rev. B*, **5**, 4226 |1972).
|248) C. D. Jeffries, "Dynamic Nuclear Orientation," Interscience, New York, N.Y., 1963.
|249) C. H. Greene, *Sci. Amer.*, **204**, 2 |Jan. 1961).
|250) H. Imagawa, *Phys. Status Solidi*, **30**, 469 |1968).
|251) D. L. Griscom, *Solid State Commun.*, 11, 899 |1972).
|252) D. L. Griscom, P. C. Taylor, D. A. Ware, and P. J. Bray, *J. Chem. Phys.*, **48**, 5158 |1968).
|253) G. E. Peterson and C. R. Kurkjian, *Solid State Commun.*, 11, 1105 (1972).
|254) G. E. Peterson and A. Carnevale, *J. Chem. Phys.*, **56**, 4848 |1972).
|255) J. H. Mackey, J. W. Boss, and M. Kopp, *Phys. Chem. Glasses*, 11, 205 (1970).
|256) D. L. Griscom, *J. Non.-Cryst. Solids*, 13, 251 (1973/74).
|257) D. L. Griscom, *J. Non.-Cryst. Solids*, **6**, 275 (1971).
|258) J. Wong and C. A. Angell, *Appl. Spectrosc. Rev.*, **4**, 200 |1971).
|259) M. C. R. Symons, *J. Chem. Phys.*, **53**, 468 |1970).
|260) D. L. Griscom, P. C. Taylor, and P. J. Bray, *J. Chem. Phys.*, **53**, 469 (1970).
|261) S. L. Segel and R. G. Barnes, *Phys. Rev. Lett.*, **15**, 886 |1965); S. L. Segel, R. G. Barnes, and R. B. Creel, *Chem. Phys. Lett.*, **2**, 613 |1968); D. L. Macalady and R. G. Barnes, *ibid.*, **5**, 186 (1970).
|262) K. Halbach, *Phys. Rev.*, **119**, 1230 |1960).
|263) E. R. Andrew, *Phys. Rev.*, **91**, 425 (1953).
|264) C. P. Flynn and E. F. W. Seymour, *Proc. Phys. Soc., London*, **75**, 337 |1959).
|265) W. J. Spry, *J. Appl. Phys.*, **28**, 661 |1957).
|266) M. Perlman and M. Bloom, *Phys. Rev.*, **88**, 1290 |1952).
|267) G. K. Reeves and G. V. H. Wilson, *J. Phys. D*, 3, 1609 |1970).
|268) J. Talpe, *Physica*, **35**, 157 (1967).
|269) D. E. O'Reilly, *J. Chem. Phys.*, **28**, 1262 (1958).
|270) A. M. Portis, *Phys. Rev.*, **100**, 1219 (1955).
|271) B. Bleaney and K. W. H. Stevens, *Repts. Progr. Phys.*, **16**, 108 (1953).
|272) A. R. Stokes, *Proc. Phys. Soc., London*, **61**, 382 |1948).
|273) E. J. Friebele, D. L. Griscom, and G. H. Sigel, Jr., *J. Appl. Phys.*, **45**, 3424 |1974).
|274) D. L. Griscom, E. J. Friebele, and G. H. Sigel, Jr., *Solid State Commun.*, **15**, 479 |1974).
|275) E. J. Friebele, *Bull. Amer. Ceram. Soc.*, in press.
|276) P. C. Taylor and E. J. Friebele, *J. Non-Cryst. Solids*, **16**, 375 |1974).
|277) P. J. Bray, Proceedings of the Tenth International Congress on Glass, Kyoto, Japan, July 1974, in press.
|278) G. E. Peterson, C. R. Kurkjian, and A. Carnevale, *Phys. Chem. Glasses*, **15**, 52, 59 |1974).
|279) R. C. Nicklin, J. K. Johnstone, R. G. Barnes, and D. R. Wilder, *J. Chem. Phys.*, **59**, 1652 (1973).
|280) R. G. Barnes and B. K. Lunde, *J. Phys. Soc. Jap.*, **28**, 408 |1970).
|281) K. E. Haland and B. Petersen, *J. Chem. Phys.*, **53**, 2128 |1970).
|282) R. A. Forman and A. H. Kahn, *J. Chem Phys.*, **45**, 4586 |1966).
|283) H. S. Gutowsky and B. R. McGarvey, *J. Chem. Phys.*, **20**, 1472 |1952).
|284) M. Rotaru, *Rev. Roum. Phys.*, **15**, 663 |1970).